Supplementary Material

Model Compounds of Ruthenium-Alkene Intermediates in Olefin Metathesis Reactions

Donde R. Anderson,[†] Daniel D. Hickstein,[§] Daniel J. O'Leary,[§] and Robert H. Grubbs*,[†]

[†]Arnold and Mabel Beckman Laboratories of Chemical Synthesis, Division of Chemistry and Chemical Engineering, California Institute of Technology, Pasadena, California, and [§]Department of Chemistry, Pomona College, Claremont, California, 91711

Table of Contents

Experimental Section: Preparation of Ru-Olefin Complex 9

All reactions were carried out under a dry argon atmosphere using standard Schlenk techniques or in a nitrogen-filled glovebox unless otherwise noted. Benzene and benzene-d_6 were purified by passage through activated A-2 alumina solvent columns and were degassed with argon prior to use. CD_2Cl_2 was purified by distillation from CaH_2 and degassed with argon prior to use. $CDCl_2CDCl_2$ was passed through a plug of alumina, degassed with nitrogen and stored over 4Å molecular sieves. Divinylbenzene (**8**)[1] and catalyst **7**[2] were prepared according to literature procedure. High-resolution mass spectrometry (HRMS) data was obtained on a JEOL MSRoute mass spectrometer.

H_2IMes(Cl)$_2$Ru=CH(2-vinylbenzene) (**9**). To a solution of **7** (200 mg, 0.275 mmol) in benzene (10 mL) in a 20-mL vial under nitrogen was added **8** (40 mg, 1.1 eq., 0.308 mmol). The reaction was stirred for 2 h at room temperature during which time a light green precipitate is formed. The solid was filtered, washed with benzene and dried under vacuum overnight to give a light green powder (89%). HRMS $[M]^+$ = 594.1137. Calcd = 594.1143.

[1] Mitchell, R. H.; Ghose, B. N.; Williams, M. E. *Can. J. Chem.* **1977**, *55*, 210.
[2] Sanford, M. S.; Love, J. A.; Grubbs, R. H. *Organometallics* **2001**, *20*, 5314.

CALIFORNIA INSTITUTE OF TECHNOLOGY

BECKMAN INSTITUTE

X-RAY CRYSTALLOGRAPHY LABORATORY

X-ray Crystal Structure Analysis of Ru-Olefin Complex **9**

Contents

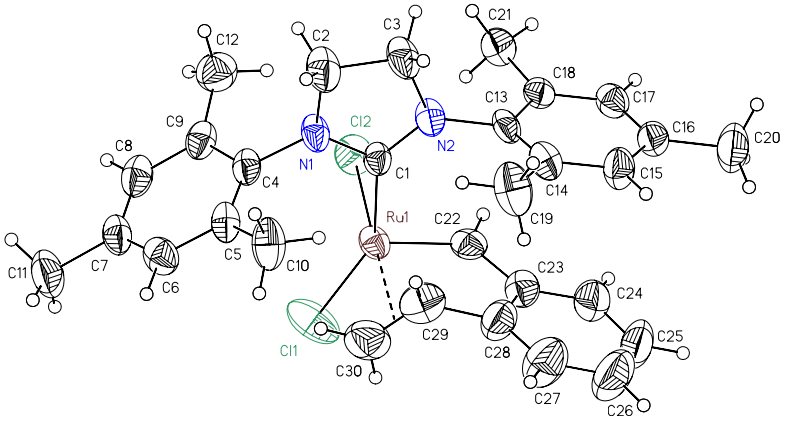

9b

Note: Crystallographic data have been deposited at the CCDC, 12 Union Road, Cambridge CB2 1EZ, UK and copies can be obtained on request, free of charge, by quoting the publication citation and the deposition number 289352.

Table S1. Crystal data and structure refinement for 9b (CCDC 289352).

Empirical formula	$C_{30}H_{34}N_2Cl_2Ru$
Formula weight	594.56
Crystallization Solvent	Dichloromethane
Crystal Habit	Blade
Crystal size	Not measured
Crystal color	Green

Data Collection

Type of diffractometer	Bruker SMART 1000
Wavelength	0.71073 Å MoKα
Data Collection Temperature	293(2) K
θ range for 15425 reflections used in lattice determination	2.20 to 25.65°
Unit cell dimensions	a = 16.4420(10) Å b = 16.5926(10) Å c = 22.4396(14) Å
Volume	6121.9(6) $Å^3$
Z	8
Crystal system	Orthorhombic
Space group	Pbca
Density (calculated)	1.290 Mg/m^3
F(000)	2448
Data collection program	Bruker SMART v5.630
θ range for data collection	1.82 to 28.43°
Completeness to θ = 28.43°	96.5 %
Index ranges	$-21 \le h \le 21$, $-22 \le k \le 22$, $-29 \le l \le 29$
Data collection scan type	ω scans at 5 ϕ settings
Data reduction program	Bruker SAINT v6.45A
Reflections collected	86972
Independent reflections	7436 [R_{int}= 0.1083]
Absorption coefficient	0.706 mm^{-1}
Absorption correction	None

Table S1 (cont.).

Structure Solution and Refinement

Structure solution program	Bruker XS v6.12
Primary solution method	Direct methods
Secondary solution method	Difference Fourier map
Hydrogen placement	Geometric positions
Structure refinement program	Bruker XL v6.12
Refinement method	Full matrix least-squares on F^2
Data / restraints / parameters	7436 / 0 / 325
Treatment of hydrogen atoms	Riding
Goodness-of-fit on F^2	1.507
Final R indices [$I>2\sigma(I)$, 3704 reflections]	R1 = 0.0477, *w*R2 = 0.0656
R indices (all data)	R1 = 0.1032, *w*R2 = 0.0680
Type of weighting scheme used	Sigma
Weighting scheme used	$w=1/\sigma^2(Fo^2)$
Max shift/error	0.004
Average shift/error	0.000
Largest diff. peak and hole	0.676 and -0.925 e.Å^{-3}

Special Refinement Details

The crystals contain solvent of crystallization, either pentane or dichloromethane. The electron density difference Fourier strongly suggested dichloromethane. However, when dichloromethane was included in the model the refinement produced unsatisfactory results with non-sensible bond distances and angles, rigid body refinement produced an unsatisfactory fit.

Squeeze[3] was used to model the electron density in the solvent regions. The eight voids within the crystal occupied approximately 122Å^3 each and represented 40.25 electrons, very near the 42 expected for either dichloromethane or pentane.

Refinement of F^2 against ALL reflections. The weighted R-factor (*w*R) and goodness of fit (S) are based on F^2, conventional R-factors (R) are based on F, with F set to zero for negative F^2. The threshold expression of $F^2 > 2\sigma(F^2)$ is used only for calculating R-factors(gt) etc. and is not relevant to the choice of reflections for refinement. R-factors based on F^2 are statistically about twice as large as those based on F, and R-factors based on ALL data will be even larger.

All esds (except the esd in the dihedral angle between two l.s. planes) are estimated using the full covariance matrix. The cell esds are taken into account individually in the estimation of esds in distances, angles and torsion angles; correlations between esds in cell parameters are only used when they are defined by crystal symmetry. An approximate (isotropic) treatment of cell esds is used for estimating esds involving l.s. planes.

[3] P. v.d. Sluis & A.L. Spek , *Acta Cryst.* (1990), A46, 194

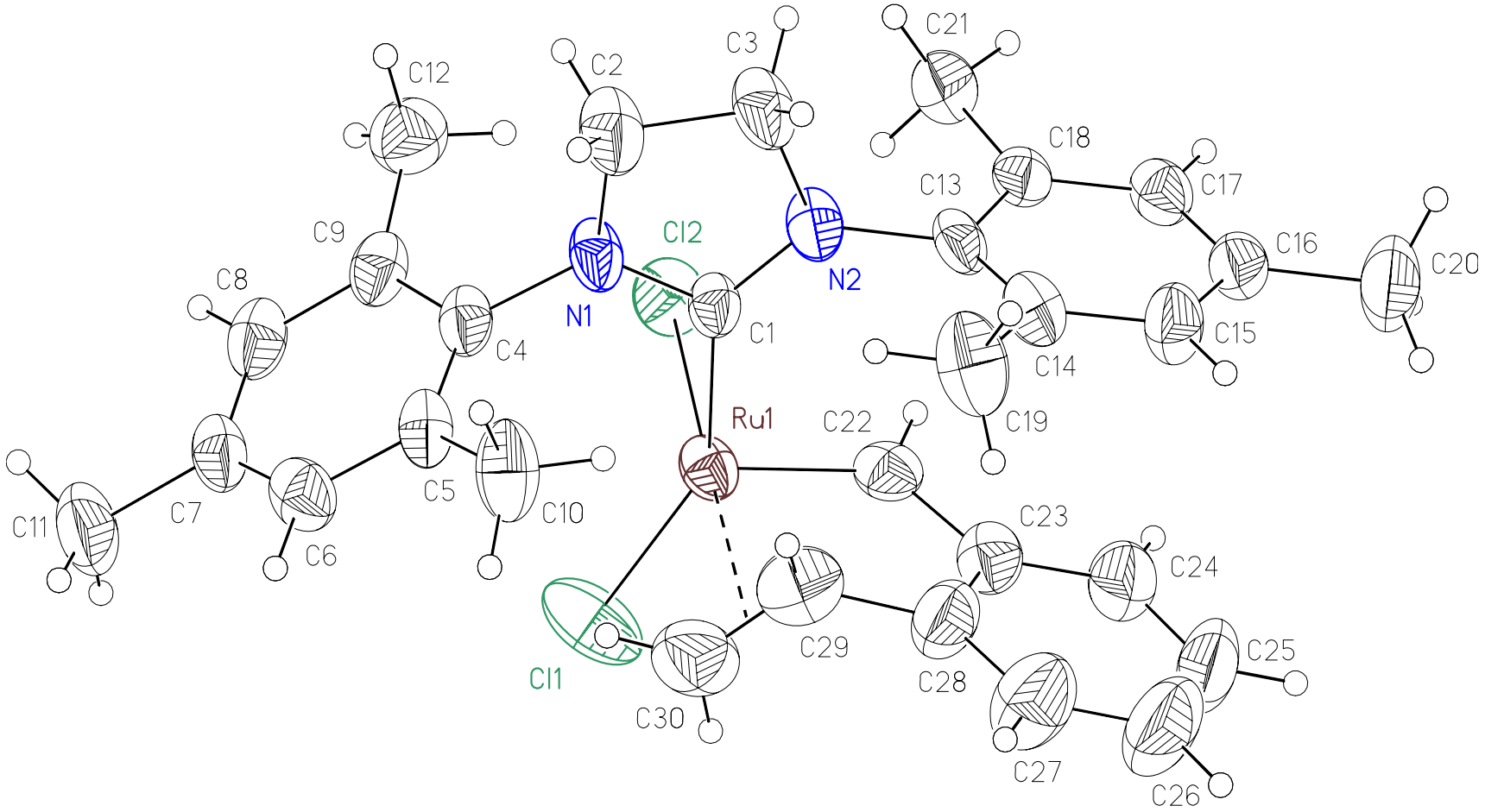

Figure S1. X-ray structure and atom-numbering scheme for **9b**.

Table S2. Atomic coordinates (Å x 10^4) and equivalent isotropic displacement parameters (Å^{2}x 10^3) for 9b (CCDC 289352). U(eq) is defined as the trace of the orthogonalized U^{ij} tensor.

	x	y	z	U_{eq}
Ru(1)	7649(1)	7980(1)	6066(1)	36(1)
Cl(1)	6661(1)	6949(1)	6244(1)	77(1)
Cl(2)	7671(1)	7446(1)	5086(1)	50(1)
N(1)	7456(2)	9527(2)	5455(1)	41(1)
N(2)	8747(2)	9367(2)	5590(1)	41(1)
C(1)	8018(2)	9043(2)	5696(1)	34(1)
C(2)	7795(2)	10246(2)	5162(2)	60(1)
C(3)	8696(2)	10127(2)	5247(2)	54(1)
C(4)	6591(2)	9403(2)	5515(2)	39(1)
C(5)	6202(2)	9687(2)	6022(2)	42(1)
C(6)	5377(2)	9535(2)	6082(2)	48(1)
C(7)	4942(2)	9130(2)	5649(2)	46(1)
C(8)	5335(2)	8915(2)	5133(2)	48(1)
C(9)	6156(2)	9059(2)	5049(2)	43(1)
C(10)	6633(2)	10197(2)	6488(2)	63(1)
C(11)	4048(2)	8946(2)	5731(2)	70(1)
C(12)	6535(2)	8872(2)	4448(2)	60(1)
C(13)	9534(2)	9096(2)	5793(2)	38(1)
C(14)	9870(2)	9412(2)	6300(2)	43(1)
C(15)	10628(2)	9138(2)	6483(2)	52(1)
C(16)	11058(2)	8581(2)	6145(2)	45(1)
C(17)	10719(2)	8313(2)	5622(2)	42(1)
C(18)	9963(2)	8562(2)	5429(2)	37(1)
C(19)	9468(2)	10078(2)	6663(2)	69(1)
C(20)	11880(2)	8295(2)	6355(2)	73(1)
C(21)	9650(2)	8285(2)	4832(2)	53(1)
C(22)	8641(2)	7517(2)	6197(2)	41(1)
C(23)	9084(2)	7575(2)	6747(2)	46(1)
C(24)	9778(2)	7154(2)	6909(2)	59(1)
C(25)	10135(2)	7281(3)	7448(2)	73(1)
C(26)	9814(3)	7850(3)	7830(2)	89(2)
C(27)	9143(3)	8293(3)	7670(2)	82(1)
C(28)	8765(2)	8147(2)	7134(2)	57(1)
C(29)	8016(3)	8581(2)	6912(2)	60(1)
C(30)	7276(2)	8267(2)	6976(2)	71(1)

Table S3. Selected bond lengths [Å] and angles [°] for 9b (CCDC 289352).

Ru(1)-C(22)	1.827(3)
Ru(1)-C(1)	2.041(3)
Ru(1)-C(30)	2.185(3)
Ru(1)-C(29)	2.228(4)
Ru(1)-Cl(2)	2.3701(9)
Ru(1)-Cl(1)	2.3926(9)
C(22)-Ru(1)-C(1)	99.36(12)
C(22)-Ru(1)-C(30)	101.10(15)
C(1)-Ru(1)-C(30)	105.94(14)
C(22)-Ru(1)-C(29)	79.02(15)
C(1)-Ru(1)-C(29)	83.05(14)
C(30)-Ru(1)-C(29)	35.10(11)
C(22)-Ru(1)-Cl(2)	88.74(11)
C(1)-Ru(1)-Cl(2)	86.63(9)
C(30)-Ru(1)-Cl(2)	162.31(11)
C(29)-Ru(1)-Cl(2)	162.45(11)
C(22)-Ru(1)-Cl(1)	106.19(9)
C(1)-Ru(1)-Cl(1)	152.57(9)
C(30)-Ru(1)-Cl(1)	79.02(11)
C(29)-Ru(1)-Cl(1)	111.21(11)
Cl(2)-Ru(1)-Cl(1)	84.15(3)

Table S4. Bond lengths [Å] and angles [°] for 9b (CCDC 289352).

Ru(1)-C(22)	1.827(3)
Ru(1)-C(1)	2.041(3)
Ru(1)-C(30)	2.185(3)
Ru(1)-C(29)	2.228(4)
Ru(1)-Cl(2)	2.3701(9)
Ru(1)-Cl(1)	2.3926(9)
N(1)-C(1)	1.340(3)
N(1)-C(4)	1.443(4)
N(1)-C(2)	1.472(4)
N(2)-C(1)	1.335(3)
N(2)-C(13)	1.443(4)
N(2)-C(3)	1.481(4)
C(2)-C(3)	1.507(4)
C(4)-C(5)	1.386(4)
C(4)-C(9)	1.390(4)
C(5)-C(6)	1.385(4)
C(5)-C(10)	1.523(4)
C(6)-C(7)	1.380(5)
C(7)-C(8)	1.374(4)
C(7)-C(11)	1.513(4)
C(8)-C(9)	1.383(4)
C(9)-C(12)	1.517(4)
C(13)-C(14)	1.368(4)
C(13)-C(18)	1.397(4)
C(14)-C(15)	1.389(4)
C(14)-C(19)	1.525(4)
C(15)-C(16)	1.388(4)
C(16)-C(17)	1.374(4)
C(16)-C(20)	1.507(4)
C(17)-C(18)	1.379(4)
C(18)-C(21)	1.507(4)
C(22)-C(23)	1.437(4)
C(23)-C(24)	1.387(4)
C(23)-C(28)	1.389(4)
C(24)-C(25)	1.362(5)
C(25)-C(26)	1.380(5)
C(26)-C(27)	1.374(5)
C(27)-C(28)	1.374(5)
C(28)-C(29)	1.511(5)
C(29)-C(30)	1.331(4)
C(22)-Ru(1)-C(1)	99.36(12)
C(22)-Ru(1)-C(30)	101.10(15)
C(1)-Ru(1)-C(30)	105.94(14)
C(22)-Ru(1)-C(29)	79.02(15)
C(1)-Ru(1)-C(29)	83.05(14)
C(30)-Ru(1)-C(29)	35.10(11)
C(22)-Ru(1)-Cl(2)	88.74(11)
C(1)-Ru(1)-Cl(2)	86.63(9)
C(30)-Ru(1)-Cl(2)	162.31(11)
C(29)-Ru(1)-Cl(2)	162.45(11)
C(22)-Ru(1)-Cl(1)	106.19(9)

C(1)-Ru(1)-Cl(1)	152.57(9)
C(30)-Ru(1)-Cl(1)	79.02(11)
C(29)-Ru(1)-Cl(1)	111.21(11)
Cl(2)-Ru(1)-Cl(1)	84.15(3)
C(1)-N(1)-C(4)	123.9(3)
C(1)-N(1)-C(2)	113.9(3)
C(4)-N(1)-C(2)	122.0(3)
C(1)-N(2)-C(13)	128.5(3)
C(1)-N(2)-C(3)	112.6(3)
C(13)-N(2)-C(3)	118.7(3)
N(2)-C(1)-N(1)	107.8(3)
N(2)-C(1)-Ru(1)	133.4(2)
N(1)-C(1)-Ru(1)	118.5(2)
N(1)-C(2)-C(3)	102.1(3)
N(2)-C(3)-C(2)	103.5(3)
C(5)-C(4)-C(9)	121.3(3)
C(5)-C(4)-N(1)	118.9(3)
C(9)-C(4)-N(1)	119.7(3)
C(6)-C(5)-C(4)	118.0(3)
C(6)-C(5)-C(10)	119.4(3)
C(4)-C(5)-C(10)	122.5(3)
C(7)-C(6)-C(5)	121.8(4)
C(8)-C(7)-C(6)	118.3(3)
C(8)-C(7)-C(11)	120.5(4)
C(6)-C(7)-C(11)	121.1(4)
C(7)-C(8)-C(9)	122.0(3)
C(8)-C(9)-C(4)	118.0(3)
C(8)-C(9)-C(12)	119.1(3)
C(4)-C(9)-C(12)	122.8(3)
C(14)-C(13)-C(18)	121.7(3)
C(14)-C(13)-N(2)	120.3(3)
C(18)-C(13)-N(2)	117.7(3)
C(13)-C(14)-C(15)	118.8(3)
C(13)-C(14)-C(19)	123.2(3)
C(15)-C(14)-C(19)	118.0(3)
C(16)-C(15)-C(14)	120.9(3)
C(17)-C(16)-C(15)	118.3(3)
C(17)-C(16)-C(20)	122.0(3)
C(15)-C(16)-C(20)	119.7(3)
C(16)-C(17)-C(18)	122.5(3)
C(17)-C(18)-C(13)	117.5(3)
C(17)-C(18)-C(21)	119.7(3)
C(13)-C(18)-C(21)	122.8(3)
C(23)-C(22)-Ru(1)	124.2(3)
C(24)-C(23)-C(28)	119.5(4)
C(24)-C(23)-C(22)	127.4(4)
C(28)-C(23)-C(22)	113.1(3)
C(25)-C(24)-C(23)	120.6(4)
C(24)-C(25)-C(26)	119.6(4)
C(27)-C(26)-C(25)	120.7(4)
C(26)-C(27)-C(28)	119.8(4)
C(27)-C(28)-C(23)	119.8(4)
C(27)-C(28)-C(29)	125.0(4)
C(23)-C(28)-C(29)	115.2(3)

C(30)-C(29)-C(28)	121.6(4)
C(30)-C(29)-Ru(1)	70.7(2)
C(28)-C(29)-Ru(1)	106.8(2)
C(29)-C(30)-Ru(1)	74.2(2)

Table S5. Anisotropic displacement parameters ($Å^2 x 10^4$) for 9b (CCDC 289352). The anisotropic displacement factor exponent takes the form: $-2\pi^2 [h^2 a^{*2} U^{11} + ... + 2 h k a^* b^* U^{12}]$.

	U^{11}	U^{22}	U^{33}	U^{23}	U^{13}	U^{12}
Ru(1)	318(1)	293(1)	478(2)	7(2)	37(2)	-28(1)
Cl(1)	721(7)	569(7)	1011(9)	-68(7)	332(6)	-325(6)
Cl(2)	519(5)	460(5)	533(6)	-106(4)	-23(5)	-78(5)
N(1)	270(18)	309(14)	662(19)	100(15)	-35(16)	-48(13)
N(2)	311(18)	276(17)	650(20)	90(15)	-18(16)	-10(14)
C(1)	290(20)	300(20)	440(20)	27(17)	-20(17)	26(17)
C(2)	400(30)	400(20)	1010(30)	200(20)	-60(20)	-84(18)
C(3)	340(20)	390(20)	880(30)	130(20)	10(20)	-86(18)
C(4)	300(20)	280(20)	590(30)	98(19)	-60(20)	-10(17)
C(5)	310(20)	330(20)	610(30)	-20(20)	-80(20)	13(15)
C(6)	440(20)	430(20)	580(30)	-10(20)	90(20)	98(17)
C(7)	310(20)	370(20)	690(30)	80(20)	-30(20)	26(18)
C(8)	420(30)	400(20)	630(30)	30(20)	-160(20)	-30(19)
C(9)	400(20)	340(20)	540(30)	36(19)	-120(20)	5(18)
C(10)	450(30)	540(30)	890(30)	-200(20)	-120(20)	120(20)
C(11)	340(20)	770(30)	980(30)	100(30)	-40(20)	-70(20)
C(12)	640(30)	570(30)	590(30)	60(20)	-30(20)	-20(20)
C(13)	240(20)	350(20)	550(30)	60(20)	46(18)	-54(17)
C(14)	360(20)	370(20)	560(30)	-90(20)	40(20)	-29(18)
C(15)	380(20)	630(30)	540(30)	-80(20)	-100(20)	10(20)
C(16)	350(20)	460(20)	520(30)	90(20)	-10(20)	-18(17)
C(17)	380(20)	360(20)	510(30)	29(19)	67(19)	47(17)
C(18)	330(20)	340(20)	440(20)	71(18)	12(18)	-61(17)
C(19)	510(30)	590(30)	970(40)	-250(30)	-30(20)	40(20)
C(20)	450(30)	980(30)	750(30)	-30(20)	-170(20)	140(20)
C(21)	420(20)	590(30)	580(30)	50(20)	10(20)	-24(19)
C(22)	460(20)	310(20)	460(20)	79(19)	66(18)	-43(17)
C(23)	440(20)	410(20)	540(30)	20(20)	-10(20)	7(19)
C(24)	500(20)	620(30)	660(30)	80(20)	-20(20)	60(20)
C(25)	530(30)	800(30)	870(40)	170(30)	-230(30)	110(20)
C(26)	860(40)	1150(50)	670(30)	10(30)	-340(30)	80(30)
C(27)	910(40)	880(40)	660(30)	-100(30)	-170(30)	180(30)
C(28)	550(30)	660(30)	510(30)	10(20)	-130(20)	30(20)
C(29)	790(30)	570(30)	460(30)	-160(20)	-10(20)	0(30)
C(30)	730(30)	900(30)	490(30)	-80(20)	60(20)	-110(30)

Experimental Section: NMR Spectroscopy Experiments

NMR spectra were obtained on a Bruker Avance DPX 400 MHz NMR spectrometer equipped with a 5 mm dual $^{1}H/^{13}C$ Z-gradient probe. Unless otherwise specified, spectra were obtained at 23 °C. For experiments requiring elevated temperatures, the probe was calibrated with a sample of ethylene glycol containing a trace amount of gaseous HCl.[4] 1D ^{1}H and ^{13}C spectra were acquired with standard pulse sequences and parameters. Details for the 2D experiments are as follows:

Gradient-enhanced 2D COSY experiment.[5] The **cosygs** pulse program was used with the following acquisition parameters. F2 and F1 sweep widths, 7184 Hz. F2 and F1 digital resolution, 7.01 Hz/pt. 256 FIDs recorded, each consisting of 4 scans and 1024 data points (AQ = 0.071 s). A recycle delay of (D1) of 1.5 s was employed. Processing parameters: unshifted sinusoidal apodization was applied in both dimensions prior to the Fourier transformation. **9b/c**: Figures S11-S12.

2D COSYLR experiment.[6] The **cosylr** pulse program was used with the following acquisition parameters. F2 and F1 sweep widths, 7184 Hz. F2 and F1 digital resolution, 7.01 Hz/pt. 128 FIDs recorded, each consisting of 8 scans and 1024 data points (AQ = 0.071 s). Refocussing delays of 100 ms and 200 ms were used in separate experiments. A recycle delay of (D1) of 2.0 s was employed. Zero-filling was applied once to achieve digital resolution of 3.5 Hz/pt in each dimension. Processing parameters: unshifted sinusoidal (SINE, SSB=0) apodization was applied in both dimensions prior to the Fourier transformation. **9b/c**: Figures S13-S15.

2D ROESY experiment.[7] The **roesytp.2** pulse program was used with the following acquisition parameters. F2 and F1 sweep widths, 7184 Hz. F2 and F1 digital resolution, 3.5 Hz/pt. 256 FIDs recorded, each consisting of 16 scans and 2048 data points (AQ = 0.142 s). The 800 ms spin lock consisted of 5404 cycles of phase-shifted pairs of 74 μs 180° pulses. A recycle delay of (D1) of 2.0 s was employed. Processing parameters: $\pi/2$ shifted sine^2 (QSINE, SSB=2) apodization was applied in both dimensions prior to the Fourier transformation. **9b/c**: Figures S16-18.

Representative 2D NOESY/EXSY experiment.[8] The **noesytp** pulse program was used with the following acquisition parameters. F2 and F1 sweep widths, 2913 Hz. F2 and F1 digital resolution, 2.8 Hz/pt. 256 FIDs recorded, each consisting of 8 scans and 1024 data points (AQ = 0.176 s). A mixing time of 800 ms was set as a simple delay. A recycle delay of (D1) of 2.0 s was employed. Processing parameters: $\pi/2$ shifted sine^2 (QSINE, SSB=2) apodization was applied in both dimensions prior to the Fourier transformation. **9b/c**: Figures S19-S24.

Gradient-enhanced 2D ^{1}H-^{13}C HMQC experiment.[9] The **inv4gp** pulse program was used with the following acquisition parameters. F2 sweep width, 7184 Hz, F1 sweep width, 32,895 Hz. F2 digital resolution, 7.01 Hz/pt, F1 digital resolution, 257 Hz/pt. 128 FIDs recorded, each consisting of 16 scans and 1024 data points (AQ = 0.071 s). The D2 delay was set to 3.57 ms (1/2J = 140 Hz). A recycle delay (D1) of 3.0 s was employed. Processing parameters: Zero-filling was applied once (SI = 2048) in F2 to achieve a digital resolution of 3.5 Hz/pt and eight times (SI = 1024) in F1 to achieve a digital resolution of 32 Hz/pt. Exponential (EM, LB = 5) apodization was applied in the F2 dimension and $\pi/3$ shifted sine^2 (QSINE, SSB=3) apodization was applied in the F1 dimension prior to the Fourier transformation. .**9b/c**: Figures S25-S26.

2D ^{1}H-^{13}C HMQC experiment without F2 decoupling.[10] The **inv4nd** pulse program was used with the following acquisition parameters. F2 sweep width, 4789 Hz, F1 sweep width, 17605 Hz. F2 digital resolution, 4.68 Hz/pt, F1 digital resolution, 137.5 Hz/pt. 128 FIDs recorded, each consisting of 64 scans and 1024 data points (AQ = 0.107 s). The D2 delay was set to 3.57 ms (1/2J = 140 Hz). A recycle delay (D1) of 2.2 s was employed. Processing parameters: Zero-filling was applied eight times (SI = 1024) in F1 to achieve a digital resolution of 17.2 Hz/pt. Processing parameters: $\pi/2$ shifted sine^2 (QSINE, SSB=2) apodization was applied in both dimensions prior to the Fourier transformation. **9b/c**: Figure S27. **8**: Figure S37.

---

[4] Braun, S.; Kalinowski, H. –O.; Berger, S. *150 and More NMR Experiments: A Practical Course*; Wiley-VCH: Weinheim, 1998.
[5] Hurd, R. *J. Magn. Reson.* **1990**, *87*, 422.
[6] Bax, A.; Freeman, R. *J. Magn. Reson.* **1981**, *44*, 542.
[7] Hwang, T. –L.; Shaka, A. J. *J. Am. Chem. Soc.* **1992**, *114*, 3157.
[8] Jeener, J.; Meier, B. H.; Bachmann, P.; Ernst, R. R. *J. Chem. Phys.* **1979**, *71*, 4546.
[9] Hurd, R. E.; John, B. K. *J. Magn. Reson.* **1991**, *91*, 648.
[10] Bax, A.; Griffey, R. H.; Hawkins, B. L. *J. Magn. Reson.* **1983**, *55*, 301.

Table S6. Tabulation of ^{1}H-detected NMR data of Ru-olefin complex **9b/9c** in CD_2Cl_2.*

assignment	proton (ppm)	integral	multiplicity (Hz)	COSY	COSYLR	NOESY	2D-exchange	HMQC	1J(C13/H)
H-22	16.34	0.75	t, J = 1.1	3.44	7.38, 3.44	2.55, 6.62	16.17	300.300	
H-22	16.17	1	t, J = 1.0	3.51	7.38, 3.51	2.91, 6.40	16.34	296.900	
	7.50-7.41	1.75	m	7.095	6.428				
	7.39-7.32	1.75	m						
H-17	7.17	1	br s		6.41, 2.91, 2.37, 1.20	2.91, 2.38	6.85		
	7.11	1	br s						
	7.10-7.00	4	m		2.72				
H-17	6.85	0.75	br s		5.99, 2.55, 2.12, 1.20	2.55, 2.12	7.17	129.395	
H-24	6.62	0.75	d, J = 7.8	7.09	7.43	16.34, 7.09	6.4	121.616	
H-15	6.41	1	br s		7.17, 2.91, 2.39, 1.20	2.38, 1.2	5.99	130.336	
H-24	6.4	1	d, J = 7.8	7.101		16.17, 7.07	6.62	121.565	
H-29	6.13	1	dd, J = 12.5, 9.9	3.51, 3.37		7.35, 3.37, 3.51	5.54	107.800	163 Hz
H-15	5.99	0.75	br s		6.85, 2.55, 2.12, 1.90	2.12, 1.9	6.62	129.068	
H-29	5.54	0.75	dd, J = 9.2, 12.6	3.59, 3.44		7.35, 3.44, 3.59, 2.43, 1.90	6.13	92.200	160 Hz
	4.23	1	app quart, J = 10.2	4.01, 3.77		3.90, 2.787		52.682	
	4.19-3.92	4.5	m						
	3.84	1	app quart, J = 11.2			4.01, 1.195		52.219	
H-30(cis 28)	3.59	0.75	dd, J = 12.6, 1.6	5.54		3.44, 5.54	3.37	86.700	166 Hz
H-30(trans 28)	3.51	1	dt, J = 9.9, 1.1	6.13		6.13, 3.37, 2.36	3.44	69.600	160 Hz
H-30(trans 28)	3.44	0.75	dt, J = 9.2, 1.5	5.54		5.54, 3.59, 2.43	3.51	86.700	159 Hz
H-30(cis 28)	3.37	1	dd, J = 12.5, 1.0	6.13		6.13, 3.51, 2.36. 1.20	3.59	69.600	160 Hz
Me-21	2.91	3	s		6.41, 7.17, 1.20	7.17, 4.01, 16.17	2.55, 2.36	19.713	
Me-12	2.75	3	s			7.104	1.2		
Me-12	2.72	2.1	s		7.05	7.13			
Me-21	2.55	2.1	s		5.99, 6.85, 1.90	16.34, 6.85			
	2.44-2.36	13	m						
Me-20	2.12	2	s		5.99, 6.85, 1.90	5.99, 6.85	2.39		
Me-19	1.9	2	s		5.99, 6.85, 2.55, 2.12	5.54, 5.99	1.2		
Me-19	1.2	3	s		2.40, 2.91, 6.41, 7.17	6.41, 3.37	1.90, 2.75		

*Assignments colored in red correspond to the minor isomer (**9b**), those in black to the major isomer (**9c**). Columns for COSY, COSYLR, NOESY, EXSY, and HMQC data list cross-peaks observed for the assigned resonance in that row to a particular ^{1}H or ^{13}C resonance value in ppm.

DU=/disk2, USER=doleary, NAME=do_ct_44, EXPNO=6, PROCNO=1
F1=323.293ppm, F2=-3.651ppm, MI=0.03cm, MAXI=10000.00cm, PC=1.400

#	ADDRESS	FREQUENCY [Hz]	[PPM]	INTENSITY
1	4604.3	30216.305	300.3229	0.08
2	5284.3	29874.982	296.9305	0.12
3	22712.4	21127.234	209.9857	0.07
4	22837.8	21064.326	209.3605	0.13
5	33062.7	15932.086	158.3506	0.26
6	34816.5	15051.789	149.6012	0.12
7	34892.4	15013.684	149.2225	0.21
8	36560.0	14176.657	140.9032	0.13
9	36649.4	14131.794	140.4573	0.22
10	36794.5	14058.965	139.7335	0.12
11	36889.1	14011.470	139.2614	0.27
12	36892.4	14009.834	139.2451	0.25
13	36975.9	13967.902	138.8284	0.14
14	37001.1	13955.243	138.7026	0.24
15	37156.1	13877.482	137.9297	0.15
16	37421.0	13744.479	136.6078	0.27
17	37615.3	13646.979	135.6387	0.23
18	37648.8	13630.183	135.4718	0.18
19	37678.4	13615.305	135.3239	0.13
20	37818.1	13545.170	134.6268	0.10
21	38082.2	13412.638	133.3096	0.18
22	38525.8	13189.959	131.0963	0.21
23	38547.3	13179.176	130.9892	0.10
24	38559.5	13173.047	130.9282	0.35
25	38621.1	13142.133	130.6210	0.37
26	38650.9	13127.169	130.4722	0.35
27	38702.1	13101.457	130.2167	0.22
28	38754.5	13075.198	129.9557	0.37
29	38829.2	13037.701	129.5830	0.22
30	38840.0	13032.264	129.5290	0.37
31	38873.9	13015.220	129.3596	0.22
32	38917.2	12993.488	129.1436	0.20
33	39008.1	12947.904	128.6905	3.03
34	39346.5	12778.025	127.0021	0.34
35	39397.3	12752.537	126.7487	0.35
36	39490.8	12705.611	126.2823	0.36
37	40396.2	12251.138	121.7653	0.22
38	40492.2	12202.978	121.2866	0.37
39	43199.2	10844.217	107.7818	0.32
40	46325.6	9275.003	92.1852	0.18
41	47432.0	8719.629	86.6653	0.14
42	50849.4	7004.314	69.6166	0.24
43	53894.1	5476.076	54.4273	4.16
44	53948.3	5448.868	54.1568	8.39
45	54002.6	5421.646	53.8863	12.50
46	54056.8	5394.425	53.6157	8.39
47	54111.0	5367.219	53.3453	4.17
48	54294.1	5275.324	52.4320	0.26
49	54303.8	5270.465	52.3837	0.17
50	54356.7	5243.921	52.1199	0.27
51	54455.9	5194.099	51.6247	0.15
52	60544.6	2137.988	21.2497	0.31
53	60563.1	2128.697	21.1573	0.25
54	60613.8	2103.267	20.9046	0.19
55	60622.3	2098.969	20.8619	0.27
56	60683.7	2068.159	20.5556	0.15

Table S7. ^{13}C chemical shifts of Ru-olefin complex **9b/c** in CD_2Cl_2.

57	60855.8	1981.769	19.6970	0.26
58	60883.0	1968.115	19.5613	0.15
59	60941.3	1938.852	19.2704	0.27
60	61131.9	1843.206	18.3198	0.16
61	61204.9	1806.583	17.9558	0.18
62	61260.9	1778.474	17.6764	0.32

Table S7. ^{13}C chemical shifts of Ru-olefin complex **9b/c** in CD_2Cl_2 (cont.)

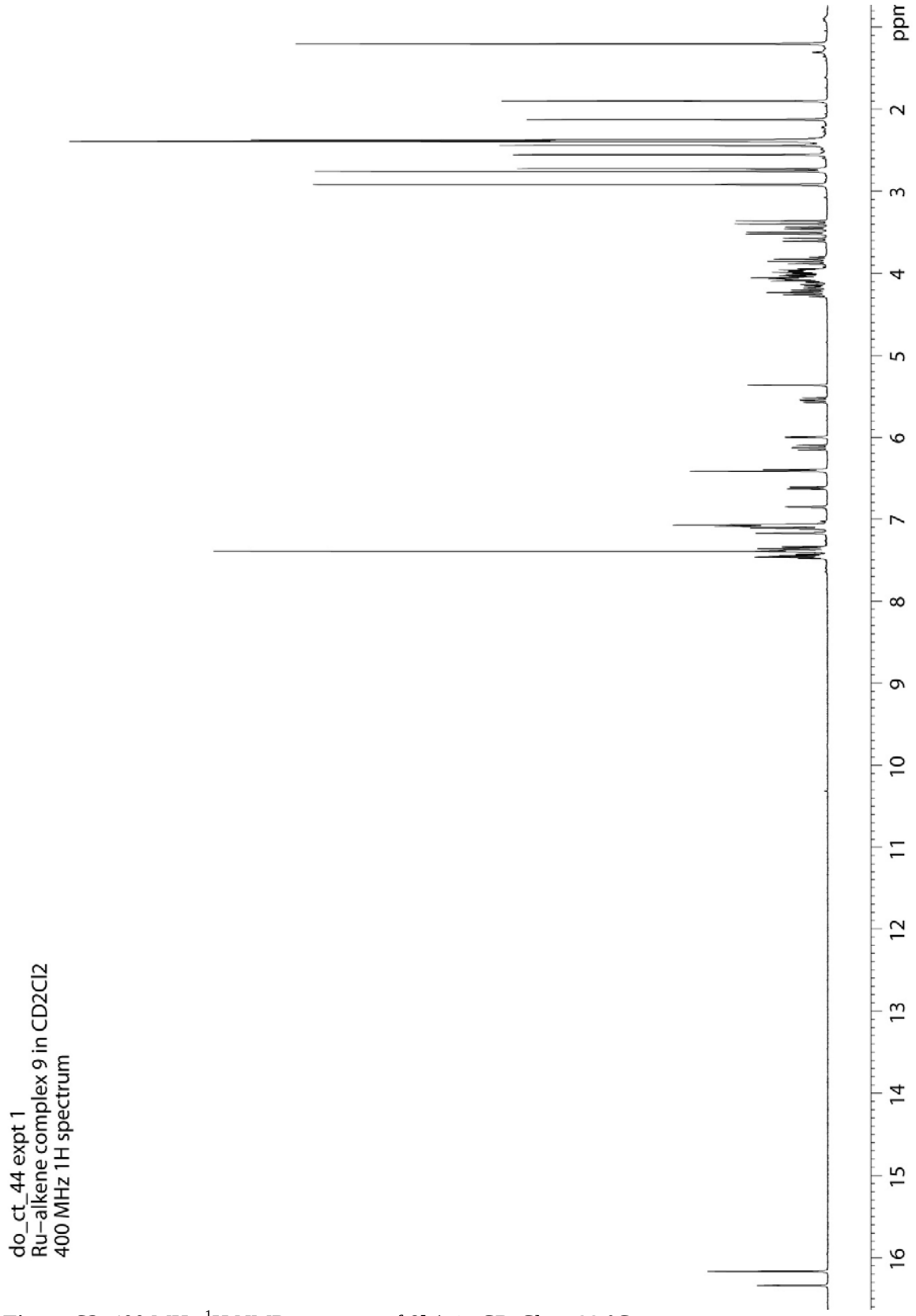

Figure S2. 400 MHz ^{1}H NMR spectrum of **9b/c** in CD_2Cl_2 at 22 °C.

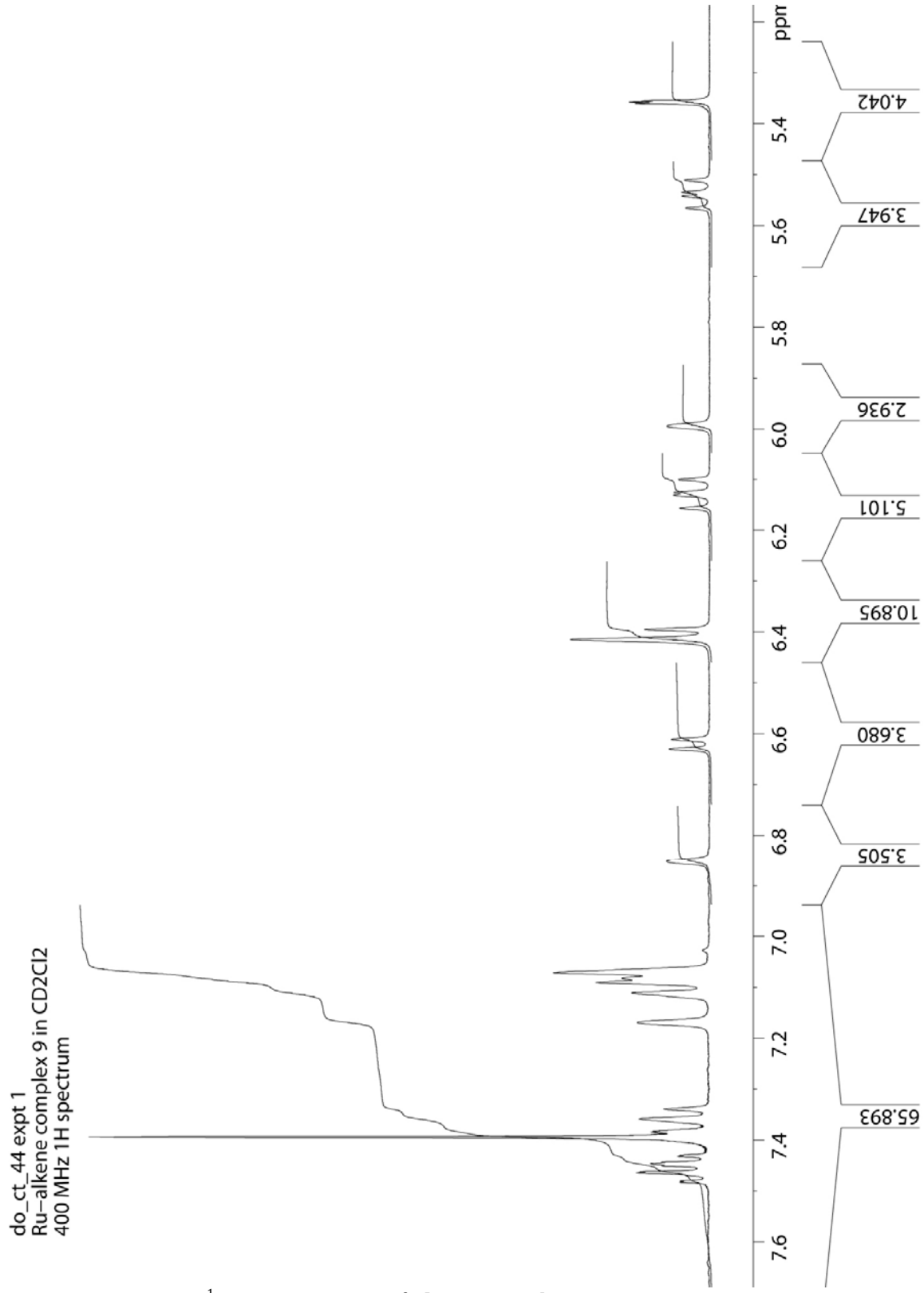

Figure S3. 400 MHz ^{1}H NMR spectrum of **9b/c** in CD_2Cl_2 at 22 °C.

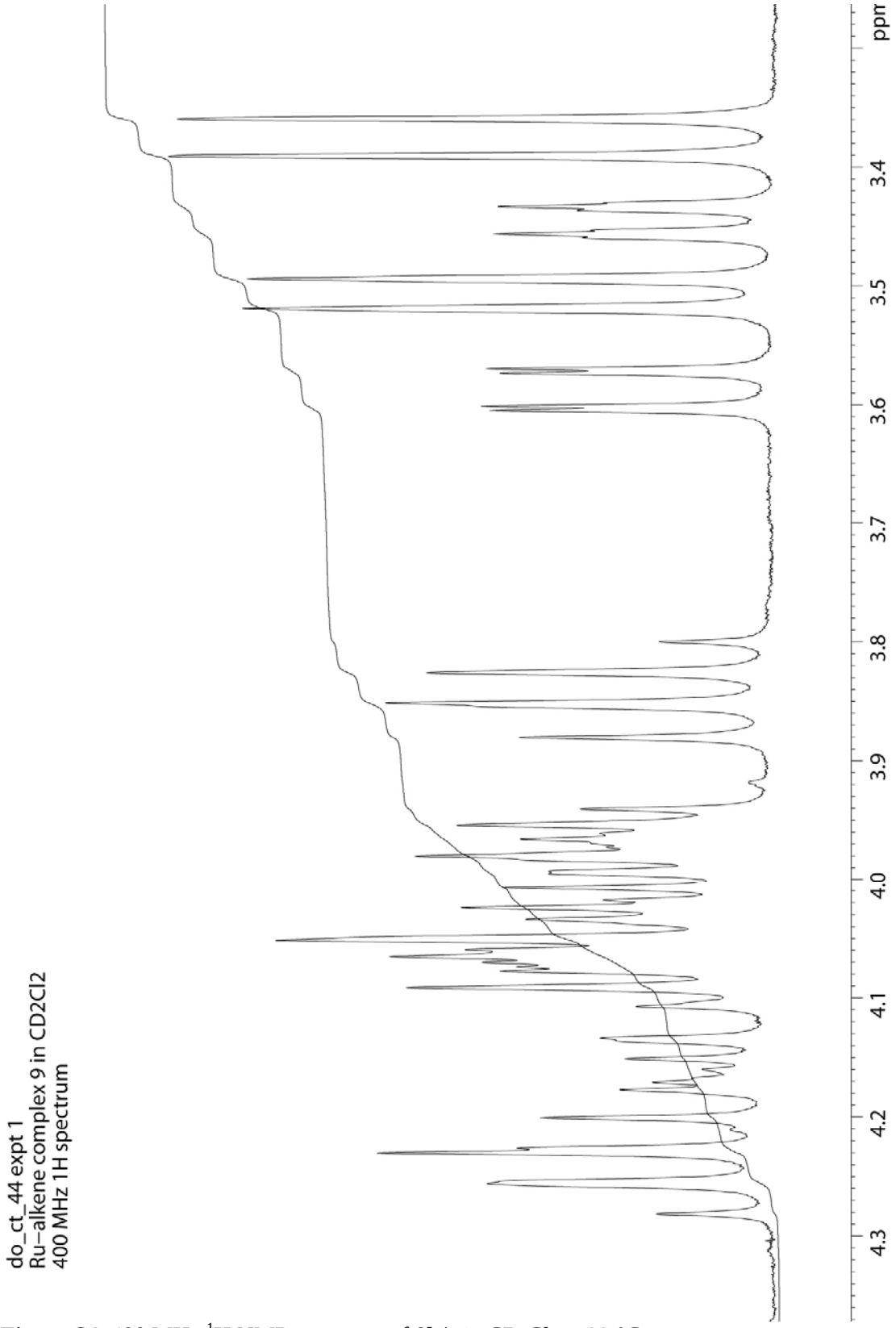

Figure S4. 400 MHz ^{1}H NMR spectrum of **9b/c** in CD_2Cl_2 at 22 °C.

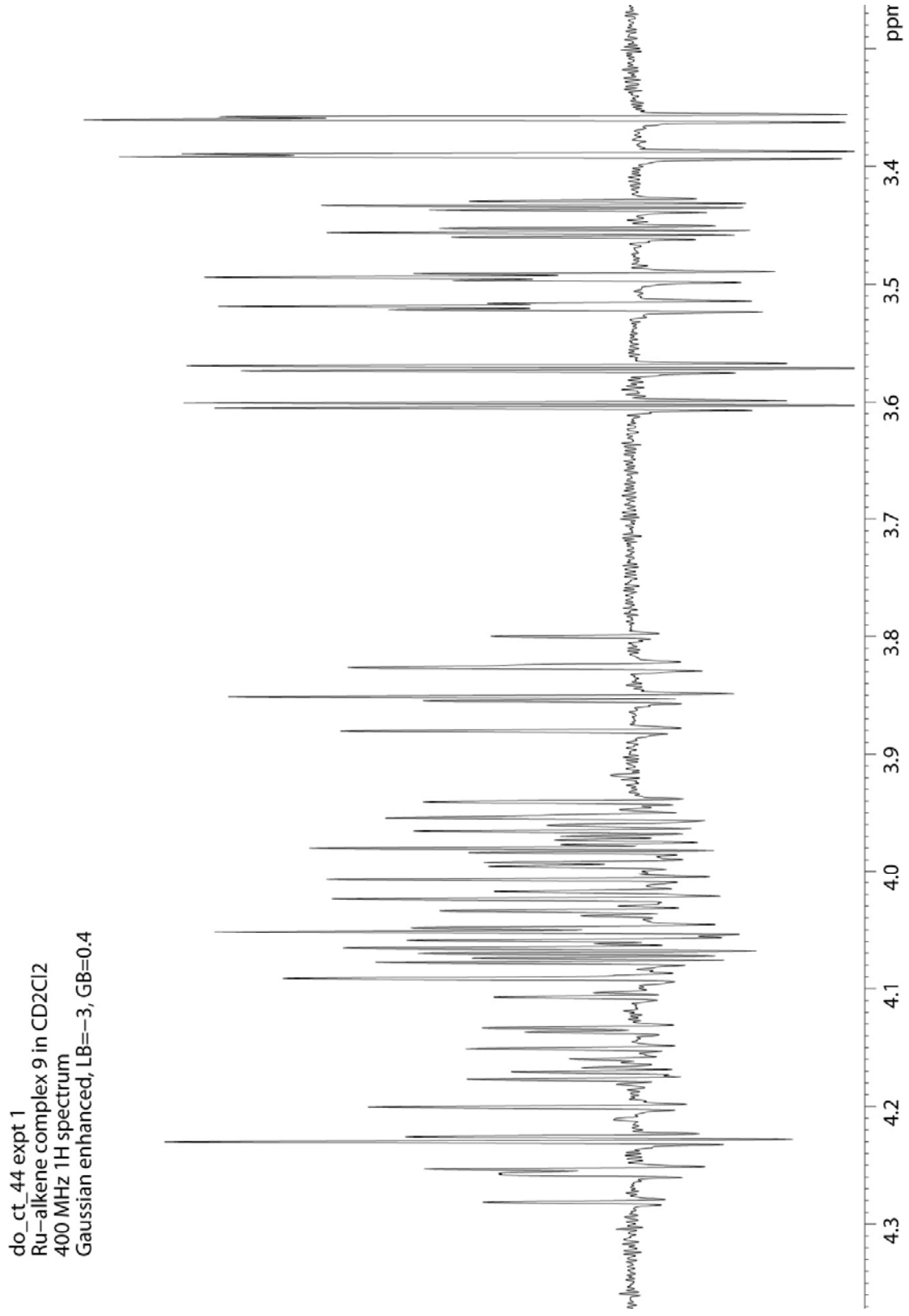

Figure S5. 400 MHz ^{1}H NMR spectrum of **9b/c** in CD_2Cl_2 at 22 °C.

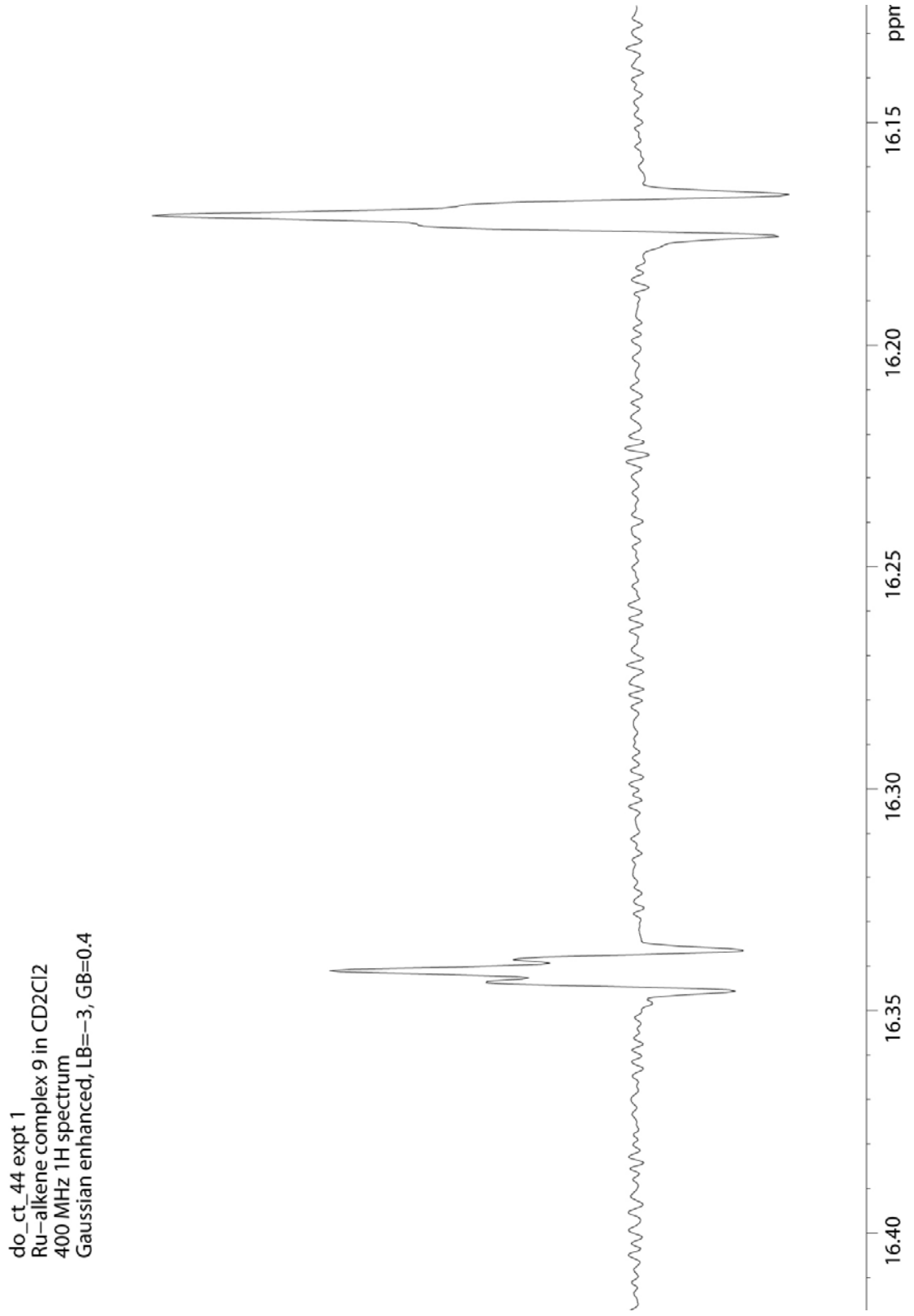

Figure S6. 400 MHz ^{1}H NMR spectrum of **9b/c** in CD_2Cl_2 at 22 °C.

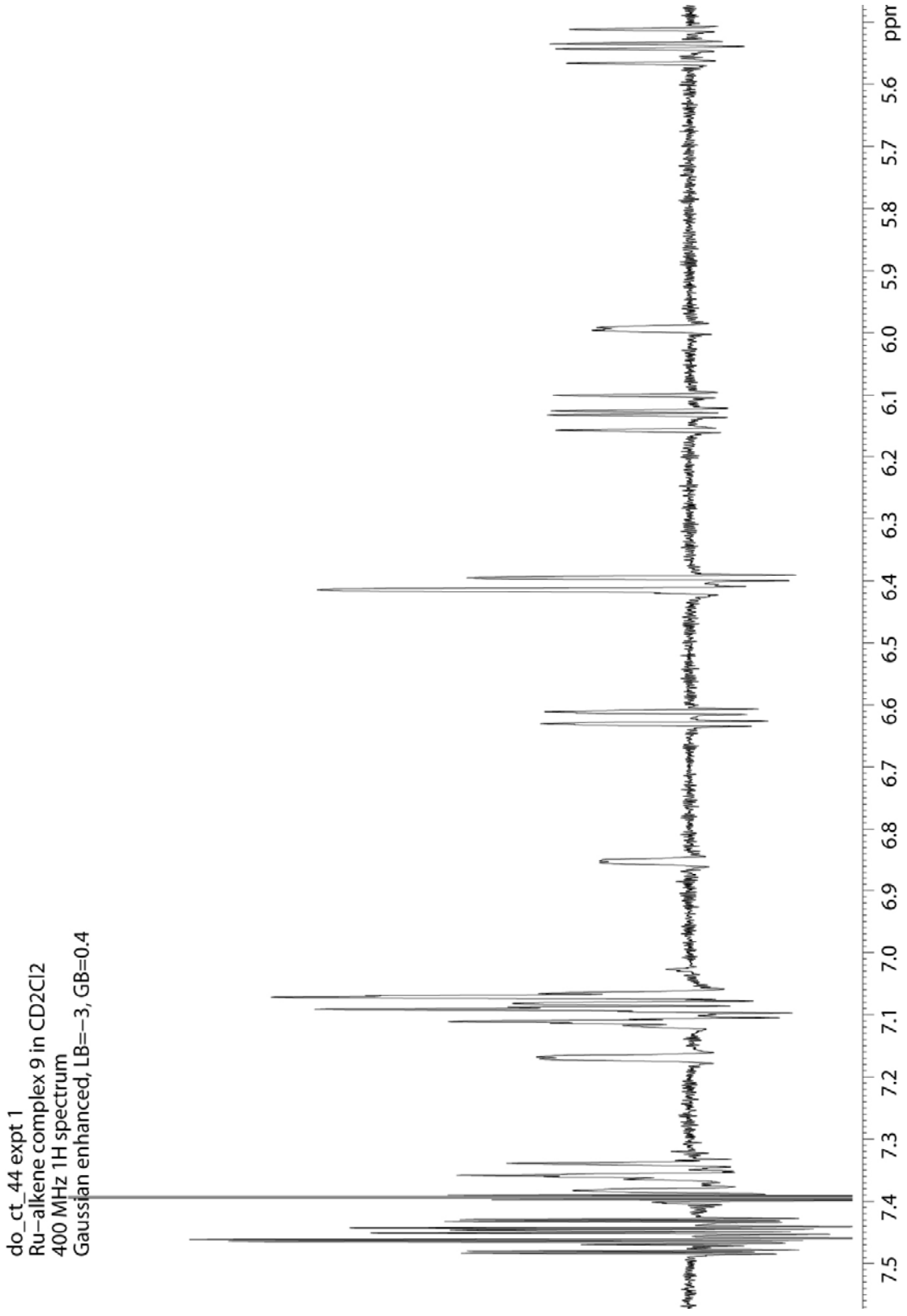

Figure S7. 400 MHz ^{1}H NMR spectrum of **9b/c** in CD_2Cl_2 at 22 °C.

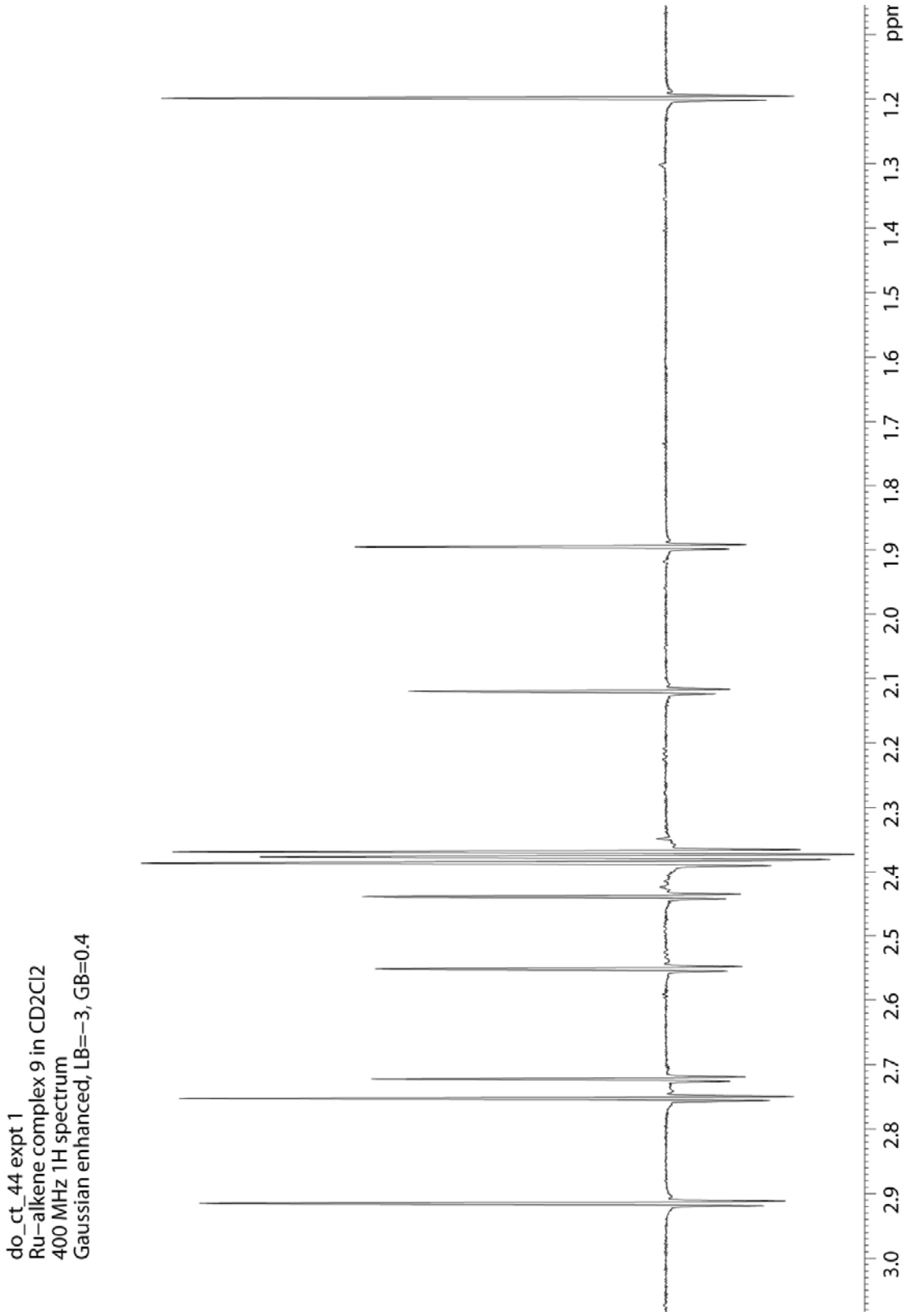

Figure S8. 400 MHz ^{1}H NMR spectrum of **9b/c** in CD_2Cl_2 at 22 °C.

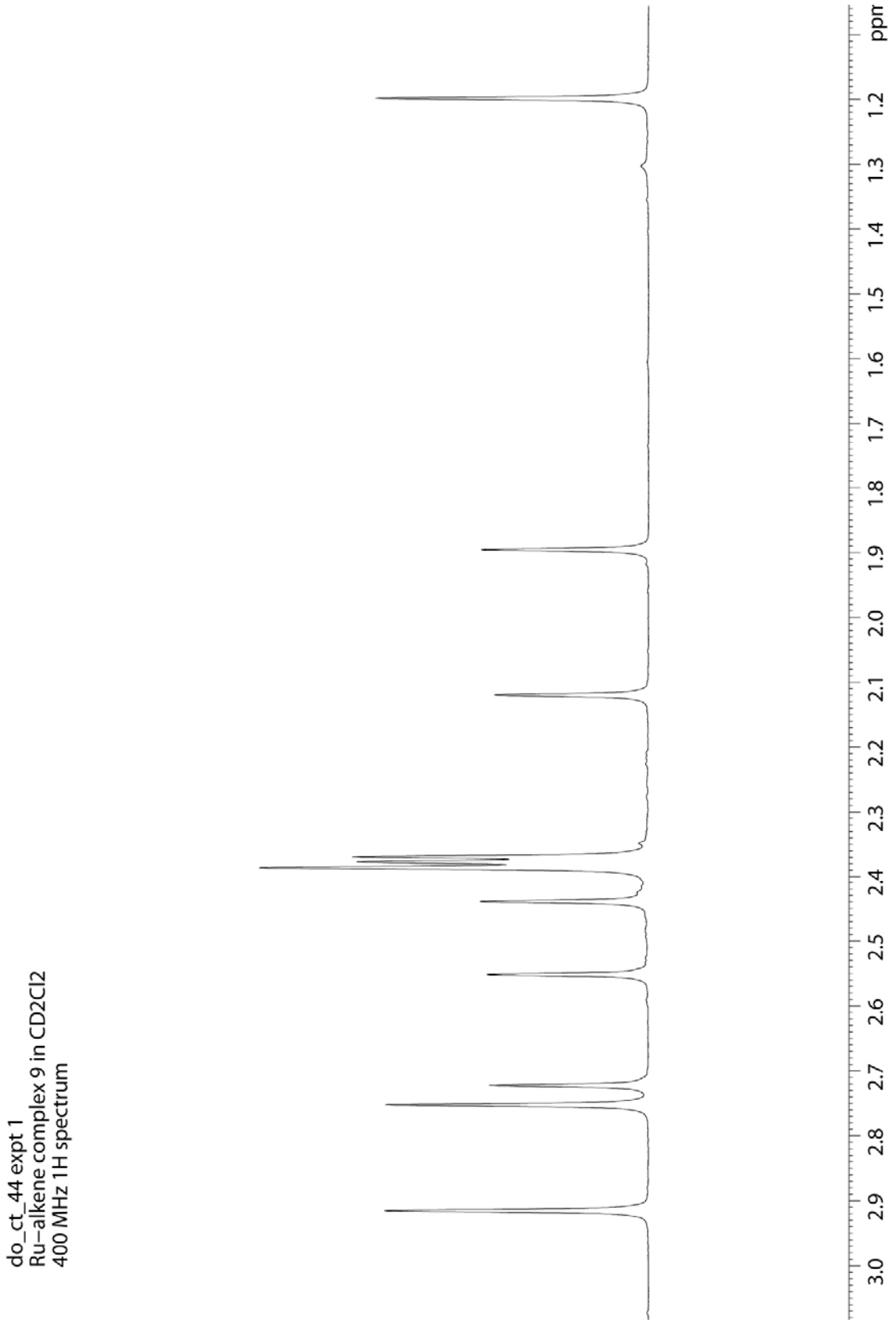

Figure S9. 400 MHz ^{1}H NMR spectrum of **9b/c** in CD_2Cl_2 at 22 °C.

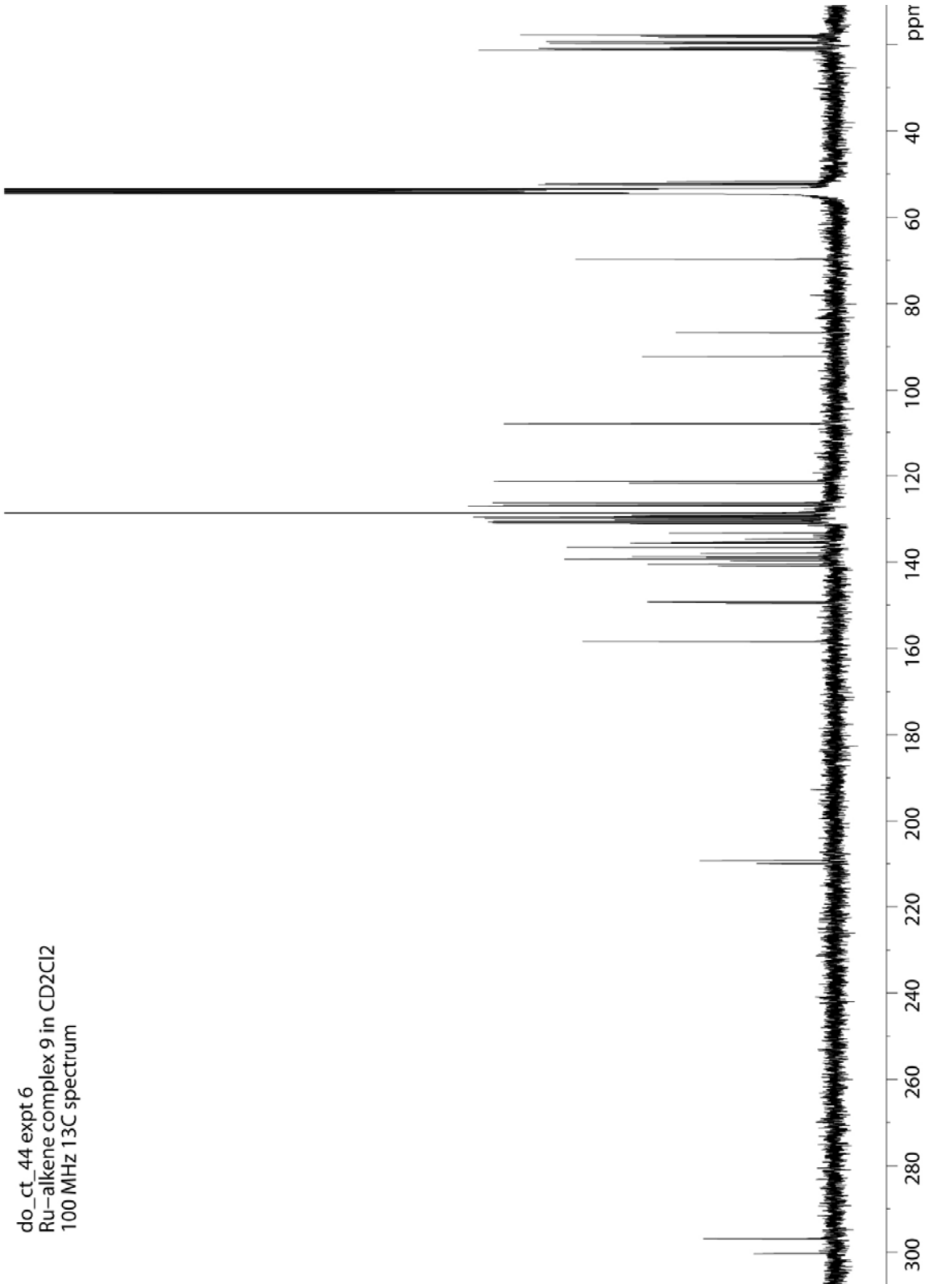

Figure S10. 100 MHz ^{13}C NMR spectrum of **9b/c** in CD_2Cl_2 at 22 °C.

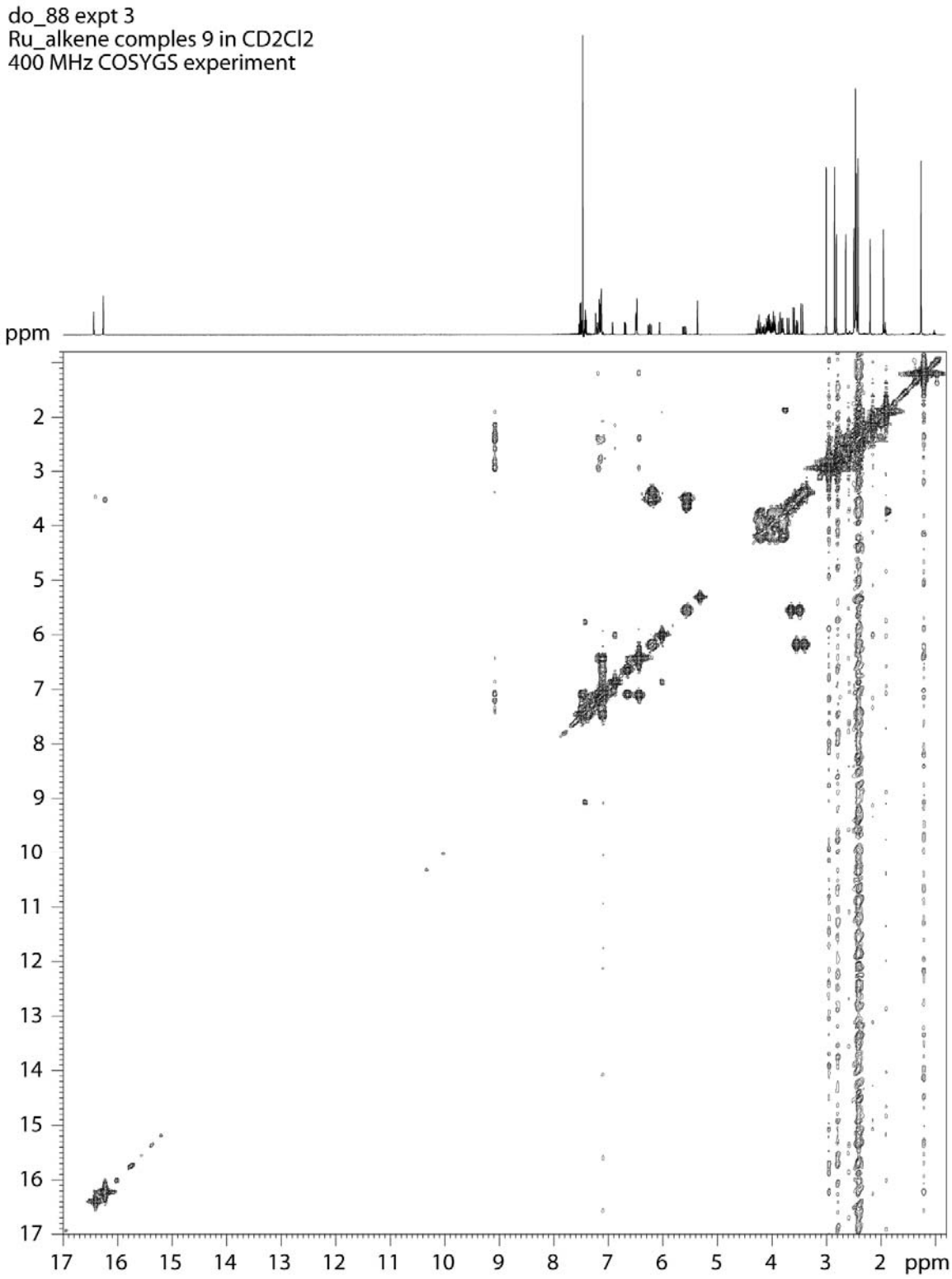

Figure S11. 400 MHz ^{1}H-^{1}H COSY spectrum of **9b/c** in CD_2Cl_2 at 22 °C.

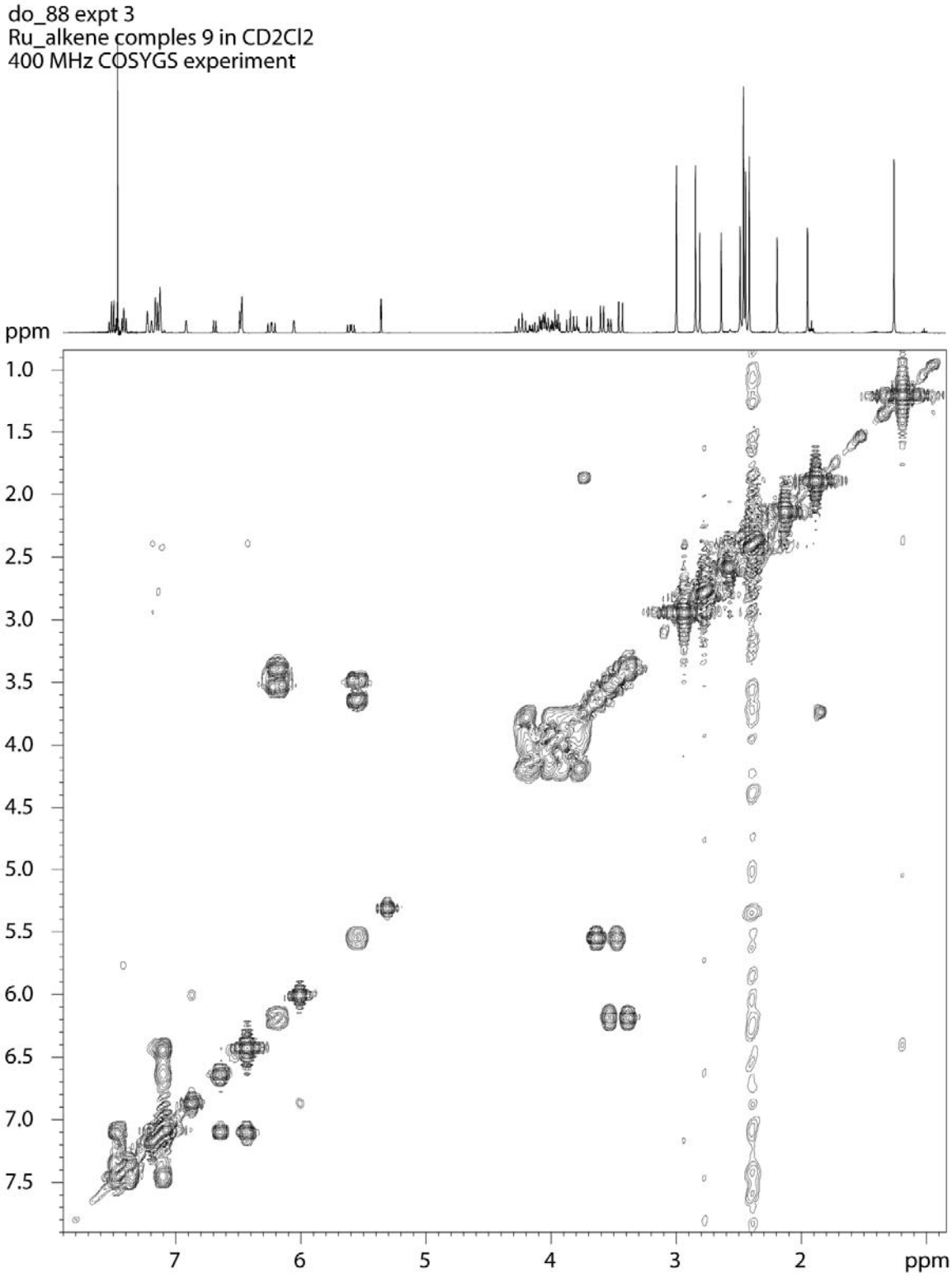

Figure S12. 400 MHz ^{1}H-^{1}H COSY spectrum of **9b/c** in CD_2Cl_2 at 22 °C.

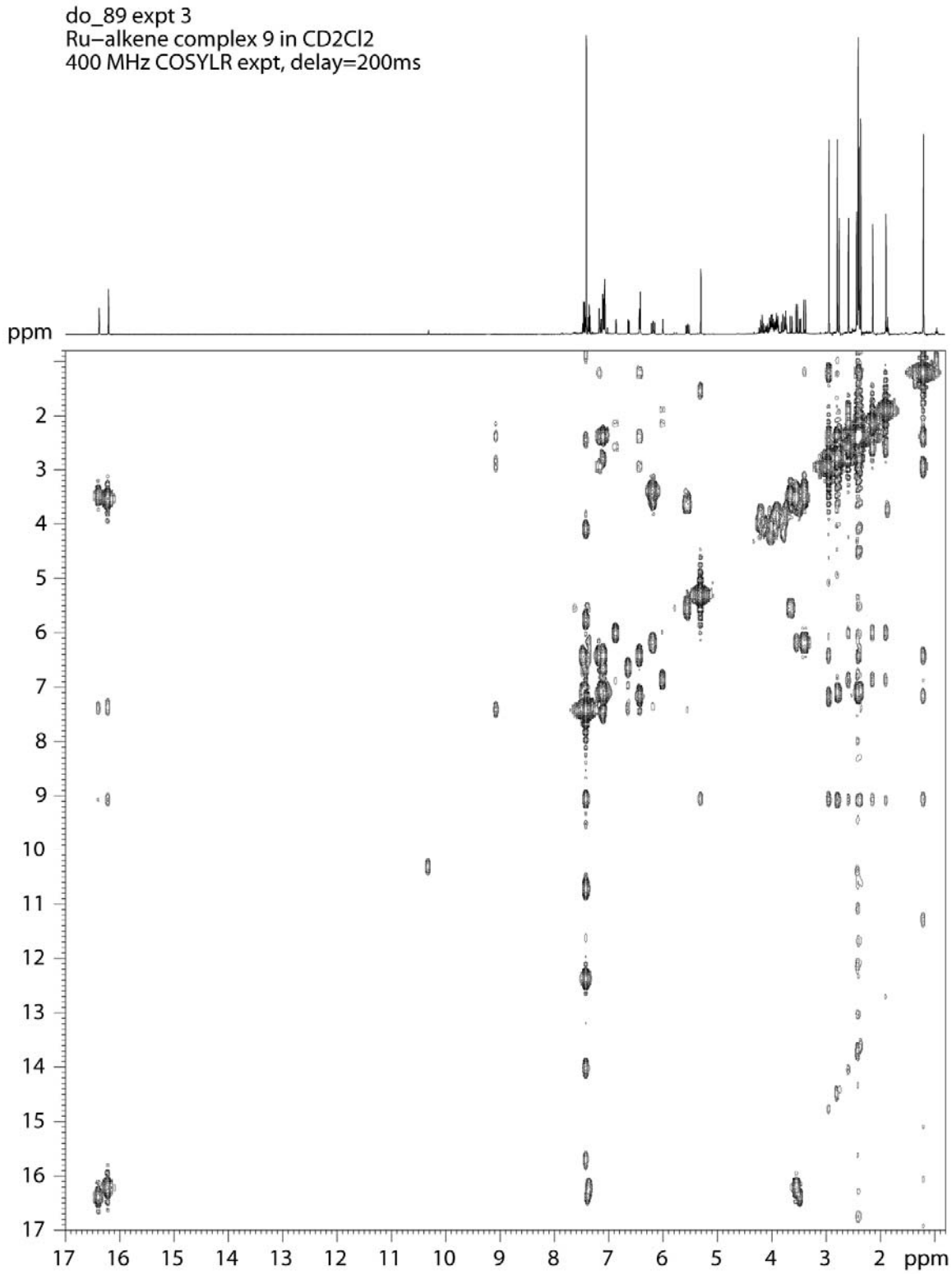

Figure S13. 400 MHz ^{1}H-^{1}H COSYLR spectrum of **9b/c** in CD_2Cl_2 at 22 °C.

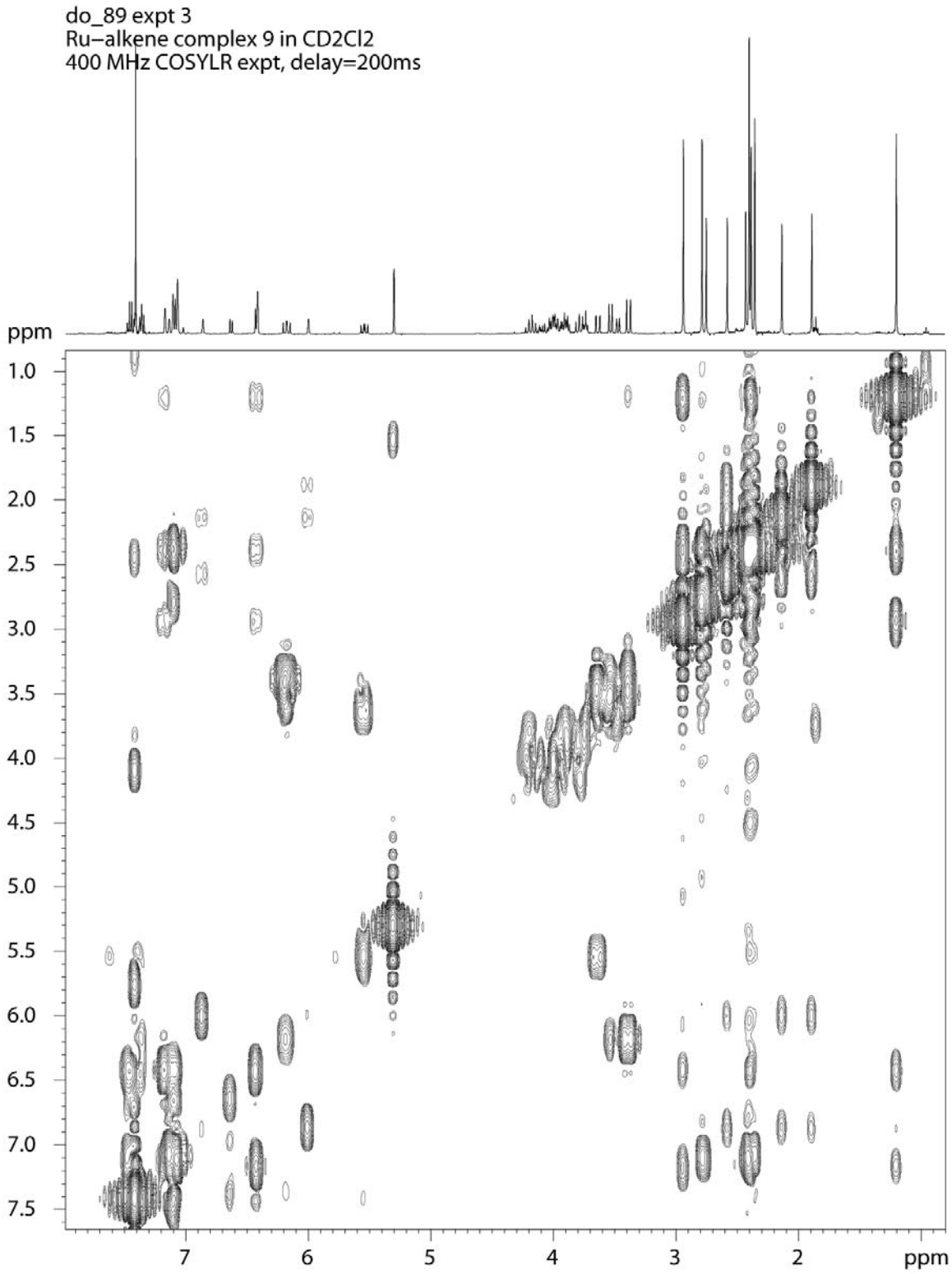

Figure S14. 400 MHz ^{1}H-^{1}H COSYLR spectrum of **9b/c** in CD_2Cl_2 at 22 °C.

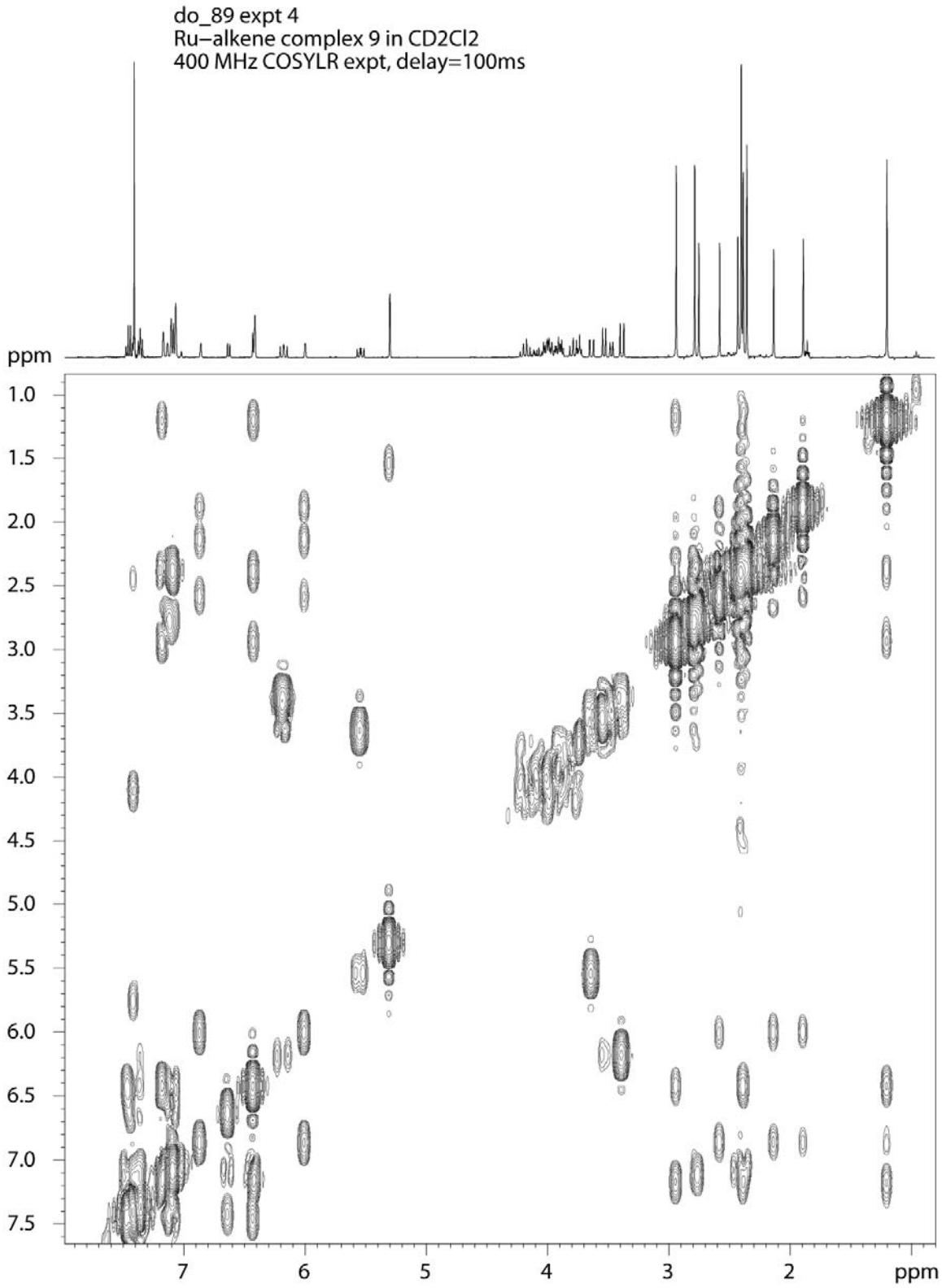

Figure S15. 400 MHz ^{1}H-^{1}H COSYLR spectrum of **9b/c** in CD_2Cl_2 at 22 °C.

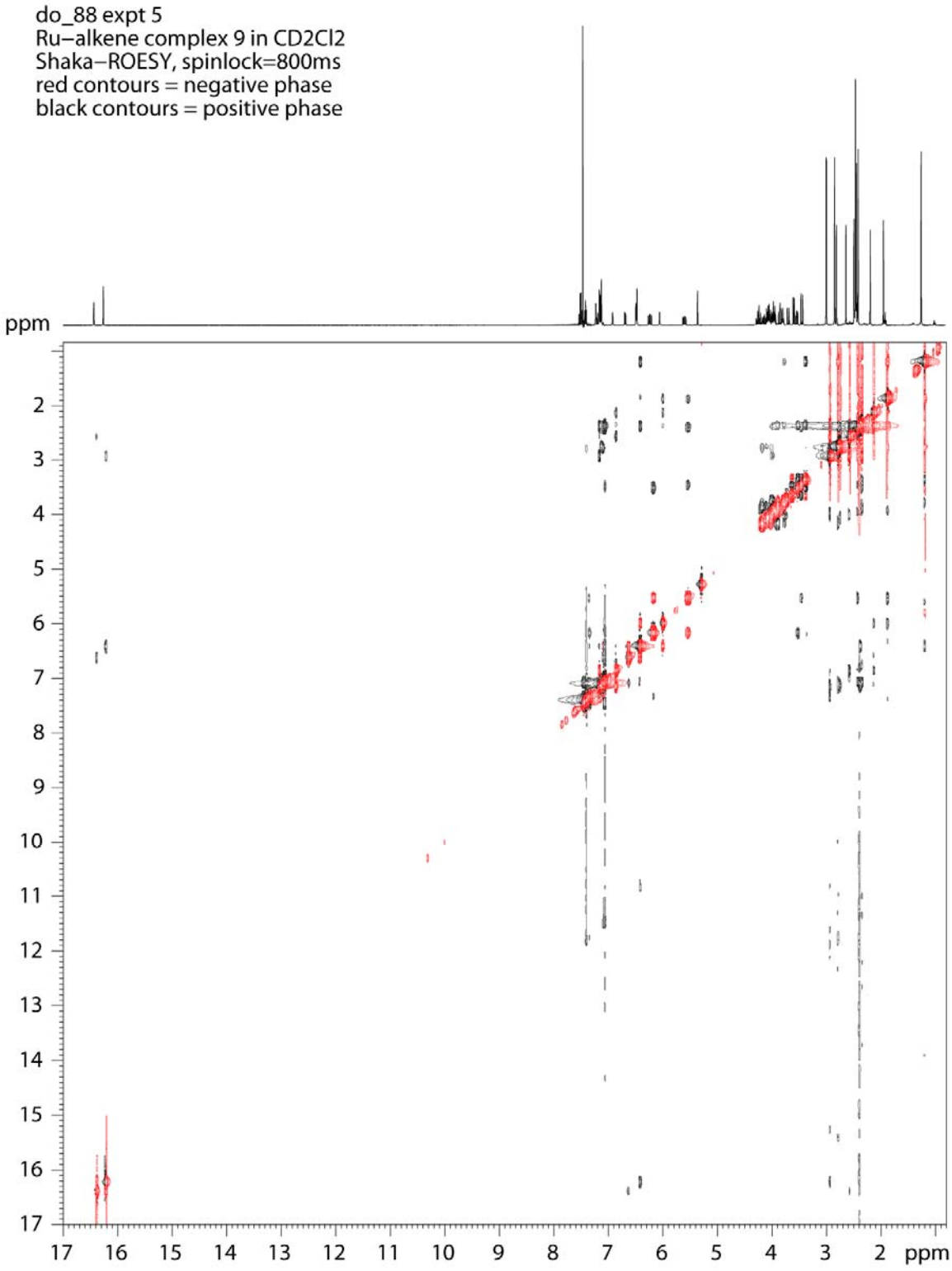

Figure S16. 400 MHz ^{1}H-^{1}H ROESY spectrum of **9b/c** in CD_2Cl_2 at 22 °C. Overhauser-derived crosspeaks are colored black, diagonal and exchange-derived crosspeaks are colored red.

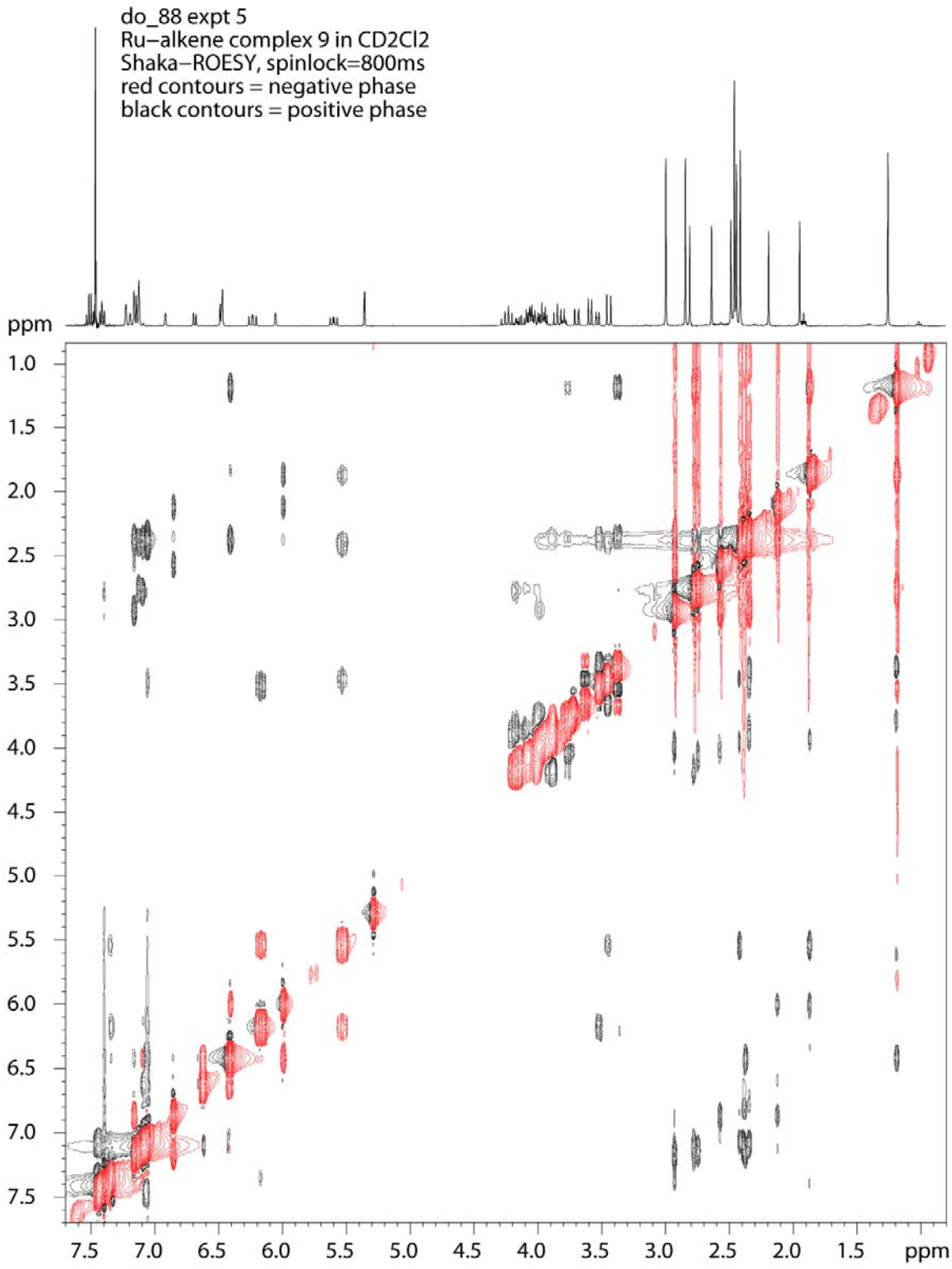

Figure S17. 400 MHz ^{1}H-^{1}H ROESY spectrum of **9b/c** in CD_2Cl_2 at 22 °C. Overhauser-derived crosspeaks are colored black, diagonal and exchange-derived crosspeaks are colored red.

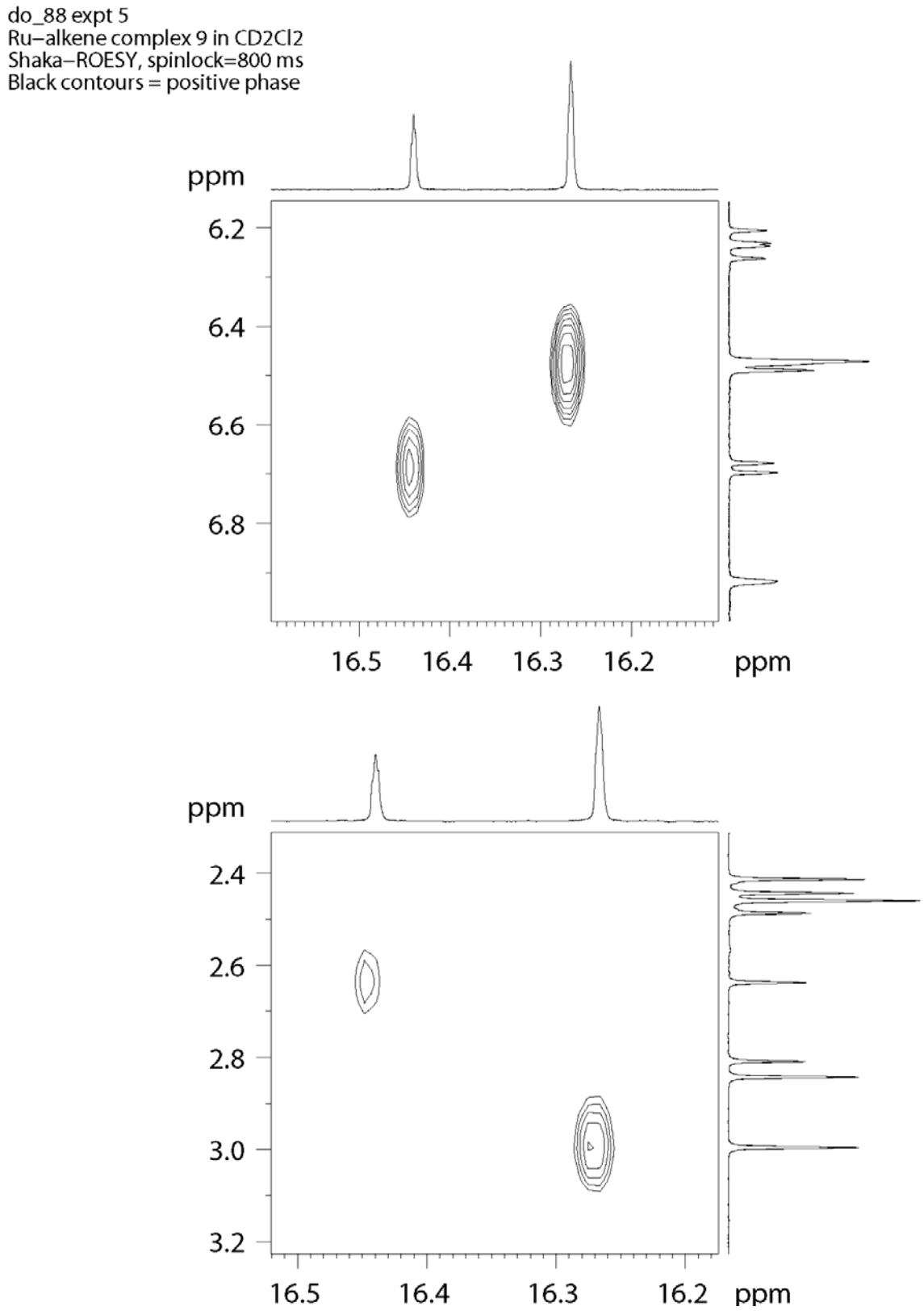

Figure S18. 400 MHz ^{1}H-^{1}H ROESY spectrum of **9b/c** in CD_2Cl_2 at 22 °C. Overhauser-derived crosspeaks are colored black, diagonal and exchange-derived crosspeaks are colored red.

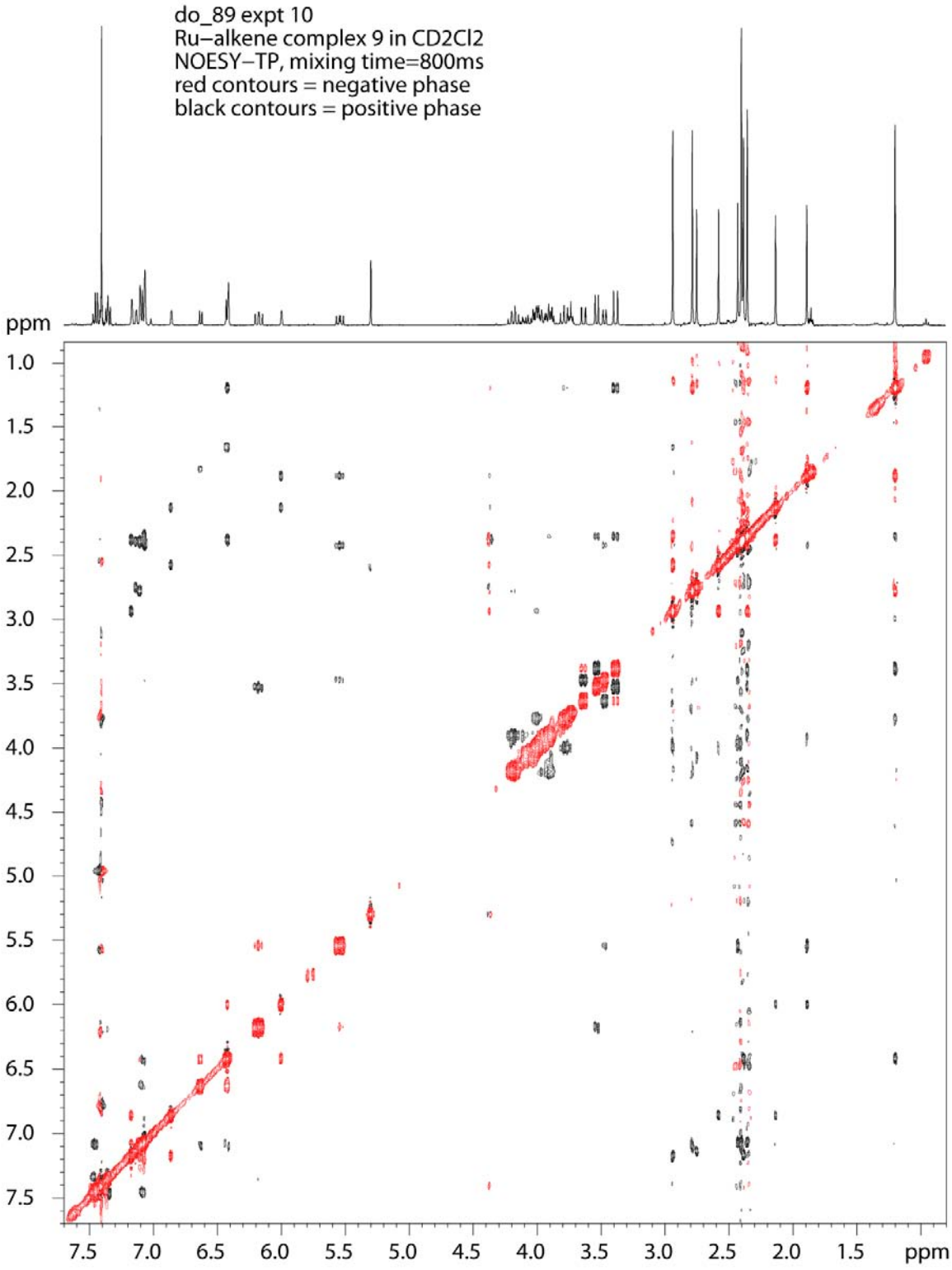

Figure S19. 400 MHz ^{1}H-^{1}H NOESY/EXSY spectrum of **9b/c** in CD_2Cl_2 at 22 °C. Overhauser-derived crosspeaks are colored black, diagonal and exchange-derived crosspeaks are colored red.

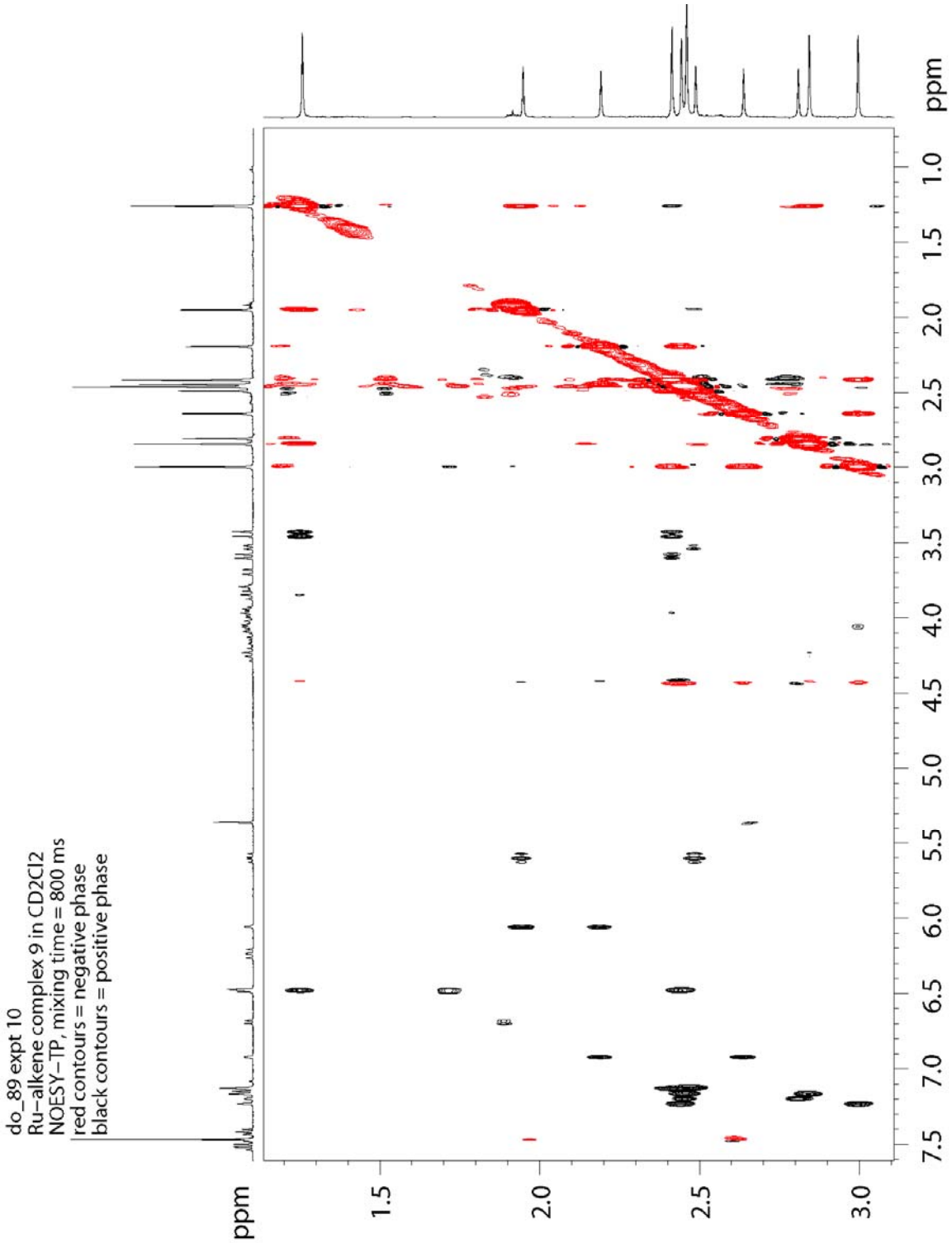

Figure S20. 400 MHz ^{1}H-^{1}H NOESY/EXSY spectrum of **9b/c** in CD_2Cl_2 at 22 °C. Overhauser-derived crosspeaks are colored black, diagonal and exchange-derived crosspeaks are colored red.

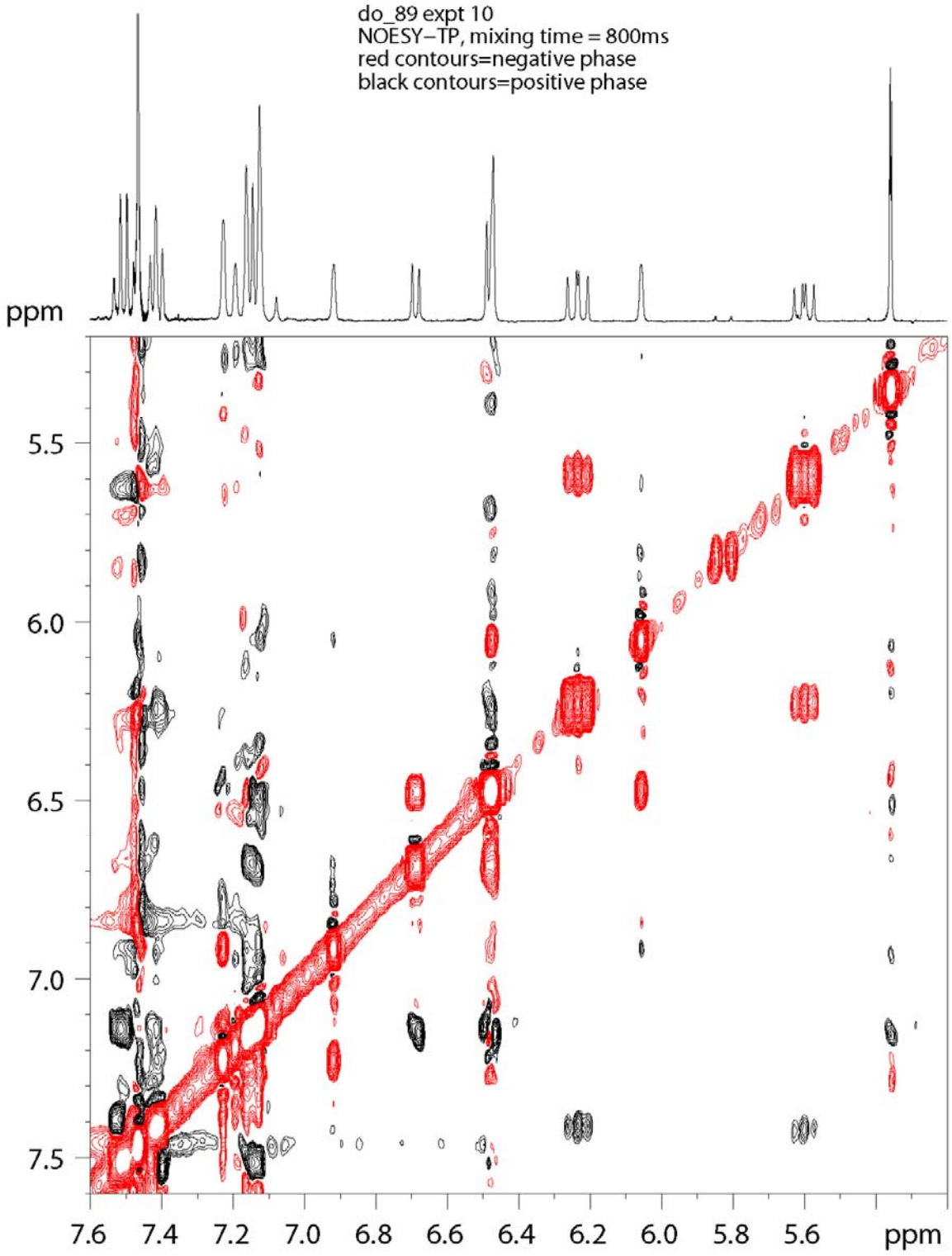

Figure S21. 400 MHz ^{1}H-^{1}H NOESY/EXSY spectrum of **9b/c** in CD_2Cl_2 at 22 °C. Overhauser-derived crosspeaks are colored black, diagonal and exchange-derived crosspeaks are colored red.

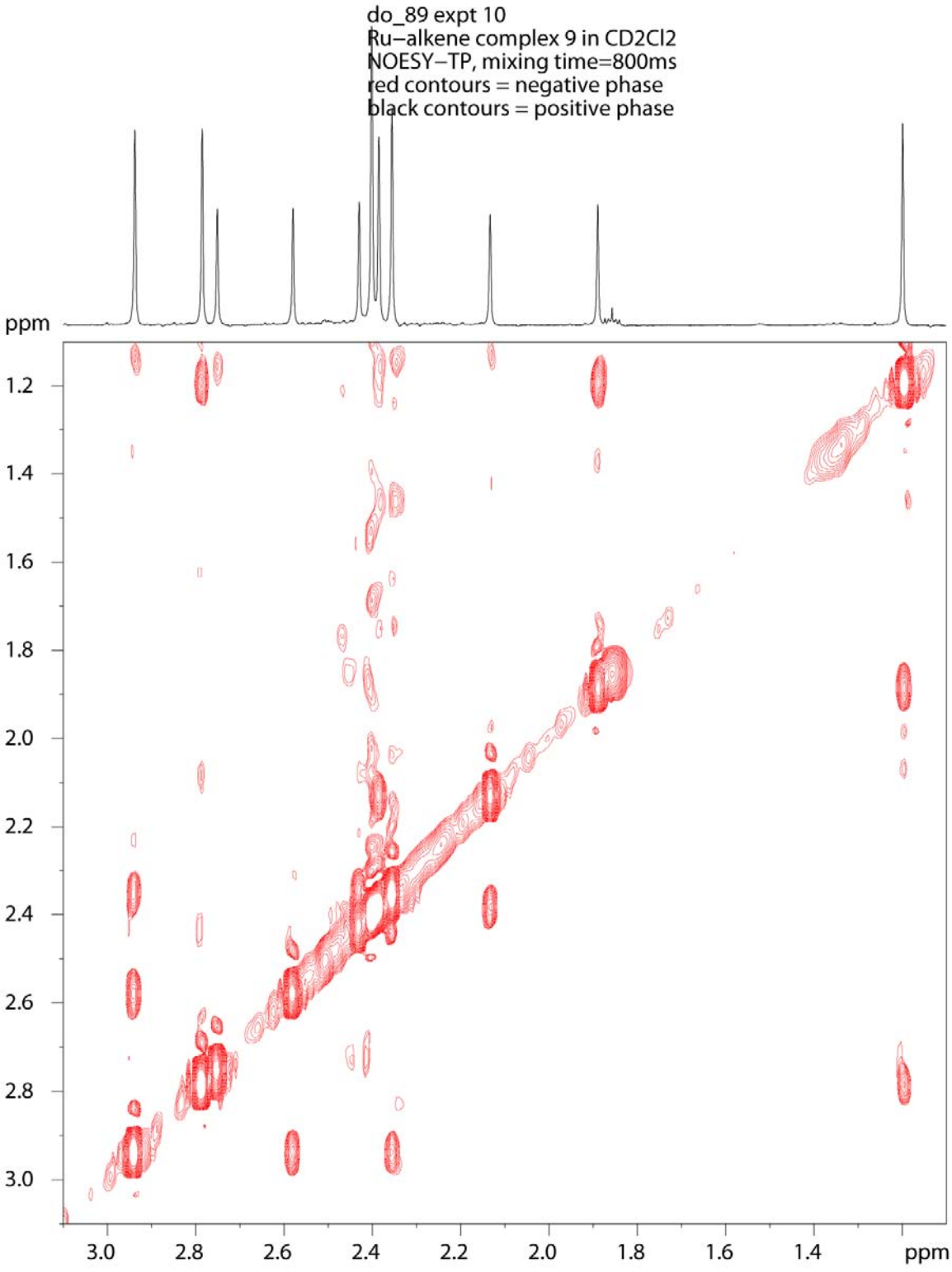

Figure S22. 400 MHz ^{1}H-^{1}H NOESY/EXSY spectrum of **9b/c** in CD_2Cl_2 at 22 °C. Overhauser-derived crosspeaks are colored black, diagonal and exchange-derived crosspeaks are colored red.

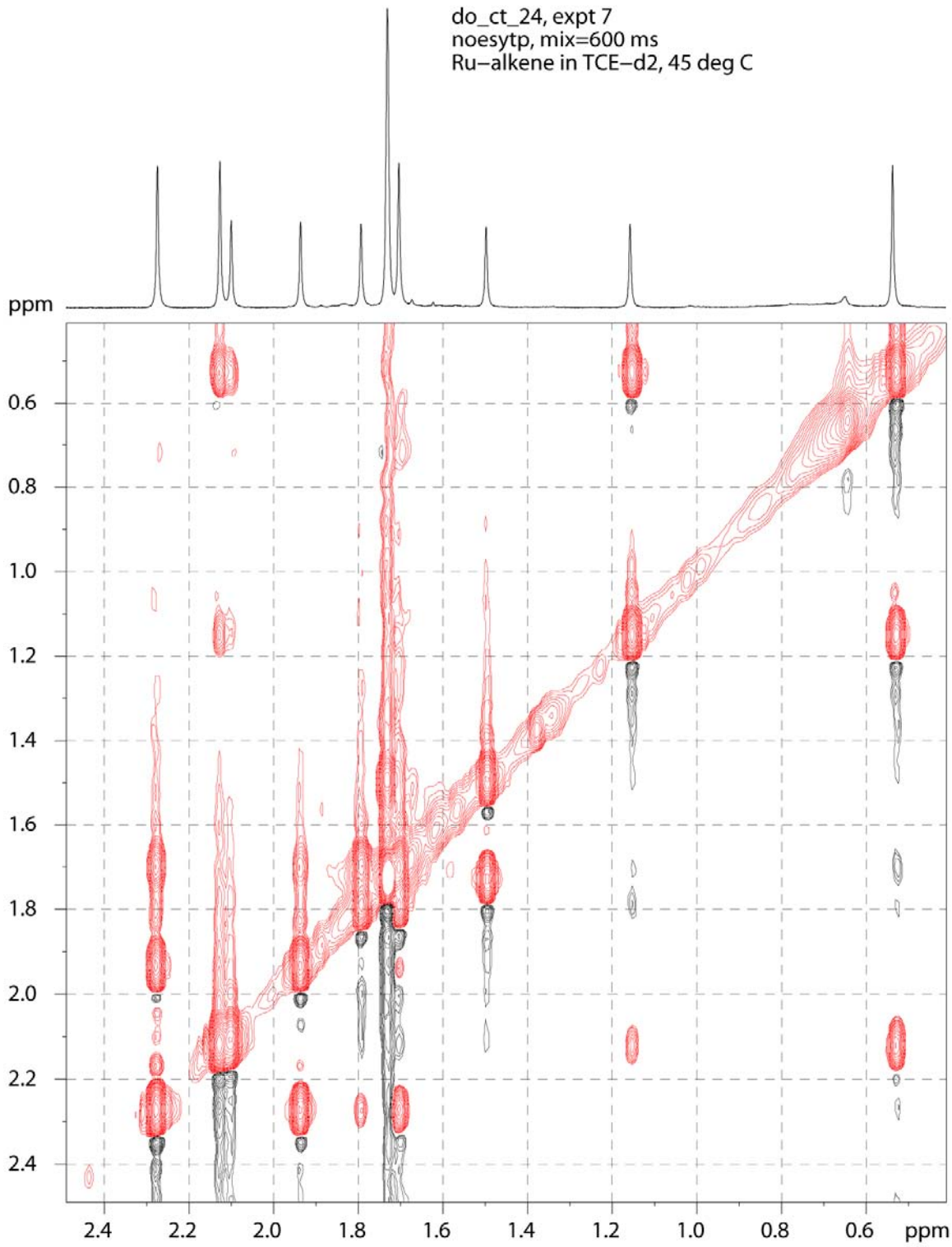

Figure S23. 400 MHz ^{1}H-^{1}H NOESY/EXSY spectrum of **9b/c** in CD_2Cl_2 at 45 °C. Overhauser-derived crosspeaks are colored black, diagonal and exchange-derived crosspeaks are colored red.

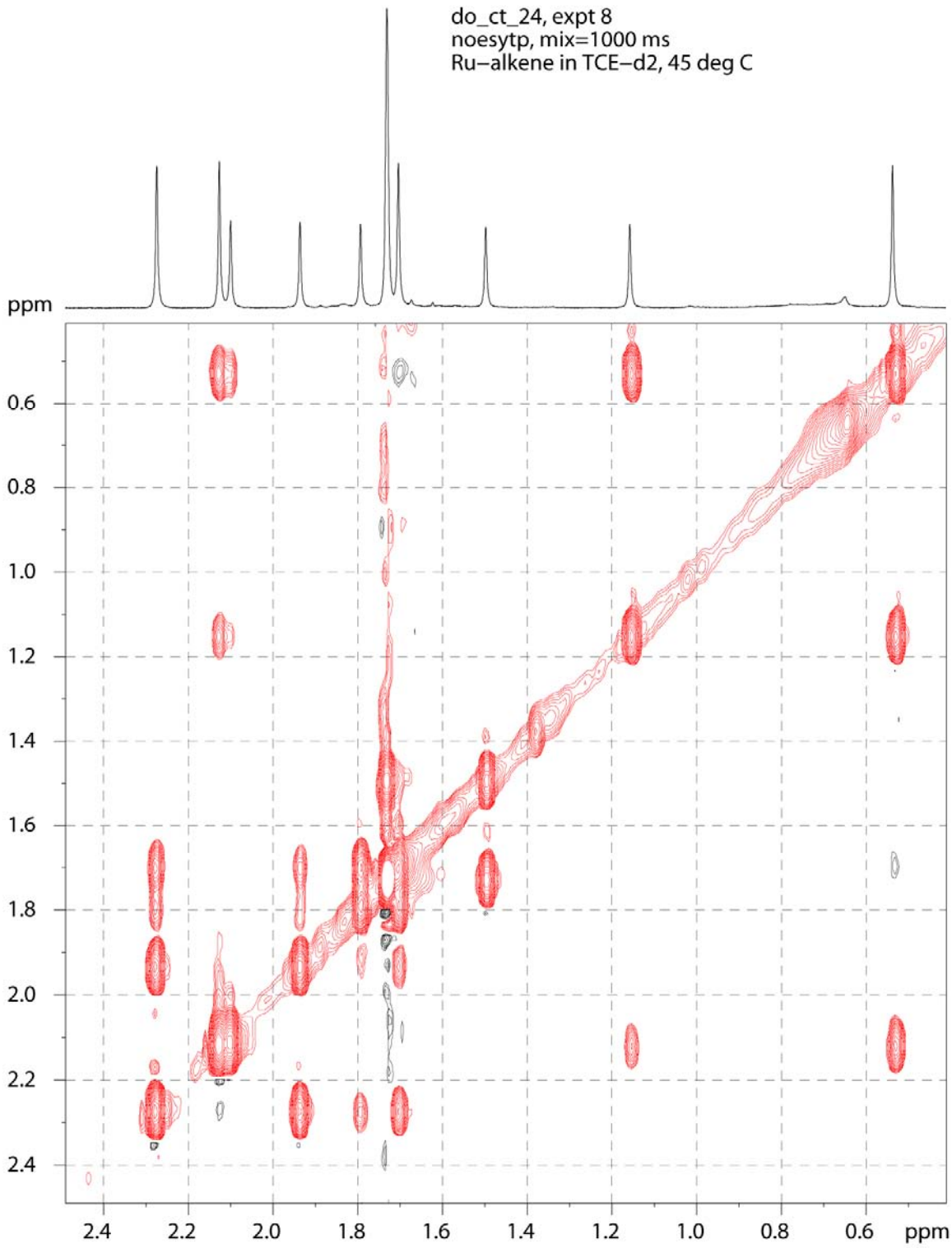

Figure S24. 400 MHz ^{1}H-^{1}H NOESY/EXSY spectrum of **9b/c** in CD_2Cl_2 at 45 °C. Overhauser-derived crosspeaks are colored black, diagonal and exchange-derived crosspeaks are colored red.

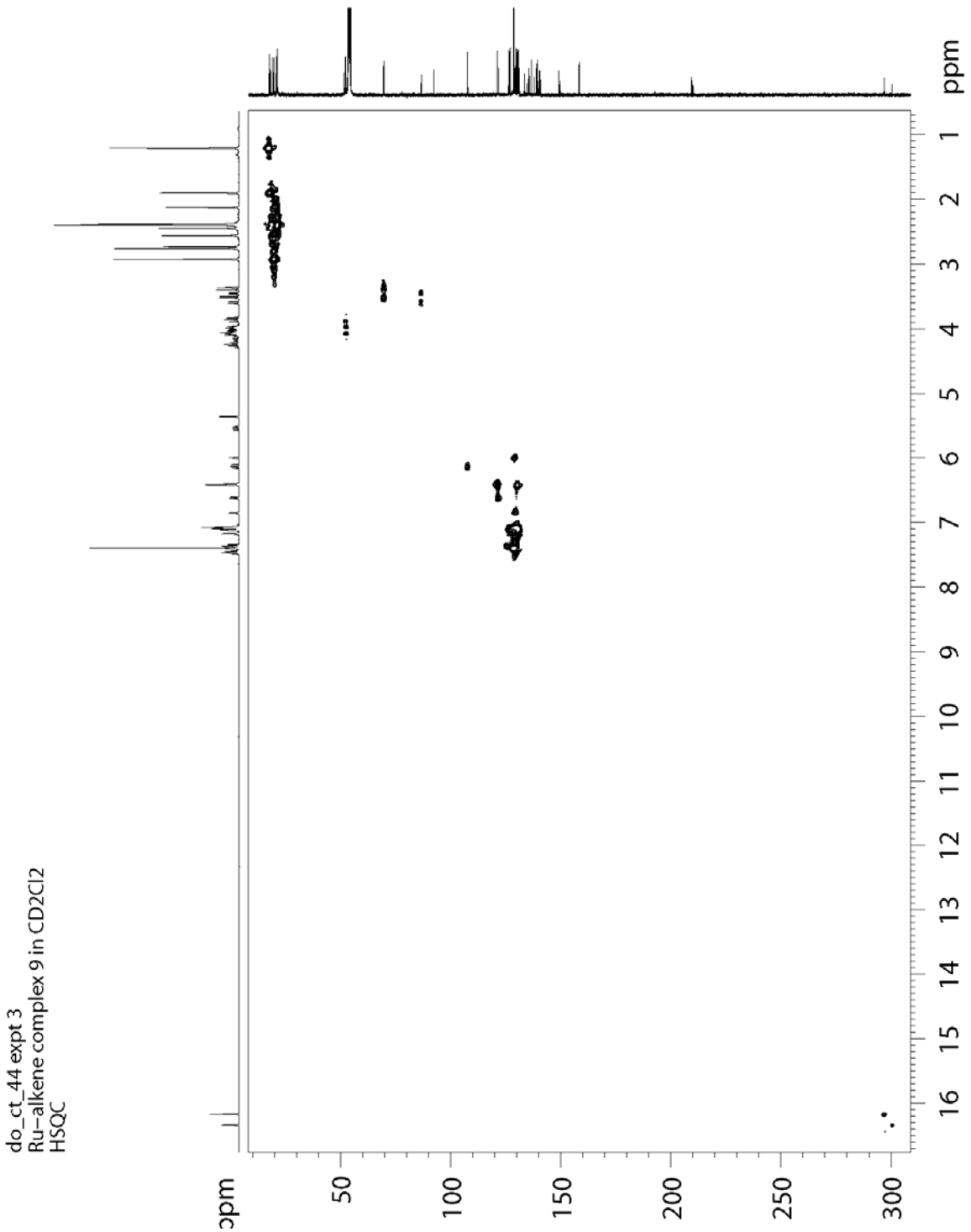

Figure S25. 400 MHz ^{1}H-^{13}C HMQC spectrum of **9b/c** in CD_2Cl_2 at 22 °C. This experiment correlates proton chemical shifts with carbon chemical shifts via the one-bond heteronuclear scalar coupling.

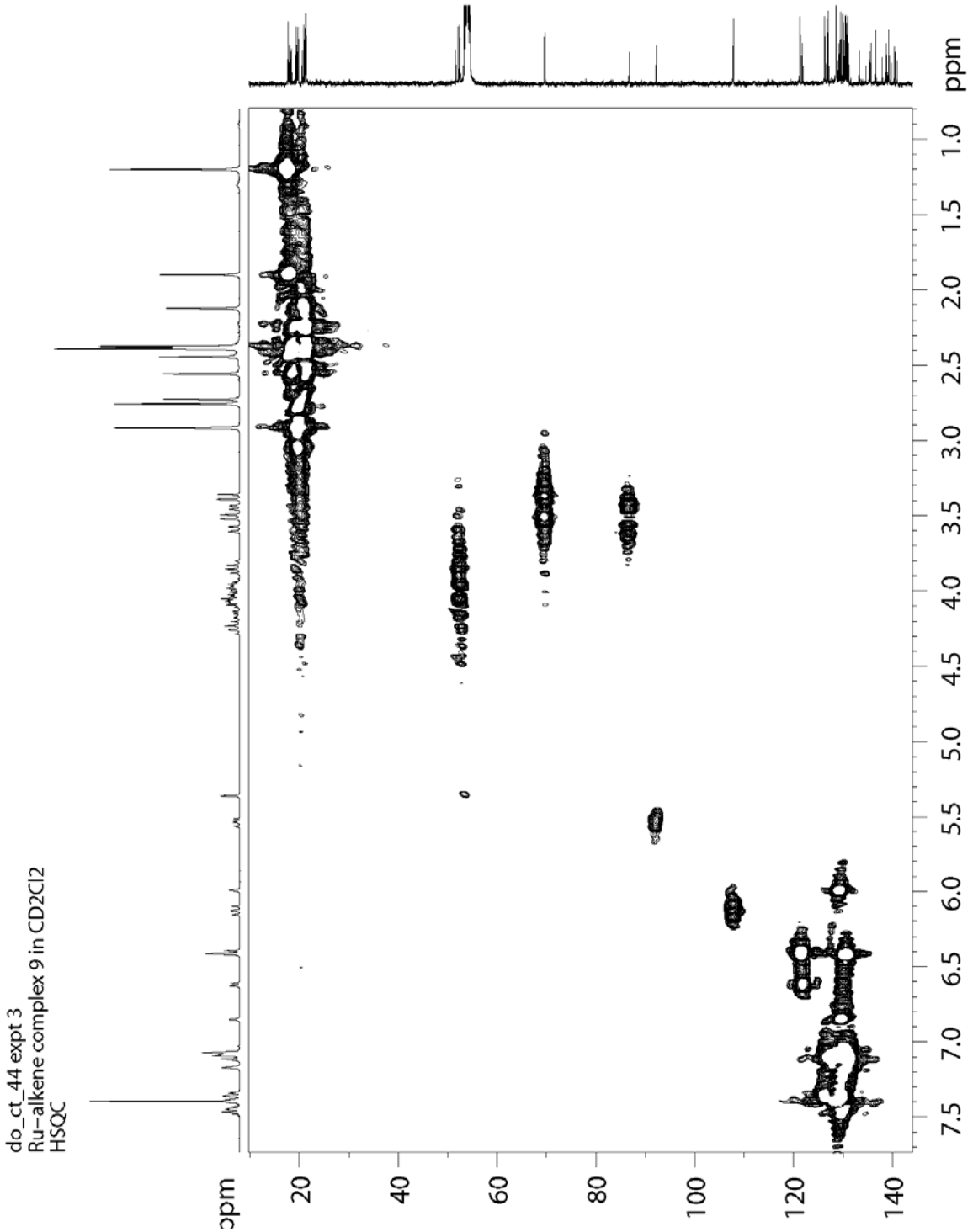

Figure S26. 400 MHz ^{1}H-^{13}C HMQC spectrum of **9b/c** in CD_2Cl_2 at 22 °C. This experiment correlates proton chemical shifts with carbon chemical shifts via the one-bond heteronuclear scalar coupling.

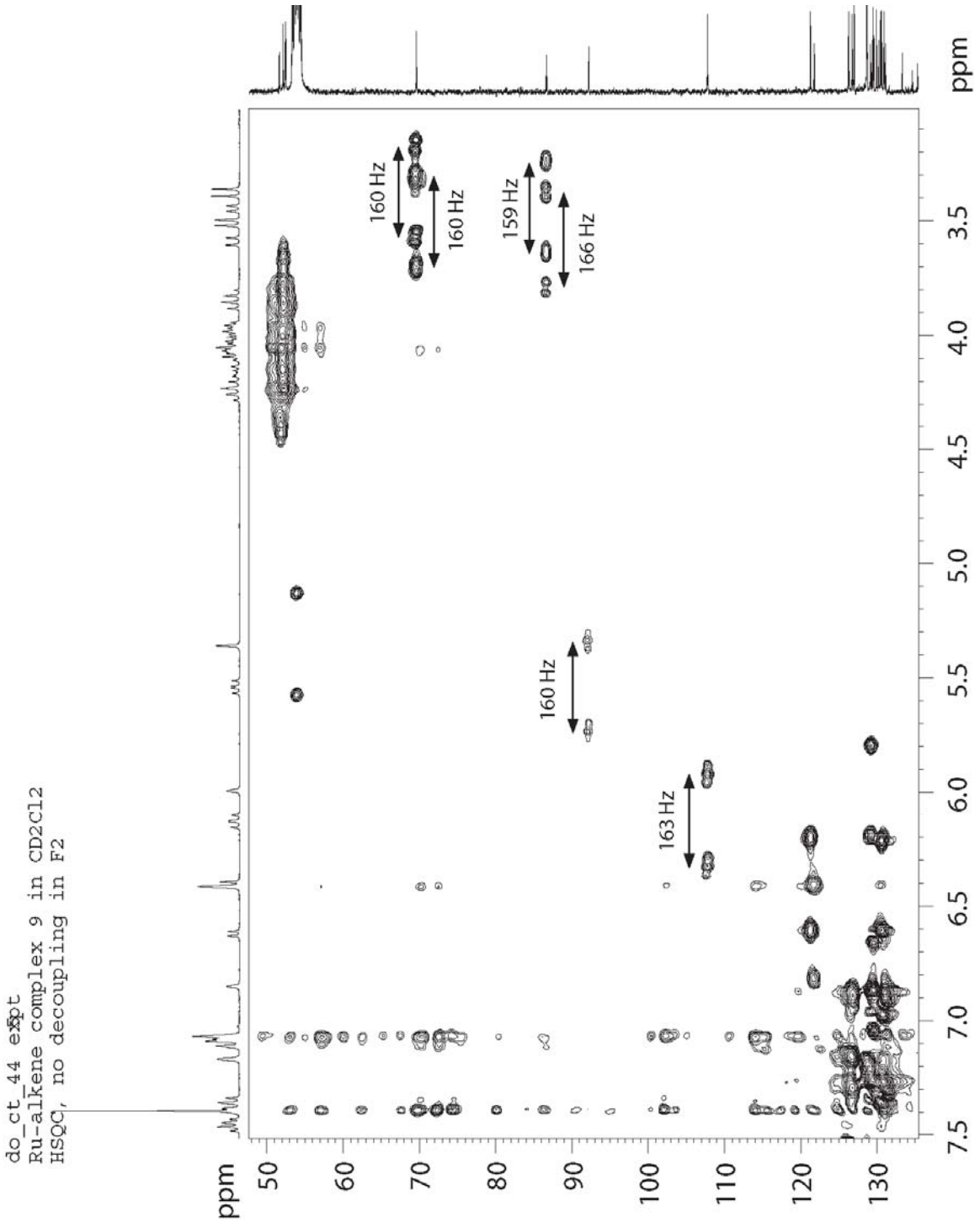

Figure S27. 400 MHz ^{1}H-^{13}C HMQC spectrum of **9b/c** in CD_2Cl_2 at 22 °C. This experiment correlates proton chemical shifts with carbon chemical shifts via the one-bond heteronuclear scalar coupling. Decoupling was not used in the f2 dimension, which allows the one-bond C-H coupling constants to be measured.

Discussion of the Expected and Observed NOEs in 9a-c

The structures of isomers **9a**, **9b**, and **9c** as shown in Figure S28 were computed with the B3LYP/LACVP** level of theory. The details of these calculations are described in a later section of this report (p. S62). The structures are used here for the purpose of comparing measured nuclear Overhauser effects with those predicted from a consideration of internuclear distances.

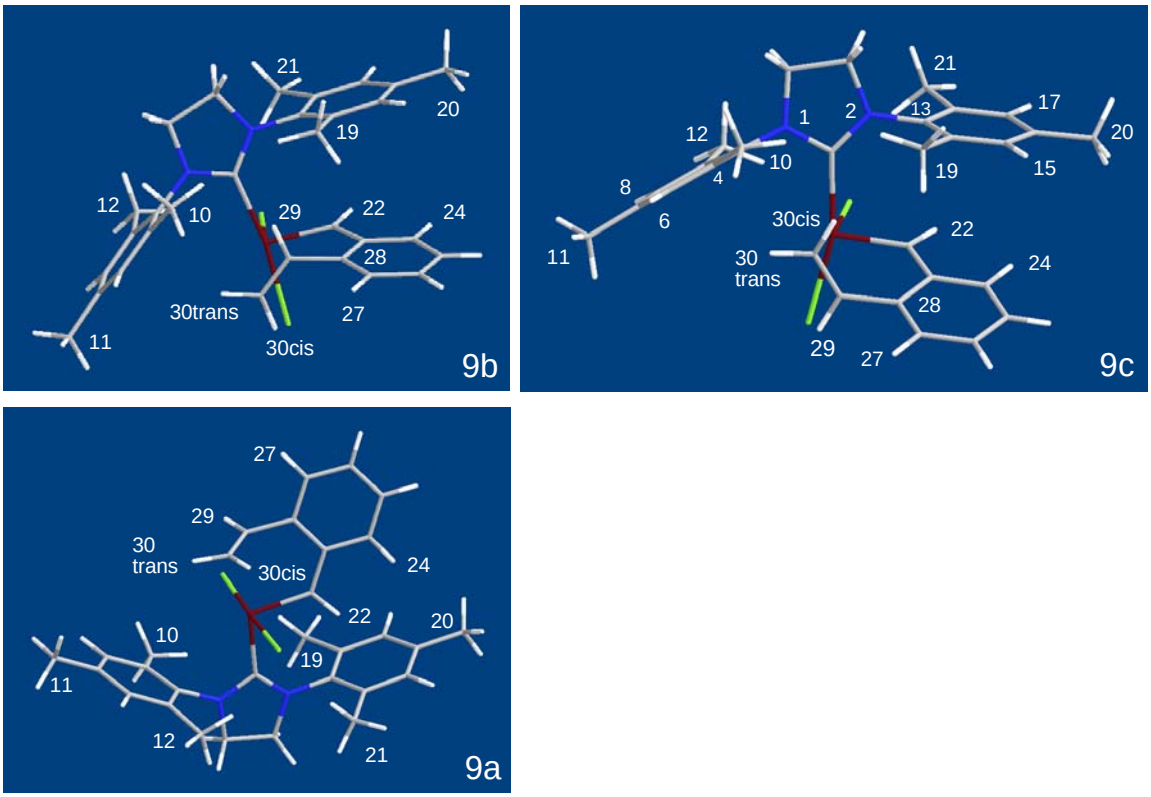

Figure S28. Atom-numbering scheme used to define selected H-H distances in structural isomers **9a-c**.

As shown in Table S8, NOEs are expected to arise between the olefin resonances and the mesityl methyl groups in the side-bound isomers **9b** and **9c**, whereas no such interaction is expected in the bottom-bond isomer **9a**. This is not surprising, as the olefin ligand in **9a** is trans to and distal from the NHC ligand. In the side-bound isomers **9b** and **9c**, the benzylidene H-22 is also in proximity to the C-21 methyl group. The only analogous interactions in bottom-bound **9a** would arise from the benzylidene H-22, which is in proximity to both mesityl C-21 and C-19 methyl groups. Examination of the models shows that the side-bound isomers should be differentiable on the basis of the olefin-mesityl methyl interactions: in **9b**, H-29 is located roughly equidistant from Me-19 and Me-10 and H-30(trans) is proximal to Me-10. In **9c**, olefinic H-29 is oriented away from the NHC ligand and only the geminal protons on C-30 are in proximity to the mesityl methyl groups. In this structural isomer, H-30(cis) is equidistant between Me-10 and Me-19, whereas H-30(trans) is located closer to Me-10.

Table S8. Computed distances (Å) in structural isomers **9b**, **9c** and **9a** $H^{\cdots}CH_3$ and $CH_3^{\cdots}CH_3$ distances are reported as the $H^{\cdots}C$ and $C^{\cdots}C$ distances, respectively. Distances less than 3.8 Å are highlighted; Overhauser effects might be measurable for these interactions. Short-range intra-olefin and benzylidene-*ortho*-H distances, which are expected to produce NOEs, are colored in green. Highlighted in yellow are through-space interactions unique to each structural isomer. Red boxes identify observed NOEs.

Isomer 9b

Label	10	11	12	19	20	21	22	24	27	29	30c	30t
10	--											
11	5.033	--										
12	5.117	5.036	--									
19	4.502	9.201	7.159	--								
20	9.221	13.226	9.943	5.028	--							
21	7.112	9.858	5.494	5.117	5.040	--						
22	6.591	8.888	5.951	5.126	5.477	3.677	--					
24	8.038	10.860	8.450	5.548	4.538	5.385	2.578	--				
27	5.433	9.092	8.771	4.181	7.008	7.831	5.542	4.984	--			
29	2.877	6.913	5.926	2.817	6.904	5.839	4.413	5.310	3.020	--		
30cis	4.690	6.305	6.261	5.706	8.532	7.143	4.289	5.171	3.766	3.088	--	
30trans	2.980	4.923	5.250	5.260	8.987	7.048	5.049	6.374	4.298	2.481	1.837	--

Isomer 9c

Label	10	11	12	19	20	21	22	24	27	29	30c	30t
10	--											
11	5.034	--										
12	5.108	5.038	--									
19	4.706	9.211	7.127	--								
20	9.452	13.360	9.837	5.036	--							
21	7.099	9.878	5.391	5.115	5.039	--						
22	6.568	9.118	5.819	4.222	4.986	3.555	--					
24	8.043	11.086	8.308	4.490	3.955	5.359	2.555	--				
27	6.653	9.064	8.825	5.381	8.281	8.696	5.534	4.983	--			
29	5.275	6.630	6.189	5.472	8.671	7.344	4.430	5.303	2.954	--		
30cis	3.062	6.755	5.786	2.870	7.329	6.099	4.271	5.216	3.932	3.081	--	
30trans	2.873	5.115	5.044	4.667	8.896	6.915	5.033	6.377	4.360	2.427	1.845	--

Isomer 9a

Label	10	11	12	19	20	21	22	24	27	29	30c	30t
10	--											
11	5.037	--										
12	5.095	5.044	--									
19	4.358	8.944	7.050	--								
20	9.196	13.272	9.981	5.048	--							
21	7.049	9.992	5.605	5.099	5.052	--						
22	6.209	9.167	6.064	3.739	4.638	3.423	--					
24	7.996	11.061	8.454	4.759	4.069	5.390	2.482	--				
27	8.214	9.314	8.742	7.290	8.970	8.821	5.537	4.979	--			
29	5.765	6.621	6.203	6.010	8.912	7.492	4.674	5.417	2.805	--		
30cis	7.148	7.813	5.366	6.742	8.222	5.884	3.759	4.917	4.201	3.096	--	
30trans	6.285	6.112	4.633	7.000	9.470	6.804	4.845	6.243	4.497	2.441	1.843	--

Both isomers observed in solution were found to have Overhauser interactions between olefinic resonances and mesityl-derived methyl groups, which is consistent with both isomers being side-bound. Furthermore, NOE interactions arising from each benzylidene resonance were found to involve only one mesityl methyl resonance each (Figure S18), which is additional evidence for a side-bound isomer. We were able to assign the resonances corresponding to the minor form as structural isomer **9b** on the basis of Overhauser interactions involving H-29 and two mesityl methyl groups, one well-resolved at 1.90 ppm and one at 2.43 ppm, in a region of several overlapping methyl resonances. The H-30(trans) resonance in the minor form also exhibited an NOE to a methyl resonance at 2.43 ppm. No methyl-derived NOEs were observed for the H-30(cis) resonance of the minor isomer. The resonances corresponding to the major form were assigned to structural isomer **9c** on the basis of Overhauser effects between H-30(cis) and two methyl resonances at 1.20 ppm and 2.36 ppm, the latter being in a region of overlapping methyl resonances. The H-30(trans) resonance was found to have an NOE arising from only one methyl group, situated at 2.36 ppm. The H-29 resonance for the major form in solution did not show any measurable NOEs to any methyl resonances, which is consistent with the geometry of **9c** (Table S8).

Assignment of the ^{1}H NMR Spectrum of 9b and 9c

Isomer 9b. The olefin resonances were assigned on the basis of coupling constants and the geminal nature of the H-30 resonances was confirmed by a 2D-HMQC experiment which correlated these resonances to a single carbon resonance (**9b**: 86.70 ppm). The H-29 resonance was likewise correlated to a carbon resonance, thus identifying the C-29 carbon chemical shift (**9b**: 92.20 ppm). These olefinic proton and carbon chemical shifts are discussed in detail in a later section that compares this data with the free ligand (p. S58). To summarize the olefinic proton assignments, H-29 (5.54 ppm) was found to have a large coupling (12.6 Hz) to the trans-disposed H-30(cis) (3.59 ppm) and a smaller coupling (9.2 Hz) to the cis-disposed H-30(trans) (3.44 ppm). A small (1.0 Hz) geminal coupling was observed between the H-30 protons. A small coupling (1.1 Hz) was also observed between H-30(trans) and the benzylidene H-22. Formally a six-bond scalar coupling, this small coupling may arise from a favorable orientation of the C-H backside bond vectors.

As predicted from consideration of the internuclear distances, a strong NOE was observed between the benzylidene H-22 and a doublet (J = 7.8 Hz) proton resonance at 6.62 ppm, identifying it as H-24 on the divinylbenzene-derived ligand. Attempts to fully assign the benzylidene aromatic spin system were hindered by overlap between the remaining protons; H-22 couples as shown by 2D-COSY into the 7.00-7.10 ppm region, but this region is further complicated by overlap with the same resonances corresponding to the **9c** isomer.

NOEs between the olefin/benzylidene resonances and methyl resonances were used to assign resolved methyl resonances. A benzylidene H-22/Me NOE was used to assign the methyl resonance at 2.55 ppm as Me-21. Me-19 (1.90 ppm) was assigned on the basis of its NOE with H-29. Both H-29 and H-30(trans) showed an NOE to 2.43 ppm, which is in a region of several overlapping methyl groups. Using the Me-19 resonance at 1.90 ppm as a reference point, an NOE from it to a broad singlet at 5.99 ppm identifies that resonance as H-15. The H-15 resonance shows one additional NOE to a methyl resonance at 2.12 ppm, identifying it as Me-20. The Me-20 resonance shows an NOE to a broad singlet at 6.85 ppm, identifying it as H-17. The H-17 resonance shows one additional NOE to a methyl resonance at 2.55, identifying it as Me-21 and supporting the assignment made on the basis of the benzylidene H-22 NOE. It was thus possible to assign the mesityl methyl resonances of the portion of the NHC ligand situated over the divinylbenzene-derived ligand. The greater dispersion of these resonances, seen in both **9b**

and **9c**, is probably due to the chemical shift anisotropy induced by the divinylbenzene-derived ligand.

The methyl resonance at 2.72 ppm was assigned as Me-12 on the basis of exchange crosspeaks, observed at 45 °C, correlating it to Me-19 in both **9b** and **9c**. The details of the exchange processes will be discussed in a separate section (vide infra). To add further support for the Me-12 assignment, the H-30/Me NOE in **9b** involved a methyl resonance in the region of overlap (2.36-2.44 ppm), which would be consistent with Me-10 (and not Me-12) being located in the region of overlap.

Isomer 9c. For the most part, the strategy used to assign the resonances of **9b** was also found successful for **9c**. The olefin resonances were assigned on the basis of coupling constants and the geminal nature of the H-30 resonances was confirmed by a 2D-HMQC experiment which correlated these resonances to a single carbon resonance (**9c**: 69.60 ppm). The H-29 resonance was likewise correlated to a carbon resonance, thus identifying the C-29 carbon chemical shift (**9c**: 107.80 ppm). To summarize the olefinic proton assignments, H-29 (6.13 ppm) was found to have a large coupling (12.5 Hz) to the trans-disposed H-30(cis) (3.37 ppm) and a smaller coupling (9.9 Hz) to the cis-disposed H-30(trans) (3.51 ppm). A small coupling (1.1 Hz) was also observed between H-30(trans) and the benzylidene H-22.

A strong NOE was observed between the benzylidene H-22 and a doublet (J = 7.8 Hz) at 6.40 ppm, identifying it as H-24 on the divinylbenzene-derived ligand. None of the remaining divinylbenzene-derived aromatic protons were assigned because of peak overlap problems.

As was done for **9b**, NOEs between the olefin/benzylidene resonances and methyl resonances were used to assign resolved methyl resonances in **9c**. A benzylidene H-22/Me NOE was used to assign the methyl resonance at 2.91 ppm as Me-21. Me-19 (1.20 ppm) was assigned on the basis of its NOE with H-30(cis). H-30(cis) also showed an NOE to 2.36 ppm, which is in a region of several overlapping methyl groups. Using the Me-19 resonance at 1.20 ppm as a reference point, an NOE from it to a broad singlet at 6.41 ppm identifies that resonance as H-15. The H-15 resonance shows one additional NOE to a methyl resonance at 2.38 ppm, identifying Me-20 as one of the resonances within the region of overlap. The H-17 resonance was assigned on the basis of its NOE with the well-resolved Me-21 at 2.91 ppm. Data from a 2D-COSYLR experiment was used to provide further corroboration of the assignments for this mesityl ring. In this experiment, which detects small H-H scalar couplings, correlations between aromatic hydrogens and methyl groups were readily detected (Table S6). For example, the H-17 resonance shows correlations with H-15 (6.41 ppm) and three methyl groups: Me-21 (2.91 ppm), Me-19 (1.2 ppm), and Me-20 (2.37 ppm). As was the case for **9b**, the mesityl methyl and aromatic resonances of the portion of the NHC ligand situated over the divinylbenzene-derived ligand exhibited a pronounced dispersion in their chemical shifts.

The methyl resonance at 2.75 ppm was assigned as Me-12 on the basis of a room-temperature NOESY exchange crosspeak correlating it to Me-19 at 1.20 ppm. The details of the exchange process will be discussed later. The remaining methyl groups, Me-11 and Me-10, resonate in the region of overlap between 2.36-2.44 ppm. The evidence for this assignment is that Me-21 (2.91 ppm) has an exchange crosspeak with this region, which would be consistent with Me-21 exchanging with Me-10. Me-11 is assigned to the 2.36-2.44 region by virtue of not being assignable to any of the well-resolved methyl resonances corresponding to the major isomer.

Dynamic NMR Behavior of Complex 9b/c in CD_2Cl_2 at Room Temperature

Evidence from 2D-EXSY experiments suggested that two exchange processes were operative at room temperature (Figure S29). The first, identified as a **9b↔9c** interconversion, is a process that exchanges all resolved resonances in **9b** with those of **9c**. This exchange is readily apparent from the 2D-EXSY data, in which exchange crosspeaks have the same phase as the diagonal resonances (Figures S16-S24; Table S6). We believe this corresponds to a conformational process that involves the Ru-bound olefin changing its orientation by rotation about the C-29/C-28 single bond. The second process involves methyl group interchange in **9c** (and not **9b**) at room temperature. For example, Me-19 exchanges with Me-12 in **9c** (Table S6). Such an exchange is consistent with rotation about the Ru–C bond of the NHC ligand (Figure S29B). An alternative process that might be responsible for methyl exchange in **9c** is rotation about the N1/C4 or N2/C13 bond within the NHC ligand. We don't believe that this process is responsible for the methyl exchange in **9c** because exchange is not observed to occur between Me-19 and Me-21. Rotation about the Ru–C_{NHC} bond appears to occur at a measurable rate at room temperature in **9c**. The corresponding bond rotation in **9b** does not. If it did, we should see an exchange crosspeak between Me-19 in **9b** with Me-12 in **9b**. This exchange is not observed at room temperature, but does perhaps become evident at 45 °C (Figure S23-S24). This result could arise from purely a Ru–C_{NHC} bond rotation in **9b**. However, a Me-12/Me-19 interchange in **9b** could also arise from a combination of the two processes (**9b↔9c**, Ru–C_{NHC} bond rotation) already described.

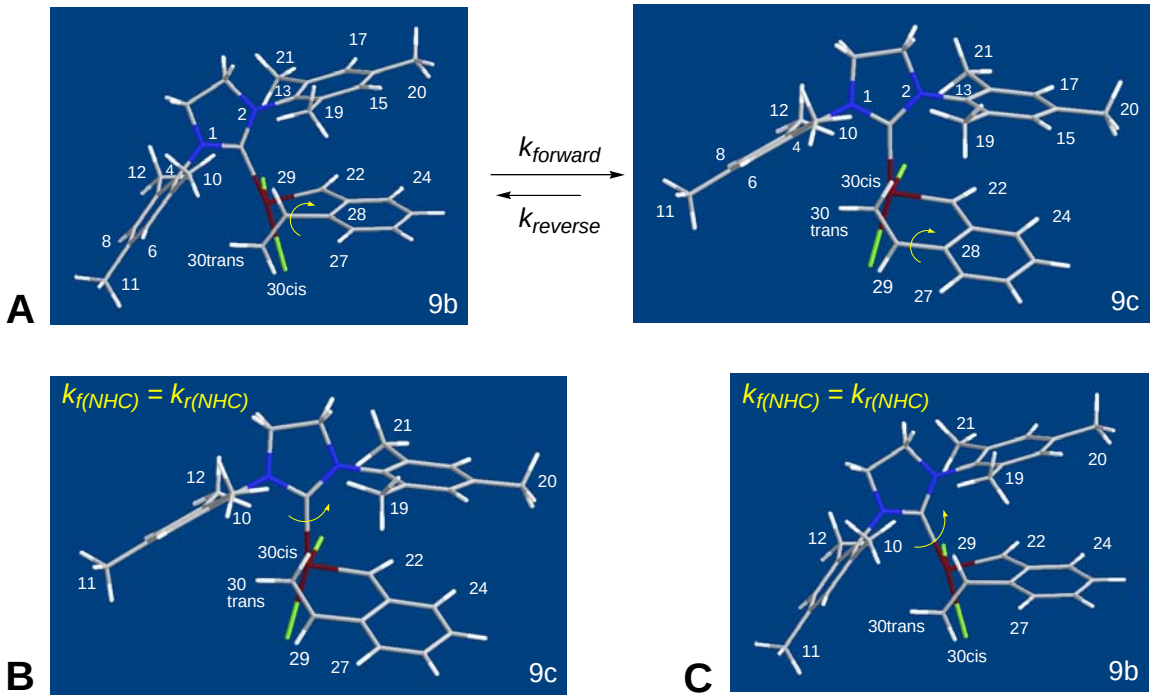

Figure S29. Exchange processes hypothesized as operative in **9b/9c**. (A) The **9b↔9c** interconversion is caused by rotation about the C-29/C-28 bond. This process is supported by the presence of exchange crosspeaks between **9b/9c** resonances (Table S6). (B) and (C) Degenerate interconversion is due to rotation about the Ru–C_{NHC} bond. At room temperature, only the exchange process shown in B is clearly evident.

The dynamics of the **9b↔9c** interconversion was measured by quantifying the off-diagonal NOESY (this experiment might also be referred to as EXSY) exchange peaks corresponding to the benzylidene resonances (Figure S30). The methodology for extracting the exchange rate constants is well-known. To accomplish this, we have written a Matlab implementation of the Full Matrix Analysis (FMA) method described by Zolnai.[11] In tests, our program (Figure S31) provided identical results with those obtained using the now-commercial EXSYCalc[12] program. The forward and reverse rate constants were found to be 0.07 and 0.04 s^{-1}, respectively.

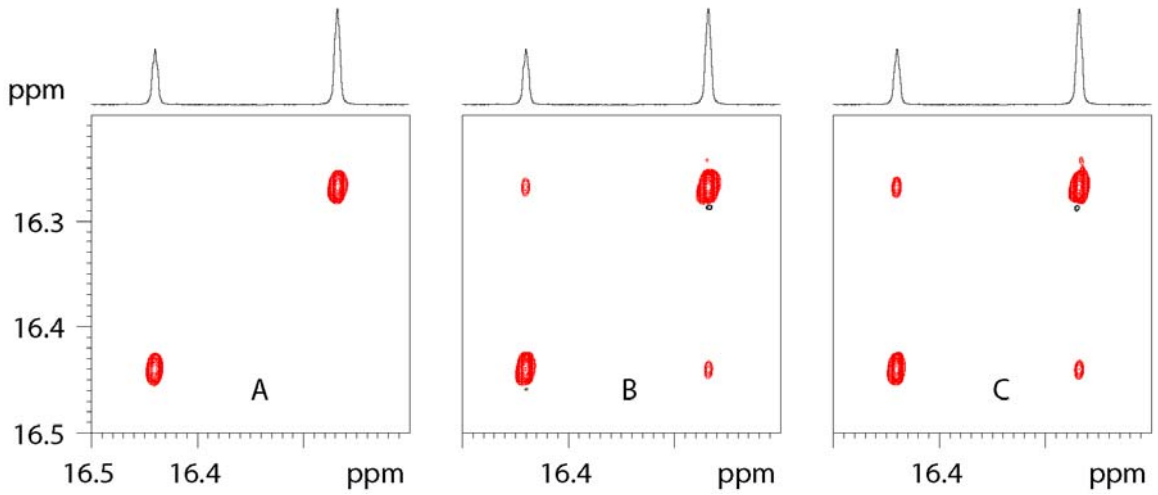

Figure S30. 400 MHz ^{1}H NOESY experiments for the carbene region of Ru-olefin complex **9b/c** in CD_2Cl_2 at room temperature. Positive peak intensity is colored black and negative peak intensity is colored red. (A) mixing time = 0 s, (B) mixing time = 600 ms, (C) mixing time = 1200 ms. Peak intensities are listed clockwise, starting at the high field diagonal resonance. The off-diagonal intensities have been corrected for background intensity. A: -161.55, -92.75. B: −129.68, −2.67, −73.42, −3.22. C: −102.96, −4.85, −58.34, −4.82.

Table S9. Rate constants for **9b↔9c** interconversion, using the benzylidene H-22 exchange from matrix analysis of 2D NOESY data.

Mixing Time	k_r (s^{-1})	k_f (s^{-1})	Ratio
600 ms	0.035	0.073	0.479
1200 ms	0.040	0.068	0.588
Mean	**0.038**	**0.071**	**0.533**

The dynamics of the **9b↔9c** interconversion were also measured by an identical analysis of the Me/Me exchange processes in **9b/9c**. The forward and reverse rate constants determined in this manner were comparable with those determined using the benzylidene resonances.

[11] *J. Chem. Inf. Comput. Sci.* **2000,** *40,* 611-621.
[12] http://www.mestrec.com.

Table S10. Forward and reverse rate constants for the methyl region from matrix analysis of two 2D-NOESY spectra.

		Tmix = 600			Tmix = 1200		
Process	**Exchange**	k_r (s^{-1})	k_f (s^{-1})	**Ratio**	k_r (s^{-1})	k_f (s^{-1})	**Ratio**
9b↔9c	Me-21/Me-21	0.050	0.093	0.538	0.052	0.091	0.572
9b↔9c	Me-19/Me-19	0.058	0.091	0.630	0.053	0.089	0.598
9b↔9c	**mean**	**0.054**	**0.092**	**0.584**	**0.053**	**0.090**	**0.585**
Ru–C_{NHC} rotation in **9c**	Me-21/Me-10	0.036	0.026	1.406	0.031	0.026	1.189
Ru–C_{NHC} rotation in **9c**	Me-19/Me-12	0.030	0.036	0.823	0.030	0.034	0.872
Ru–C_{NHC} rotation in **9c**	**mean**	**0.033**	**0.031**	**1.115**	**0.031**	**0.030**	**1.030**

Averaging the four k_f values for the **9b↔9c** interconversion, we obtain 0.08 ± 0.01 s^{-1}. Using the upper and lower 95% confidence intervals, these rate constants provide an estimate of the Gibbs Free Energy of Activation of 18.9 ± 0.1 kcal/mol at 298 K, according to the expression

$$\Delta G^{\ddagger} = RT\,[\ln (k_B/h) - \ln (k/T)].$$

Reported value for 9b↔9c $\Delta G^{\ddagger}$(25 °C): 18.9 ± 0.1 kcal/mol

The rate of Ru–C_{NHC} rotation in **9c** was determined from the Me/Me exchange processes (Table S10). The rate constant for this process was determined to be 0.03 s^{-1} at room temperature. Interestingly, this rate constant is very similar to that measured for the **9b↔9c** interconversion. This rate constant corresponds to $\Delta G^{\ddagger}$ = 19.5 kcal/mol at 298 K.

File: hickstein.m

Available: http://pages.pomona.edu/~ddh02002/hickstein.m

```
function R = hickstein (I, M, t)

%Created by Dan Hickstein, Pomona College
%Last Modified December 9, 2005
%DanHickstein@gmail.com
%This program finds the matrix -R using the right side of equation 26
%from Perrin's paper. (CHEMICAL REVIEWS 90 (6): 935-967 SEP-OCT 1990)
%NOTICE: This finds NEGATIVE R.  Thus the k values
%can be read directly off this matrix.
%Instructions:
%Open Matlab
%Create a matrix I equal to your n-by-n intensity matrix (peak volumes).
%Create (n-x-1) matrix M of the cross peak volumes from the Tm=0 matrix
%Create a constant t equal to the mixing time.
%Call the function from matlab like this:
%"hickstein (I,M,t)"    but don't use the quotes.

[b,c]=size(I);
i=1;
I=transpose(I);
disp('Transpose of I:');
disp(I);

while i<(b+1)
    j=1;
    while j<(c+1)
        Q = I(i,j)/M(j,1);
        %Q = 0.5*(I(i,j)+I(j,i))/sqrt(M(j,1)*M(i,1)) (See Below)
        A(i,j)=Q;
        j=j+1;
    end
    i=i+1;
end

%The matrices of the eigenvalues and vectors are just displayed
%to make sure the calculations are going alright.
%Negative eigenvalues spell trouble and generally mean that your
%data isn't very precise.  Go back and integrate again.
%If that doesn't fix it you can try averaging the each ij element of
%the matrix with the corresponding ji element.  Perrin talks about this
%it works well, but you lose forward & reverse information.
%If you want to do averaging, uncomment the commented line above (line 29)
%and comment the line above it (line 28).

disp ('Symmetrized A is:');
disp (A);
[X,l]=eig(A);
disp ('Matrix of EigenVECTORS:');
disp (X);
disp ('Diagonalized Matrix of EigenVALUES');
disp (l);

lnV=logm(abs(l));
disp ('Natural log of Eigenvalues');
disp (lnV);

                              R=(X*(lnV)*(inv(X)))/t;
```

Figure S31. Matlab implementation for extracting rate constants from NOESY/EXSY data.

Dynamic NMR behavior of complex 9b/c in $CDCl_2CDCl_2$ from 22-105 °C

To obtain a more accurate estimate of $\Delta G^{\ddagger}$ for the **9b↔9c** interconversion, we performed a lineshape analysis of a series of 1D ^{1}H NMR spectra of the benzylidene region of complex **9** acquired at elevated temperatures. To be able to access the coalescence temperature, the Ru-olefin complex was dissolved in deuterated tetrachloroethane in a J-Young NMR tube. A preliminary experiment (using a probe not yet temperature-calibrated) showed that complex **9** could be heated to ca. 130 °C and returned to room temperature with only a minimal amount of sample decomposition, none of which interfered with the benzylidene resonances (Figure S32).

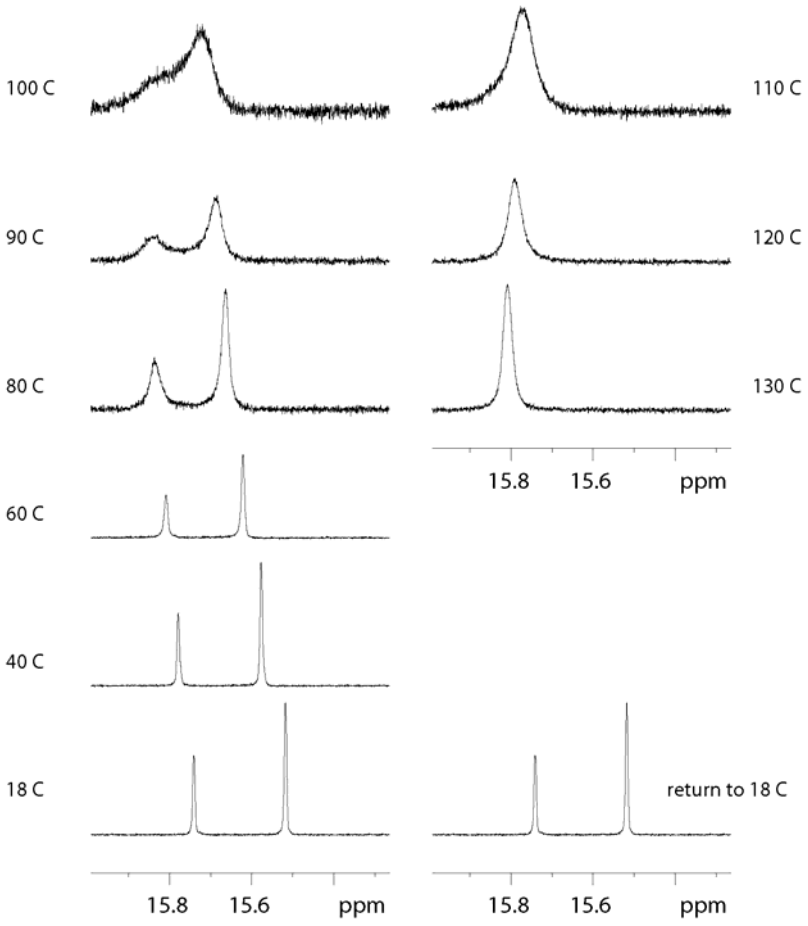

Figure S32. Compound stability test: 400 MHz ^{1}H VT-NMR spectra for Ru-olefin complex **9** dissolved in $CDCl_2CDCl_2$.

We note that using the benzylidene resonances provides a good estimate for the **9b↔9c** interconversion because these resonances are 'blind' to the process involving Ru-C_{NHC} rotation in either isomer. Put another way, the NHC ligand rotation is a degenerate process that does not alter the magnetic environment of the benzylidene resonances. The same is not true for the methyl resonances, as our earlier analysis showed.

Another variable-temperature data set was acquired, this time the probe was calibrated at each temperature with a glycol standard for each measurement. These spectra, together with their overlaid fit spectra, are shown in Figure S33.

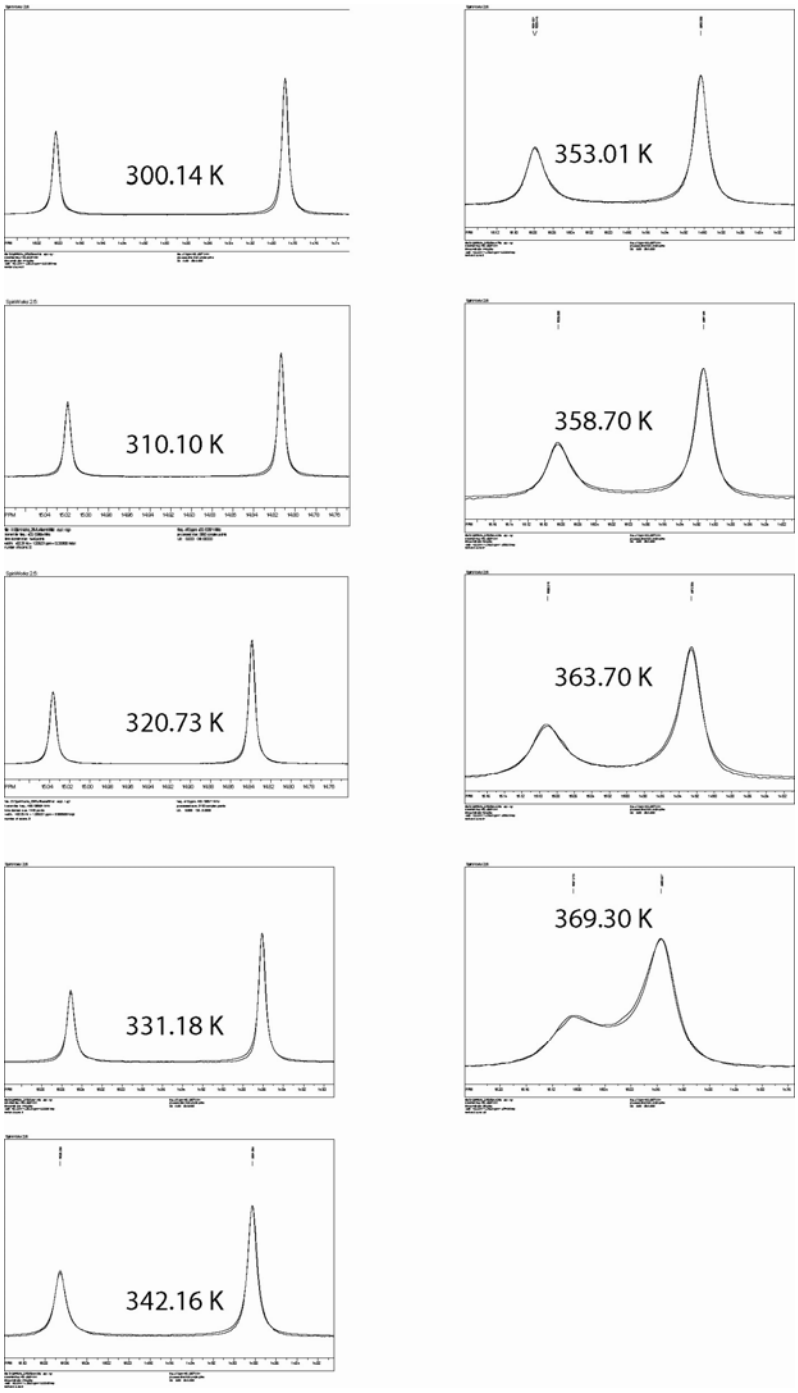

Figure S33. Experimental spectra and MEXICO fits of the benzylidene resonances of Ru-olefin complex **9b/c** in $CDCl_2CDCl_2$ at temperatures ranging from 300.14 K to 369.30 K.

We simulated our experimental spectra using the MEXICO[13] set of programs written by Professor Alex Bain. We were able to get good results using the non-interative version of MEXICO (mexicon), and we found the most effective way to utilize the manual simulation capability of MEXICO is to use it through SpinWorks[14] NMR program. The SpinWorks program allows the MEXICO simulation to be called from within SpinWorks and displays the simulated spectrum and the RMS value immediately. After getting a good general fit, the RMS value displayed in the upper left corner of the screen can be invaluable for fine-tuning the rate constant and the frequencies of the peaks to get the best possible fit. It is important to note that SpinWorks displays the RMS value for the portion of the spectrum being displayed. Thus, it is important not to change the viewing area while trying to minimize the RMS. The fits are overlaid on the experimental data shown in Figure S33. The parameters used for each fit are summarized in Table S11. For an exchange process involving unequal populations, as is the case for **9b↔9c**, MEXICO fits input values of the forward rate constant, k_f.

Table S11. Simulation parameters used for the manual MEXICO fitting. $1/T_1$ was .120 s^{-1} and the equilibrium ratio was 1:0.610.

Expt #	Temp (K)	Left Pk (Hz)	Right Pk (Hz)	k_f (s^{-1})	−1/T	R*ln(hk/k_bT)
5	310.10	6009.74	5927.36	0.25	−0.0032	−61.371
9	320.73	6016.51	5937.39	0.76	−0.0031	−59.229
11	331.18	6022.48	5946.42	2.25	−0.0030	−57.135
15	342.16	6028.26	5954.96	7.05	−0.0029	−54.931
17	353.01	6033.90	5963.00	20.1	−0.0028	−52.911
22	358.70	6036.60	5967.00	30.9	−0.0028	−52.088
25	363.70	6040.20	5971.60	44.5	−0.0027	−51.391

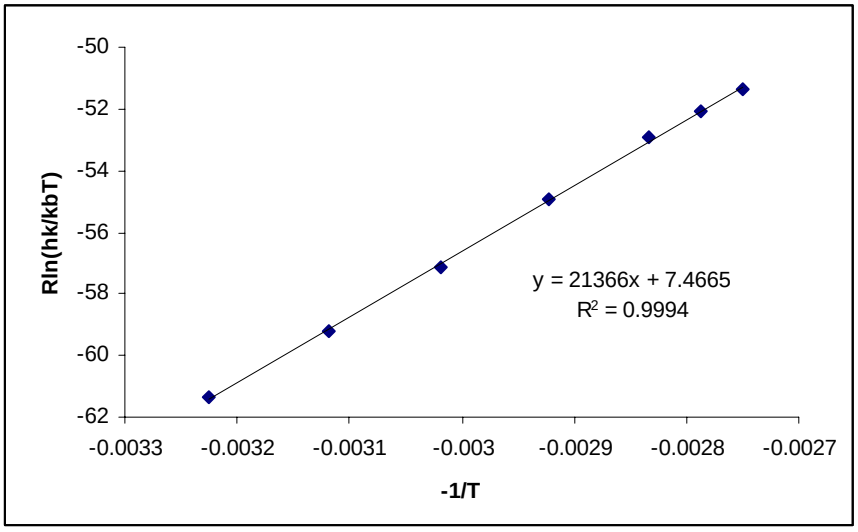

Figure S34. Eyring plot of the MEXICO lineshape data. The slope is $\Delta H^{\ddagger}$ and the intercept is $\Delta S^{\ddagger}$.

[13] http://www.chemistry.mcmaster.ca/faculty/bain/
[14] Marat, Kirk. SpinWorks. http://www.umanitoba.ca/chemistry/nmr/spinworks/index.html

An Eyring plot for data collected over the range of 310-363 K was used to extract the entropy and enthalpy of activation from the temperature dependence of the rate constant (Figure S34). Here, $R\ln(hk/k_BT)$ is plotted vs. $-1/T$. From this plot, the slope is the enthalpy of activation ($\Delta H^{\ddagger}$), and the entropy of activation ($\Delta S^{\ddagger}$) is equal to the intercept. We found $\Delta H^{\ddagger}$ = 21.4 ± 0.6 kcal/mol and $\Delta S^{\ddagger}$ = 7.5 ± 1.8 e.u. Thus, the estimated $\Delta G^{\ddagger}$ at 298 K is **19.1** ± **0.1 kcal/mol**. This is in good agreement with the value of **18.9 ± 0.1 kcal/mol** calculated using the 2D-NOESY experiments at room temperature.

Eyring Plots and Error Analysis

According to the Activated Complex Theory of Henry Eyring,

$$k = \frac{k_B T}{h} e^{-\Delta G^{\ddagger}/RT}$$

and $\Delta G^{\ddagger} = \Delta H^{\ddagger} - T\Delta S^{\ddagger}$, or

$$k = \left(\frac{k_B T}{h} e^{\Delta S^{\ddagger}/R}\right) e^{-\Delta H^{\ddagger}/RT}.$$

This can be re-worked to yield a linear equation in traditional y = mx + b format:

$$R\ln\frac{hk}{k_B T} = \Delta S^{\ddagger} + \left(\frac{-1}{T}\right)\Delta H^{\ddagger},$$

where k is the rate in s^{-1}, k_B is Boltzmann's constant (3.29957×10^{-24} cal K^{-1}), h is Planck's constant (1.58355×10^{-34} cal s), R is the gas constant (1.9872 cal mol^{-1} K^{-1}), and T is the temperature in Kelvin.

The uncertainty in the slope ($\Delta H^{\ddagger}$) and intercept ($\Delta S^{\ddagger}$) was determined directly from the output provided by the linear regression function of the NCSS statistical software package.[15]

Reported value for $\Delta H^{\ddagger}$: 21.4 ± 0.6 kcal/mol

Reported value for $\Delta S^{\ddagger}$: 7.5 ± 1.8 cal/(mol · K)

[15] http://www.ncss.com/

Page/Date/Time 1 3/4/2006 2:01:03 PM
Database
Y = R_ln_hk_over_kbT_ X = neg_1_over_T

Linear Regression Plot Section

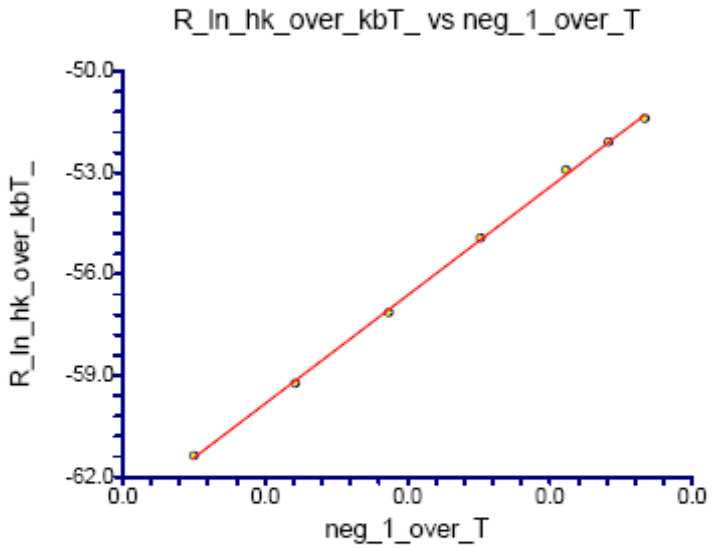

Run Summary Section

Parameter	Value	Parameter	Value
Dependent Variable	R_ln_hk_over_kbT_	Rows Processed	7
Independent Variable	neg_1_over_T	Rows Used in Estimation	7
Frequency Variable	None	Rows with X Missing	0
Weight Variable	None	Rows with Freq Missing	0
Intercept	7.466584	Rows Prediction Only	0
Slope	21366.39	Sum of Frequencies	7
R-Squared	0.9994	Sum of Weights	7
Correlation	0.9997	Coefficient of Variation	-0.0019
Mean Square Error	1.084188E-02	Square Root of MSE	0.1041243

Linear Regression Report

Page/Date/Time 2 3/4/2006 2:01:03 PM
Database
Y = R_ln_hk_over_kbT_ X = neg_1_over_T

Regression Estimation Section

Parameter	Intercept B(0)	Slope B(1)
Regression Coefficients	7.466584	21366.39
Lower 95% Confidence Limit	5.649426	20751.5
Upper 95% Confidence Limit	9.283743	21981.27
Standard Error	0.7069055	239.2004
Standardized Coefficient	0	0.9996868
T Value	10.56235	89.3242
Prob Level (T Test)	1.31423E-04	3.333307E-09
Reject H0 (Alpha = 0.05)	Yes	Yes
Power (Alpha = 0.05)	1	1
Regression of Y on X	7.466584	21366.39
Inverse Regression from X on Y	7.506093	21379.78
Orthogonal Regression of Y and X	7.506093	21379.78

Table S12. NCSS output (part 1) for Eyring plot shown in Figure S34.

Estimated Model
(7.4665841615395) + (21366.3860922965) * (neg_1_over_T)

Correlation and R-Squared Section

Parameter	Pearson Correlation Coefficient	R-Squared	Spearman Rank Correlation Coefficient
Estimated Value	0.9997	0.9994	1.0000
Lower 95% Conf. Limit (r dist'n)	0.9973		
Upper 95% Conf. Limit (r dist'n)	0.9998		
Lower 95% Conf. Limit (Fisher's z)	0.9978		1.0000
Upper 95% Conf. Limit (Fisher's z)	1.0000		1.0000
Adjusted (Rbar)		0.9992	
T-Value for H0: Rho = 0	89.3242	89.3242	
Prob Level for H0: Rho = 0	3.333307E-09	3.333307E-09	0

Analysis of Variance Section

Source	DF	Sum of Squares	Mean Square	F-Ratio	Prob Level	Power (5%)
Intercept	1	21623.37	21623.37			
Slope	1	86.50529	86.50529	7978.812	3.333307E-09	1
Error	5	5.420938E-02	1.084188E-02			
Adj. Total	6	86.55949	14.42658			
Total	7	21709.93				

s = Square Root(1.084188E-02) = 0.1041243

Page/Date/Time 3 3/4/2006 2:01:07 PM
Database
Y = R_ln_hk_over_kbT_ X = neg_1_over_T

Summary Matrices

Index	X'X 0	X'X 1	X'Y 2	X'X Inverse 0	X'X Inverse 1
0	7	-2.065491E-02	-389.0547	46.09123	15572.02
1	-2.065491E-02	6.113598E-05	1.152033	15572.02	5277394
2 (Y'Y)			21709.93		
Determinant		1.326412E-06			753913.4

Variance - Covariance Matrix of Regression Coefficients

Index	VC(b) 0	VC(b) 1
0	0.4997154	168.8299
1	168.8299	57216.85

Table S12. NCSS output (part 2) for Eyring plot shown in Figure S34.

Error in $\Delta G^{\ddagger}$:

Computing the uncertainty in $\Delta G^{\ddagger}$, given that $\Delta H^{\ddagger}$ and $\Delta S^{\ddagger}$ are correlated:

$$S^2_{\Delta G^{\ddagger}} = \left(\frac{\partial \Delta G^{\ddagger}}{\partial \Delta H^{\ddagger}}\right)^2 S^2_{\Delta H^{\ddagger}} + \left(\frac{\partial \Delta G^{\ddagger}}{\partial \Delta S^{\ddagger}}\right)^2 S^2_{\Delta S^{\ddagger}} + 2\left(\frac{\partial \Delta G^{\ddagger}}{\partial \Delta H^{\ddagger}}\right)\left(\frac{\partial \Delta G^{\ddagger}}{\partial \Delta S^{\ddagger}}\right) S^2_{\Delta H^{\ddagger}\Delta S^{\ddagger}}$$

$$\frac{\partial G^{\ddagger}}{\partial H^{\ddagger}} = \frac{\partial(\Delta H^{\ddagger} - T\Delta S^{\ddagger})}{\partial \Delta H^{\ddagger}} = 1$$

$$\frac{\partial \mathrm{G}^{\ddagger}}{\partial S^{\ddagger}} = \frac{\partial(\Delta H^{\ddagger} - T\Delta S^{\ddagger})}{\partial \Delta S^{\ddagger}} = -T$$

substituting gives,

$$S^2_{\Delta \mathrm{G}^{\ddagger}} = 1^2 S^2_{\Delta \mathrm{H}^{\ddagger}} + \mathrm{T}^2 S^2_{\Delta \mathrm{S}^{\ddagger}} - 2\mathrm{T}S^2_{\Delta \mathrm{H}^{\ddagger}\Delta \mathrm{S}^{\ddagger}}$$

where the first two terms are positive but the last term can be positive or negative depending upon the sign of the covariance $S^2_{\Delta \mathrm{H}^{\ddagger}\Delta \mathrm{S}^{\ddagger}}$.

The covariance is the off-diagonal component of the variance-covariance matrix created by NCSS. In the calculation reported here, the covariance is positive, which causes the uncertainty in $\Delta G^{\ddagger}$ to be lower than that in $\Delta H^{\ddagger}$.

Sample calculation for kinetic parameters for 9 dissolved in $CDCl2_2CDCl_2$:

$\Delta G^{\ddagger}$ (25 °C) = $\Delta H^{\ddagger}$ – $T\Delta S^{\ddagger}$ = 21370 cal/mol – (298K)(7.7 cal/mol K)/1000 = 19.135 kcal/mol

Uncertainty in $\Delta G^{\ddagger}$ (25 °C):

$$S^2_{\Delta \mathrm{G}^{\ddagger}} = S^2_{\Delta \mathrm{H}^{\ddagger}} + \mathrm{T}^2 S^2_{\Delta \mathrm{S}^{\ddagger}} - 2\mathrm{T}S^2_{\Delta \mathrm{H}^{\ddagger}\Delta \mathrm{S}^{\ddagger}}$$
$$= (239.2 \text{ cal/mol})^2 + (298 \text{ K})^2(0.7069 \text{ cal/K·mol})^2 - 2(298 \text{ K})(168.83 \text{ cal/mol})$$
$$= 970.8 \text{ cal/mol}$$

$$95\% C.I. = 2.365\sqrt{970.8} = 73.7(cal / mol)$$

$\Delta G^{\ddagger}$ (25 °C) = 19.135 ± 0.074 kcal/mol

Reported value for $\Delta G^{\ddagger}$(25 °C): 19.1 ± 0.1 kcal/mol

Calculation of rate at 25 °C:

$k_f = 2.084\text{x}10^{10}\,\mathrm{T}e^{-\Delta \mathrm{G}^{\ddagger}/1.9872\mathrm{T}}$ (units of $\Delta G^{\ddagger}$ is cal/mol)[16]

$k_f = 0.06 \pm 0.01$ s^{-1}

[16] Eliel, E. L.; Wilen, S. H. *Stereochemistry of Organic Compounds*; Wiley: New York, 1994; p. 635.

Comparison of NMR Parameters of 9b/c with Divinylbenzene (8)

Table S13 summarizes the relevant ^{1}H and ^{13}C NMR parameters for the divinylbenzene-derived ligand in **9b/c** with divinylbenzene (**8**). The data are shown in Figures S35-S37.

Table S13. Comparison of olefin NMR parameters for ruthenium-olefin complexes **9b**, **9c**, and divinylbenzene (**8**) in CD_2Cl_2.

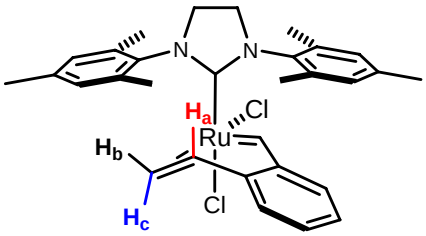

9b

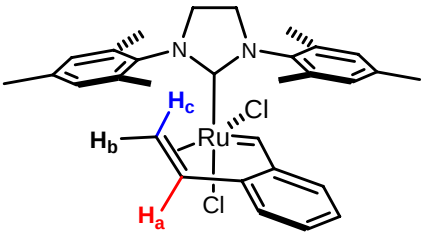

9c

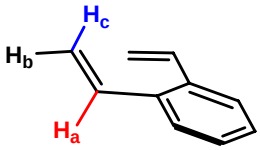

8

parameter (units)	Compound **9b**	**9c**	**8**
δH_a (ppm)	5.54	6.13	7.07
δH_b (ppm)	3.44	3.51	5.37
δH_c (ppm)	3.59	3.37	5.67
$^{3}J_{ab}$ (Hz)	9.2	9.9	11.0
$^{3}J_{ac}$ (Hz)	12.6	12.5	17.4
$^{3}J_{bc}$ (Hz)	1.1	1.0	1.4
δC_a (ppm)	92.20	107.80	135.1
δC_{bc} (ppm)	86.70	69.60	116.5
$^{1}J_{C\text{-}Ha}$ (Hz)	160	163	155
$^{1}J_{C\text{-}Hb}$ (Hz)	159	160	160
$^{1}J_{C\text{-}Hc}$ (Hz)	166	160	155

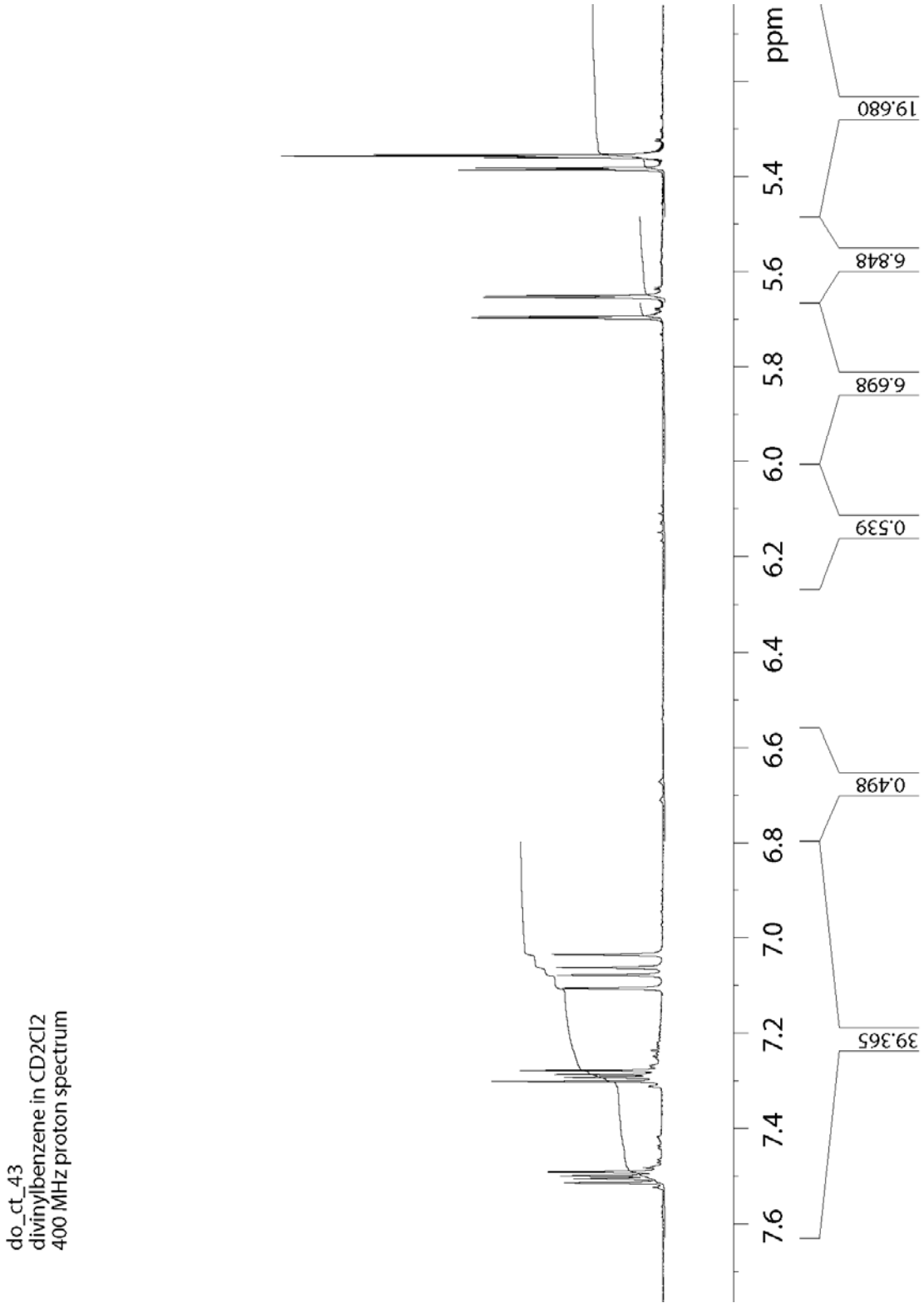

Figure S35. 400 MHz ^{1}H NMR spectrum of divinylbenzene (**8)** in CD_2Cl_2.

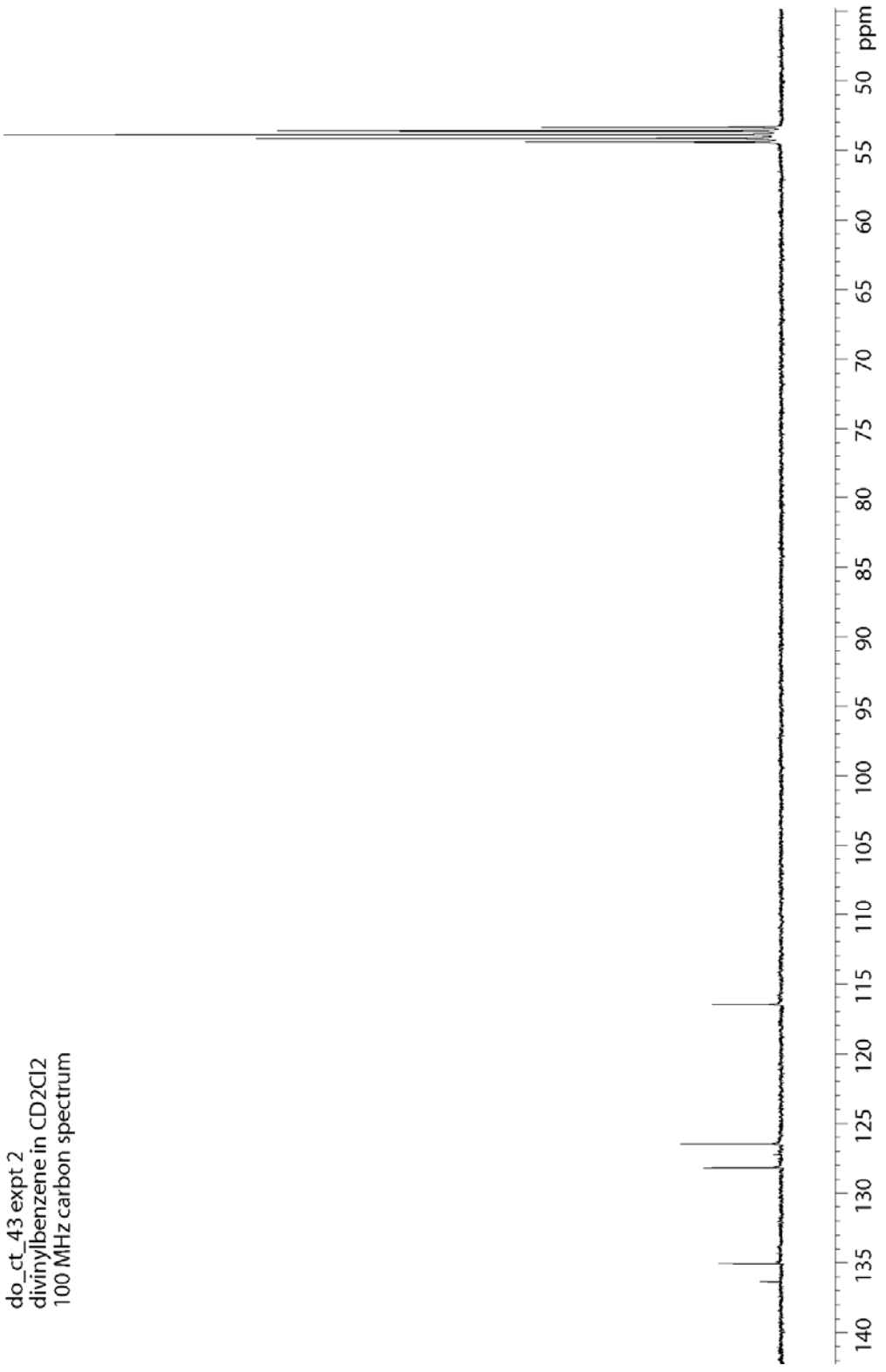

Figure S36. 100 MHz ^{13}C NMR spectrum of divinylbenzene (**8)** in CD_2Cl_2.

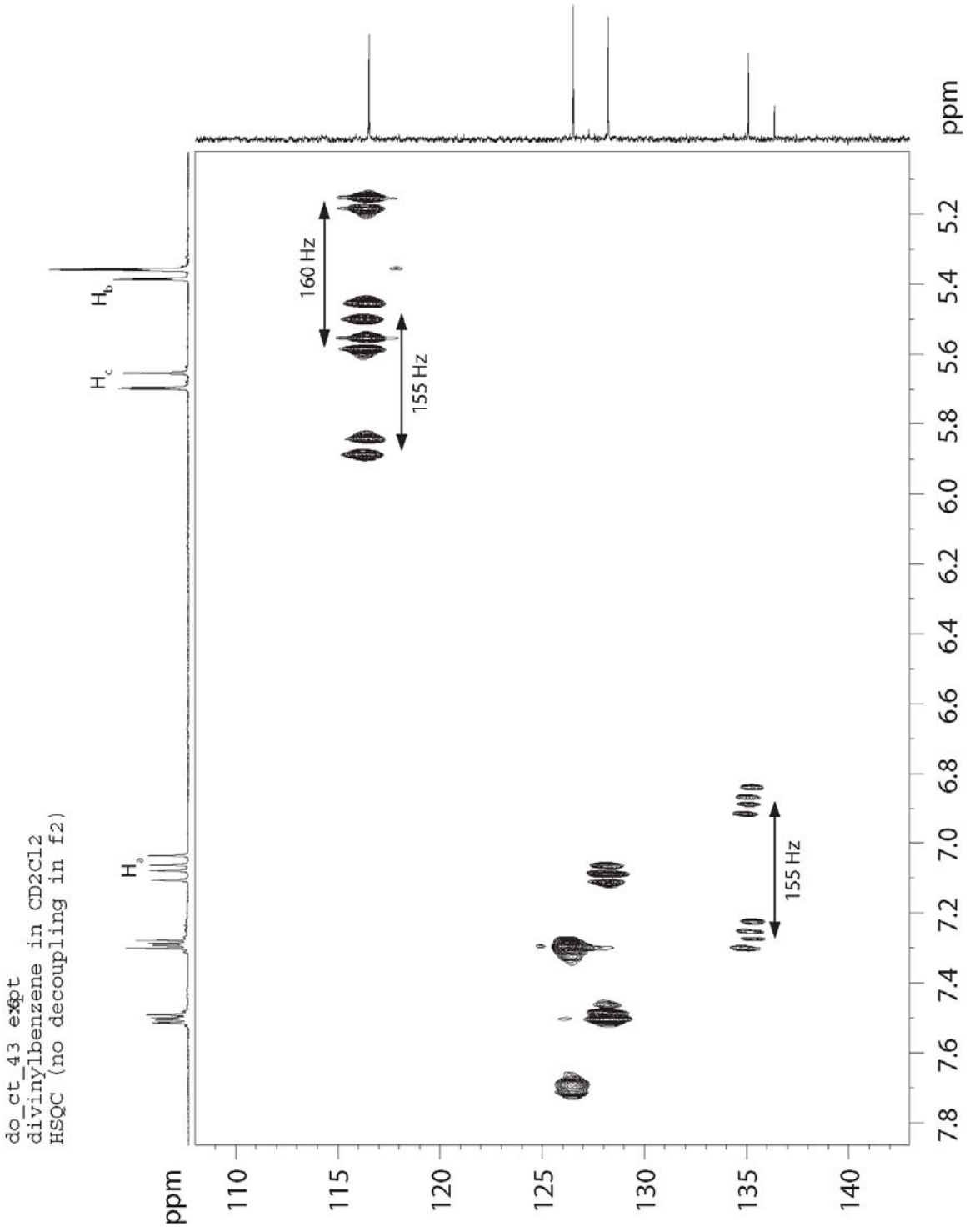

Figure S37. 400 MHz ^{1}H-^{13}C HMQC spectrum of divinylbenzene (**8)** in CD_2Cl_2 at 22 °C. This experiment correlates proton chemical shifts with carbon chemical shifts via the one-bond heteronuclear scalar coupling. Decoupling was not used in the f2 dimension, which allows the one-bond C-H coupling constants to be measured.

DFT Calculations of Ru-olefin Complexes 9a-c

DFT calculations were used to explore the gas-phase geometries and gas-phase and solvent-continuum energies of isomers **9a**, **9b**, and **9c**. The relative and absolute energies are summarized in Tables S14-S17.

Table S14. Relative gas phase energy comparison (kcal/mol) for **9a-c**.

	structural isomer		
method	**9b**	**9a**	**9c**
B3LYP/LANL2DZ	5.55	0.00	3.86
B3LYP/LACVP**	4.80	0.00	3.13
MPW1K/LACVP**	5.53	0.00	2.87

Table S15. Relative energy comparison (kcal/mol) for **9a-c** using a solvent continuum model (CH_2Cl_2, see following page for details) for single-point energy calculations using structures optimized in the gas phase.

	structural isomer		
method	**9b**	**9a**	**9c**
B3LYP/LANL2DZ	0.51	2.55	0.00
B3LYP/LACVP**	1.12	3.80	0.00
MPW1K/LACVP**	1.53	3.93	0.00

Table S16. Gas phase energies (Hartrees) for **9a-c**.

	structural isomer		
method	**9b**	**9a**	**9c**
B3LYP/LANL2DZ	-1396.836962	-1396.845806	-1396.839657
B3LYP/LACVP**	-2287.551002	-2287.558644	-2287.553650
MPW1K/LACVP**	-2287.956559	-2287.965370	-2287.960792

Table S17. Solution phase (CH_2Cl_2) energies (Hartrees) for **9a-c**.

	structural isomer		
method	**9b**	**9a**	**9c**
B3LYP/LANL2DZ	-1396.869770	-1396.866509	-1396.870576
B3LYP/lacvp**	-2287.583968	-2287.579686	-2287.585747
MPW1K/lacvp**	-2287.993397	-2287.989561	-2287.995828

Methodology

Gaussian '03W[17] was used to optimize geometries using the B3LYP/LANL2DZ level of theory. As described in the Gaussian '03 User's Reference, LANL2DZ uses the D95V basis on first row elements and Los Alamos Hay-Wadt ECP plus DZ on Ru. The D95V basis is also known as the Dunning/Huzinaga valence double-zeta basis set.

Jaguar[18] was used for geometry optimizations of **9a-c** using the B3LYP and MPW1K density functionals, using an effective core potential to describe the core electrons of Ru. The LACVP** basis set was used for each calculation employing the Los Alamos ECP of Hay and Wadt with 18 explicit electrons on Ru and the Pople 6-31G** basis on all other atoms.

Frequency calculations were also performed for each structure optimized with the MPW1K/LACVP** level of theory The MPW1K gas phase optimized structures returned normal modes which were all greater than 40 cm^{-1}. Cartesian coordinates and computed frequencies for these structures are provided in Tables S17-S22.

Once the gas phase structures were optimized, these geometries were subject to single-point energy calculations using a CH_2Cl_2 solvent continuum model at the same level of theory. In Gaussian 03W, this was done using the default PCM methodology [SCRF=(solvent=dichloromethane)]. In Jaguar, the PBF approach was used with parameters input [using MW = 84.9, dielectric constant = 9.08, and density = 1.3255] for dichloromethane [epsout=9.08, radprb=2.33274].

[17] Gaussian 03, Revision C.02, Frisch, M. J.; Trucks, G. W.; Schlegel, H. B.; Scuseria, G. E.; Robb, M. A.; Cheeseman, J. R.; Montgomery, Jr., J. A.; Vreven, T.; Kudin, K. N.; Burant, J. C.; Millam, J. M.; Iyengar, S. S.; Tomasi, J.; Barone, V.; Mennucci, B.; Cossi, M.; Scalmani, G.; Rega, N.; Petersson, G. A.; Nakatsuji, H.; Hada, M.; Ehara, M.; Toyota, K.; Fukuda, R.; Hasegawa, J.; Ishida, M.; Nakajima, T.; Honda, Y.; Kitao, O.; Nakai, H.; Klene, M.; Li, X.; Knox, J. E.; Hratchian, H. P.; Cross, J. B.; Bakken, V.; Adamo, C.; Jaramillo, J.; Gomperts, R.; Stratmann, R. E.; Yazyev, O.; Austin, A. J.; Cammi, R.; Pomelli, C.; Ochterski, J. W.; Ayala, P. Y.; Morokuma, K.; Voth, G. A.; Salvador, P.; Dannenberg, J. J.; Zakrzewski, V. G.; Dapprich, S.; Daniels, A. D.; Strain, M. C.; Farkas, O.; Malick, D. K.; Rabuck, A. D.; Raghavachari, K.; Foresman, J. B.; Ortiz, J. V.; Cui, Q.; Baboul, A. G.; Clifford, S.; Cioslowski, J.; Stefanov, B. B.; Liu, G.; Liashenko, A.; Piskorz, P.; Komaromi, I.; Martin, R. L.; Fox, D. J.; Keith, T.; Al-Laham, M. A.; Peng, C. Y.; Nanayakkara, A.; Challacombe, M.; Gill, P. M. W.; Johnson, B.; Chen, W.; Wong, M. W.; Gonzalez, C.; and Pople, J. A.; Gaussian, Inc., Wallingford CT, 2004.

[18] Jaguar, version 6.5, Schrodinger, LLC, New York, NY, 2005

Table S17. Cartesian coordinates for **9a** optimized at the MPW1K/LACVP** level of theory.

atom	x	y	z
Ru1	0.1211140189	0.0843179001	-0.0284789440
C2	0.2330973156	0.0423289885	2.3433481259
C3	1.4830384666	0.2108084919	1.8299520734
Cl4	2.0804788455	1.1839561868	-0.9617021241
C5	-0.6307870169	1.7068608163	0.3480144389
Cl6	-1.7031232582	-1.3514723518	0.6107506062
C7	-0.4370475992	-0.1385115530	-2.0210281029
N8	-0.0943482744	-1.2416955147	-2.7021536773
N9	-1.0396385122	0.6923405750	-2.8804006388
C10	-0.3417262380	-1.1305342199	-4.1349449549
H11	-0.8322853596	-2.0234176926	-4.5120487266
H12	0.6031870103	-1.0068236912	-4.6636264721
C13	-1.2150652579	0.1090383420	-4.2094284612
H14	-0.8997795992	0.8074886407	-4.9791499004
H15	-2.2671448247	-0.1254788666	-4.3737593556
C16	0.4472524815	-2.4491179803	-2.1714513991
C17	-0.4432967232	-3.4748819363	-1.8275505962
C18	0.0763734507	-4.6525503003	-1.3186160087
H19	-0.6058890812	-5.4412970911	-1.0332549439
C20	1.4439705104	-4.8471402643	-1.1713024247
C21	2.2989948745	-3.8452192455	-1.5983414372
H22	3.3678987974	-3.9987926875	-1.5414834754
C23	1.8274947629	-2.6473363338	-2.1270106525
C24	-1.9163101198	-3.3466795271	-2.0651845587
H25	-2.1421596541	-3.3971760058	-3.1316456090
H26	-2.3033844306	-2.4144217027	-1.6689959178
H27	-2.4510263549	-4.1587009568	-1.5812428160
C28	1.9700567095	-6.1162121740	-0.5728060089
H29	3.0121384090	-6.2791120893	-0.8347299811
H30	1.3971898291	-6.9783357952	-0.9077796974
H31	1.9029493682	-6.0861483141	0.5144027100
C32	2.7956648514	-1.6716944328	-2.7201240168
H33	2.9158346579	-1.8736401736	-3.7858637820
H34	3.7747670021	-1.7746498794	-2.2605897707
H35	2.4803236881	-0.6427341760	-2.5905597313
C36	-1.6786602952	1.9337138388	-2.6148697721
C37	-2.9724569434	1.9431936794	-2.0902663335
C38	-3.5871040981	3.1722558875	-1.8876109689
H39	-4.5852578306	3.1909163823	-1.4719009440
C40	-2.9585490318	4.3688626138	-2.2028308408
C41	-1.6791322573	4.3198389751	-2.7395319693
H42	-1.1730417250	5.2420256000	-2.9899582713
C43	-1.0231003678	3.1167691833	-2.9637284140
C44	-3.6788497207	0.6746309272	-1.7262465699
H45	-4.6995388589	0.8824138481	-1.4176812186
H46	-3.1754443471	0.1558837342	-0.9111420840
H47	-3.7219603866	-0.0158951901	-2.5674554704

C48	-3.6556290148	5.6811075190	-2.0006283366
H49	-2.9494881515	6.4725036363	-1.7606934769
H50	-4.3861650379	5.6235337441	-1.1974416036
H51	-4.1868232600	5.9818617265	-2.9036916632
C52	0.3598010851	3.1004062332	-3.5382870513
H53	1.0412566691	2.5403584679	-2.9005819169
H54	0.7395967600	4.1127326928	-3.6440558968
H55	0.3774577497	2.6408208692	-4.5266967136
H56	-0.7624814653	2.4757517433	-0.4068790943
C57	-1.0155501877	2.0517528950	1.6901712937
C58	-1.7926764333	3.1749767579	1.9883129434
H59	-2.0695875814	3.8512764742	1.1926808252
C60	-2.2286533326	3.3836874867	3.2799185053
H61	-2.8435933756	4.2389762358	3.5151126135
C62	-1.8863247526	2.4794923217	4.2801483572
H63	-2.2356643136	2.6423642630	5.2890145772
C64	-1.0987445228	1.3750080350	4.0017345094
H65	-0.8308176496	0.6856465188	4.7884369807
C66	-0.6404778662	1.1648660445	2.7104257267
H67	-0.0915351382	-0.9436957350	2.6406121059
H68	1.9330061093	1.1839881688	1.7172097905
H69	2.1415996931	-0.6396834408	1.7255456751

Table S18. Frequencies for **9a** computed at the MPW1K/LACVP** level of theory.

harmonic frequencies in cm**-1,

frequencies	48.08	58.12	60.18	66.42	78.05	80.71
frequencies	89.34	99.95	108.91	115.90	124.19	129.90
frequencies	131.46	143.18	152.96	161.11	171.42	181.97
frequencies	183.08	186.24	188.92	190.70	195.09	200.32
frequencies	204.87	210.56	214.69	232.45	236.31	246.23
frequencies	265.94	269.79	271.17	272.93	288.50	288.73
frequencies	297.80	304.17	314.19	324.62	329.71	336.49
frequencies	366.39	375.61	379.97	391.20	446.73	467.41
frequencies	484.56	503.86	509.50	511.08	550.25	554.57
frequencies	562.57	580.93	586.59	590.42	592.61	594.63
frequencies	599.91	605.41	615.35	622.28	645.66	684.73
frequencies	735.50	771.09	778.34	790.70	796.32	807.00
frequencies	809.00	818.13	884.34	886.00	888.39	898.57
frequencies	902.21	913.97	918.34	923.82	950.85	961.17
frequencies	961.89	970.02	986.47	990.56	991.12	998.61
frequencies	1024.45	1027.43	1032.81	1034.12	1036.35	1037.14
frequencies	1045.93	1056.46	1061.21	1062.10	1062.91	1067.14
frequencies	1067.97	1069.21	1071.05	1072.02	1072.92	1097.67
frequencies	1126.71	1140.62	1169.85	1184.24	1189.98	1194.30
frequencies	1206.79	1243.65	1248.28	1263.69	1264.32	1273.50
frequencies	1283.51	1296.25	1308.56	1336.80	1341.85	1349.15
frequencies	1355.35	1359.79	1367.15	1378.09	1397.33	1397.77
frequencies	1403.98	1405.17	1411.39	1423.29	1428.04	1432.07
frequencies	1454.46	1458.33	1459.37	1464.33	1473.70	1475.19
frequencies	1476.28	1477.80	1478.23	1478.39	1479.46	1486.97
frequencies	1495.59	1504.66	1506.34	1520.65	1523.25	1524.01
frequencies	1538.70	1540.76	1567.37	1579.24	1628.39	1673.51
frequencies	1690.62	1692.35	1703.69	1713.05	1714.96	3121.85
frequencies	3123.23	3126.09	3127.13	3130.86	3131.88	3151.14
frequencies	3155.84	3214.46	3215.21	3223.55	3224.20	3226.35
frequencies	3226.90	3229.11	3237.88	3247.00	3247.48	3247.94
frequencies	3248.10	3248.75	3260.97	3271.71	3272.57	3281.53
frequencies	3281.89	3282.99	3283.33	3291.15	3297.86	3307.52
frequencies	3309.70	3316.92	3376.63			

Table S19. Cartesian coordinates for **9b** optimized at the MPW1K/LACVP** level of theory.

atom	x	y	z
Ru1	0.0248602003	0.0583054132	-0.0145814953
C2	-0.0263628811	0.0456377789	2.0395137203
C3	1.8268879975	0.0771864730	-0.3008312437
C4	0.4865060720	-2.1625899075	0.1068063428
C5	-0.5602577919	-1.9676974234	-0.7579756435
Cl6	-0.8853826719	0.5550362637	-2.1825469061
Cl7	0.1035000213	2.4477988343	0.2516933318
N8	-1.2205042725	-0.0995860788	2.6339977685
N9	0.8716530468	0.3347374294	2.9883937612
C10	-1.2014699307	0.2174165067	4.0559723151
H11	-1.6654208253	-0.5807017899	4.6310981192
H12	-1.7522039897	1.1378652111	4.2425523402
C13	0.2895672898	0.3636205894	4.3293459188
H14	0.5348780338	1.2962230543	4.8293286999
H15	0.6938378664	-0.4560534169	4.9239571060
C16	-2.4065204179	-0.5723054631	2.0028359318
C17	-2.6911446055	-1.9398659030	2.0496488261
C18	-3.8440420309	-2.4011987688	1.4273530508
H19	-4.0594601969	-3.4610971424	1.4490321577
C20	-4.7189290020	-1.5409912427	0.7836973932
C21	-4.4413242415	-0.1809876540	0.8111652379
H22	-5.1291485599	0.5082183438	0.3422428512
C23	-3.3092033151	0.3316858521	1.4266585548
C24	-1.8238219233	-2.9261449160	2.7749914836
H25	-0.8893492450	-2.4878342582	3.1084491460
H26	-1.5905305509	-3.7798313625	2.1418599033
H27	-2.3410147503	-3.3118400065	3.6530104026
C28	-5.9306890635	-2.0582739259	0.0708679120
H29	-6.7966811047	-1.4258130959	0.2525990756
H30	-6.1768396787	-3.0693738749	0.3841674450
H31	-5.7622011754	-2.0753496870	-1.0052783543
C32	-3.1029359047	1.8117874373	1.4989136215
H33	-3.0899046501	2.1511942028	2.5345662423
H34	-3.9129479994	2.3284052214	0.9932543562
H35	-2.1666232370	2.1224119630	1.0401185253
C36	2.2867123828	0.4344783964	2.8713804910
C37	3.0591399551	-0.7251811763	2.8914617047
C38	4.4427428975	-0.6040840227	2.8109744611
H39	5.0426076371	-1.5039163059	2.8072699441
C40	5.0642785218	0.6290350654	2.7430403233
C41	4.2688660120	1.7685799839	2.7931422839
H42	4.7381089961	2.7427694611	2.7771745032
C43	2.8884678832	1.7008198806	2.8762393748
C44	2.4711756652	-2.0959377476	3.0359672256
H45	2.9247137516	-2.6115608740	3.8808028091
H46	2.6638120138	-2.6942984802	2.1487441066

H47	1.3988082571	-2.0698688636	3.1954371986
C48	6.5546477357	0.7492383173	2.6377905230
H49	6.8427570351	1.1974767742	1.6877920456
H50	7.0392382304	-0.2206298599	2.7093107716
H51	6.9543667680	1.3844515144	3.4264951982
C52	2.0845435973	2.9547619274	3.0222234677
H53	1.1939596257	2.9315285772	2.4013369130
H54	2.6740790281	3.8204459782	2.7337160805
H55	1.7873838525	3.1001661859	4.0618887477
H56	2.3312931238	1.0374394890	-0.3658450789
C57	2.5745131473	-1.1208361334	-0.5881710435
C58	3.8878466324	-1.1422729446	-1.0552082961
H59	4.4152175791	-0.2129808059	-1.2112895920
C60	4.4952021153	-2.3554147665	-1.3168297002
H61	5.5099292746	-2.3855090005	-1.6835816634
C62	3.7985022512	-3.5395308711	-1.1107453521
H63	4.2784794710	-4.4840816843	-1.3200197947
C64	2.4907858990	-3.5249743791	-0.6443460217
H65	1.9553780338	-4.4510029894	-0.4948666549
C66	1.8747682185	-2.3127523895	-0.3852824241
H67	0.2946818296	-2.5015590450	1.1135155171
H68	-0.3977233258	-1.9326070429	-1.8221310885
H69	-1.5823556370	-2.0962175819	-0.4312350795

Table S20. Frequencies for **9b** computed at the MPW1K/LACVP** level of theory.

harmonic frequencies in cm**-1,

frequencies	44.56	49.08	57.83	60.29	72.06	79.74
frequencies	91.05	98.16	107.64	118.52	121.87	132.06
frequencies	139.75	150.18	152.53	156.40	165.29	171.28
frequencies	179.30	180.59	182.85	185.14	188.06	191.70
frequencies	203.01	214.08	230.09	232.57	240.27	261.18
frequencies	263.77	265.53	266.95	271.27	288.54	289.84
frequencies	296.17	301.49	311.85	331.22	337.86	356.96
frequencies	369.88	382.52	388.60	400.75	449.75	488.84
frequencies	504.47	505.75	506.97	511.18	548.28	553.68
frequencies	555.99	580.58	583.45	587.18	592.12	600.12
frequencies	604.15	610.17	615.97	618.52	642.50	679.91
frequencies	751.17	776.74	788.27	788.64	794.65	797.70
frequencies	817.08	821.85	884.99	886.76	887.55	891.09
frequencies	901.77	918.02	920.31	921.38	947.06	951.24
frequencies	959.12	963.48	979.80	984.32	987.70	991.38
frequencies	1021.44	1026.29	1029.27	1032.38	1038.47	1040.02
frequencies	1050.05	1052.52	1053.92	1055.67	1058.91	1066.93
frequencies	1067.35	1068.85	1069.57	1072.34	1074.37	1100.03
frequencies	1127.00	1135.62	1168.05	1182.05	1185.51	1189.99
frequencies	1208.60	1229.51	1246.30	1257.37	1264.44	1265.55
frequencies	1284.90	1288.39	1311.53	1329.06	1340.92	1345.55
frequencies	1348.43	1365.31	1370.74	1380.53	1391.67	1394.38
frequencies	1396.27	1403.94	1410.06	1422.87	1425.38	1428.30
frequencies	1458.23	1459.02	1466.29	1467.08	1473.95	1474.58
frequencies	1475.29	1476.79	1478.31	1482.53	1484.56	1486.74
frequencies	1498.09	1500.98	1507.74	1519.55	1520.97	1527.60
frequencies	1539.92	1540.42	1568.34	1575.47	1605.43	1681.07
frequencies	1688.54	1694.47	1701.18	1713.70	1716.31	3121.81
frequencies	3123.50	3132.07	3134.68	3136.90	3141.74	3150.89
frequencies	3160.71	3215.49	3220.59	3221.75	3223.49	3224.04
frequencies	3228.99	3232.01	3235.31	3246.45	3248.49	3249.63
frequencies	3253.50	3258.22	3259.44	3262.09	3266.50	3277.10
frequencies	3280.26	3281.96	3290.46	3291.14	3300.02	3305.00
frequencies	3307.88	3317.68	3381.90			

Table S21. Cartesian coordinates for **9c** optimized at the MPW1K/LACVP** level of theory.

atom	x	y	z
Ru1	-0.0127951825	-0.0220791525	-0.0266216652
Cl2	0.0215802014	-0.0729163490	2.3580549062
Cl3	2.3851955848	0.0215787728	0.0598274754
C4	-2.1818831259	0.3821454807	-0.4121267702
C5	0.1054519294	-1.6936360538	-0.7639650088
C6	0.2747668494	1.0054999887	-1.7885840912
C7	-2.1096699071	-0.7523320286	0.3588063653
C8	-3.3015813057	-2.9330188502	-0.1064439486
C9	-0.9673500521	-3.9007228083	-1.2931357576
C10	-3.2494614694	-4.2187255182	-0.6236966313
H11	0.1247944029	1.6971214900	-4.7022969079
N12	0.7051476906	0.6207295617	-2.9976194327
N13	0.1977175600	2.3464659557	-1.7912476114
C14	2.1948333093	-1.1874961615	-3.6535393404
C15	-0.2051276754	-1.4115239653	-3.9877110119
C16	0.8906203713	-0.6921764114	-3.5130201468
C17	0.0152755085	-2.6696676447	-4.5394878912
C18	1.2846330078	-3.2115485051	-4.6419585986
C19	-0.3586528364	3.1864890932	-0.7816772466
C20	-1.5050002749	4.8809679950	1.1128229930
C21	-1.6753860128	3.6343094510	-0.9568263520
C22	-2.2281184148	4.4675175825	0.0012330280
C23	-2.1351721288	5.7455742005	2.1618079043
H24	-2.3865740785	0.3210840543	-1.4684897952
H25	-2.3753679391	1.3303194270	0.0672920837
H26	1.0715606838	-2.0647289167	-1.0929598220
H27	-0.8347481469	-3.2352720616	-4.8955890724
H28	-3.2485459938	4.8034644675	-0.1248171446
C29	0.4152172464	3.6349608763	0.2908741159
C30	-1.0136100862	-2.6022412088	-0.7833564751
C31	-0.1894583680	4.4665015093	1.2276839994
C32	-1.6066319019	-0.8901131088	-3.9138495278
C33	-2.4899132319	3.2701175486	-2.1631796288
C34	0.7259858839	2.9475468034	-3.0099224904
C35	2.3605958491	-2.4490519863	-4.2014500943
C36	0.8830940195	1.7409564279	-3.9195057676
C37	-2.0890800450	-4.7026948943	-1.2165742789
H38	-4.2031656720	-2.5707922729	0.3646687666
H39	-0.0533283023	-4.2649847365	-1.7375633024
H40	-4.1196770045	-4.8547836171	-0.5564432882
H41	-2.0626520391	-5.7101986341	-1.6032459689
C42	3.3924907744	-0.3827740868	-3.2537760203
C43	1.8582421127	3.2840302166	0.4660707854
C44	1.5089973294	-4.5751618453	-5.2236131640
H45	0.3998106236	4.8015908516	2.0698667539
H46	0.0351269519	3.6896759844	-3.4012199202
H47	3.3625325877	-2.8460888186	-4.2909133382
H48	1.8589810738	1.6944366669	-4.3931135580

H49	-1.4227597185	6.4596248764	2.5678325905
H50	-2.4966745104	5.1389797511	2.9915929168
H51	-2.9823759715	6.2991192543	1.7647967727
H52	3.6379608694	0.3570385321	-4.0176303785
H53	4.2604536572	-1.0262815316	-3.1418365211
H54	-2.1806528911	-1.2197538418	-4.7763030873
H55	-1.6404843669	0.1950476408	-3.8798738012
H56	-2.1083961815	-1.2686835863	-3.0243217125
H57	-2.4523707673	4.0652462702	-2.9082047525
H58	-3.5350120350	3.1316601914	-1.8973387067
H59	-2.1403386371	2.3583736364	-2.6361164266
H60	1.9780614334	2.4908037237	1.2006675986
H61	2.4092967985	4.1565239784	0.8101924896
H62	2.3114856812	2.9189297289	-0.4483672394
H63	2.0166347841	-5.2244451441	-4.5117929874
H64	2.1347061748	-4.5241969484	-6.1134444882
H65	0.5718331700	-5.0500782392	-5.5006986990
H66	1.6739996650	3.4408199769	-2.7973650262
C67	-2.1857419850	-2.1171205278	-0.1945180424
H68	3.2293631331	0.1252377564	-2.3076789490
H69	-2.2227356977	-0.6607835380	1.4292094917

Table S22. Frequencies for **9c** computed at the MPW1K/LACVP** level of theory.

harmonic frequencies in cm**-1,

frequencies	49.88	55.06	61.54	66.08	73.64	81.05
frequencies	91.63	97.18	108.26	118.01	129.78	136.49
frequencies	140.19	148.17	162.10	167.08	170.48	172.75
frequencies	178.39	179.34	183.25	185.82	188.97	201.23
frequencies	202.71	208.26	225.73	233.32	237.14	257.35
frequencies	259.31	265.20	268.91	286.13	288.91	290.15
frequencies	292.30	309.81	320.07	335.38	343.34	348.97
frequencies	372.98	383.50	395.90	400.11	453.11	491.50
frequencies	503.30	505.00	507.88	511.49	550.44	553.70
frequencies	555.72	578.93	581.97	587.43	591.49	599.02
frequencies	604.66	610.70	616.63	618.57	643.30	682.05
frequencies	756.19	773.31	785.80	788.34	793.75	797.10
frequencies	809.54	818.04	885.98	887.32	888.43	896.00
frequencies	901.42	919.15	919.55	922.25	945.83	949.63
frequencies	961.37	963.31	976.89	978.30	986.10	988.89
frequencies	1024.36	1025.70	1029.59	1031.30	1039.19	1040.00
frequencies	1044.52	1054.11	1056.46	1057.77	1061.66	1063.23
frequencies	1066.96	1068.09	1070.46	1071.95	1073.38	1099.75
frequencies	1127.32	1137.40	1168.39	1184.31	1185.38	1189.91
frequencies	1209.27	1238.50	1244.54	1264.96	1265.73	1277.09
frequencies	1281.84	1287.51	1310.50	1333.25	1340.54	1346.80
frequencies	1350.96	1358.75	1371.09	1380.16	1393.87	1395.85
frequencies	1396.19	1403.71	1404.62	1421.14	1422.75	1426.75
frequencies	1452.11	1458.28	1463.02	1466.51	1469.47	1470.99
frequencies	1474.06	1475.75	1476.57	1477.31	1481.26	1485.35
frequencies	1494.37	1499.47	1506.17	1518.95	1521.03	1526.22
frequencies	1536.70	1539.23	1565.30	1573.75	1607.52	1678.04
frequencies	1690.31	1692.33	1702.22	1714.28	1714.79	3120.53
frequencies	3132.11	3133.84	3134.79	3135.45	3146.11	3148.12
frequencies	3157.49	3220.93	3223.52	3225.39	3226.75	3228.19
frequencies	3229.62	3239.12	3241.30	3248.47	3248.98	3251.45
frequencies	3251.56	3257.96	3258.20	3262.55	3275.03	3278.16
frequencies	3282.10	3283.00	3286.14	3291.87	3301.24	3301.63
frequencies	3309.48	3317.77	3372.93			